BEHAVIOR OF DOUBLY CURVED PARTLY WRINKLED MEMBRANE STRUCTURES FORMED FROM AN INITIALLY FLAT MEMBRANE

By

Martin M. Mikulas, Jr.

Thesis submitted to the Graduate Faculty of the

Virginia Polytechnic Institute

DOCTOR OF PHILOSOPHY

in

Engineering Mechanics

APPROVED: _____

Chairman, Prof. F. J. Maher

_____ _____

Dr. R. T. Davis Prof. C. W. Smith

_____ _____

Dr. J. L. Lytton Dr. C. T. Herakovich

June 1970

Blacksburg, Virginia

TABLE OF CONTENTS

ACKNOWLEDGMENTS

The author wishes to express his appreciation to the National Aeronautics and Space Administration for permitting him to conduct this research as part of his work assignment at Langley Research Center, and to Professor Francis J. Maher of the Engineering Mechanics Department, Virginia Polytechnic Institute, and to Dr. Manuel Stein of the Structures Research Division, Langley Research Center, for their helpful criticisms and suggestions. He also wishes to express his appreciation to Mrs. Cornelia Dexter, Mathematician, Structures Research Division, Langley Research Center, for her programing of the numerical solutions and assistance in subsequent calculation of the results. Finally, the author wishes to express his gratitude to his wife, Connie, and to his children, Lynne, Marty, and Cathy, for their patience and consideration throughout his entire doctorate program.

LIST OF FIGURES

SYMBOLS

a	extent of unwrinkled region
A_i	constants in power series
A_s	cross-sectional area of stiffening cords
b	radius of rigid ring insert
d	depth of unwrinkled region
E	Young's modulus of isotropic membrane
E_s	Young's modulus of stiffening cords
h	thickness of membrane
i	station number
I	total number of stations
L	load in meridional cords
m	station number defining radius of rigid ring insert
N_ξ, N_θ	meridional and circumferential stress resultants
N_r	radial stress resultant
$\bar{N}_r, \bar{N}_\theta$	nondimensional stress resultants, see equation (52)
$\bar{N}_{r_f}, \bar{N}_{\theta_f}$	nondimensional meridional and circumferential stress resultants in the isotropic portion of a stiffened membrane
n	number of meridional cords
p	internal pressure
P	applied edge load perpendicular to membrane
P_{wr}	value of radial line load for which wrinkling begins
r	radial coordinate

R	characteristic radius
R_p	radius of cylinder after pressurization
r_ξ, r_θ	meridional and circumferential radii of curvature
S	nondimensional cord stiffness, $\frac{nE_sA_s}{2\pi aEh}(1 - \mu^2)$
s	arc length
T	applied meridional load per unit length
u	meridional displacement
w	lateral displacement in same direction as pressure p
W_m	axial coordinate defining mandrel surface
W_P	deflection at line of application of radial line load
z	axial coordinate
ϵ	station spacing
$\epsilon_\xi, \epsilon_\theta$	meridional and circumferential strains
ϵ_r	radial strain
β	meridional rotation
θ	circumferential coordinate
ϕ	meridional coordinate
μ	Poisson's ratio
ξ	meridional coordinate
ρ	nondimensional radial coordinate, $\frac{r}{a}$
ψ	meridional rotation
Π	strain energy
η	ratio of added hoop stiffness to added meridional stiffness

INTRODUCTION

The primary purpose of this research is to investigate the elastic behavior of doubly curved membrane structures which are constructed from flat sheet components. Examples of structures constructed in such a fashion are parachutes, parawings, ballutes, attached inflatable decelerators, large inflatable passive communications satellites, and very large helium-filled balloons which are used to carry large payloads to altitudes over 100,000 feet (see fig. 1). Such doubly curved flexible structures are commonly constructed from flat sheets because of the ease and economy of fabrication. In most instances, however, analysis of these structures is conducted as if they were smooth doubly curved shells and, at best, linear membrane shell theory is used. The most prevalent technique for arriving at a final design for such structures is to conduct an extensive trial and error program until a workable configuration is found. This technique is far from satisfactory when the tests involved are very expensive. In addition, although such a method will ultimately permit one to find a workable configuration, the chances of arriving at the optimum, lightweight configuration are very small.

If these design techniques are to be improved upon, it is necessary that a fundamental understanding of the mechanics of deformation of a flat membrane to a doubly curved membrane be developed. For instance, if an unloaded flat membrane is deformed to a doubly curved surface, wrinkling must occur over the entire membrane. This

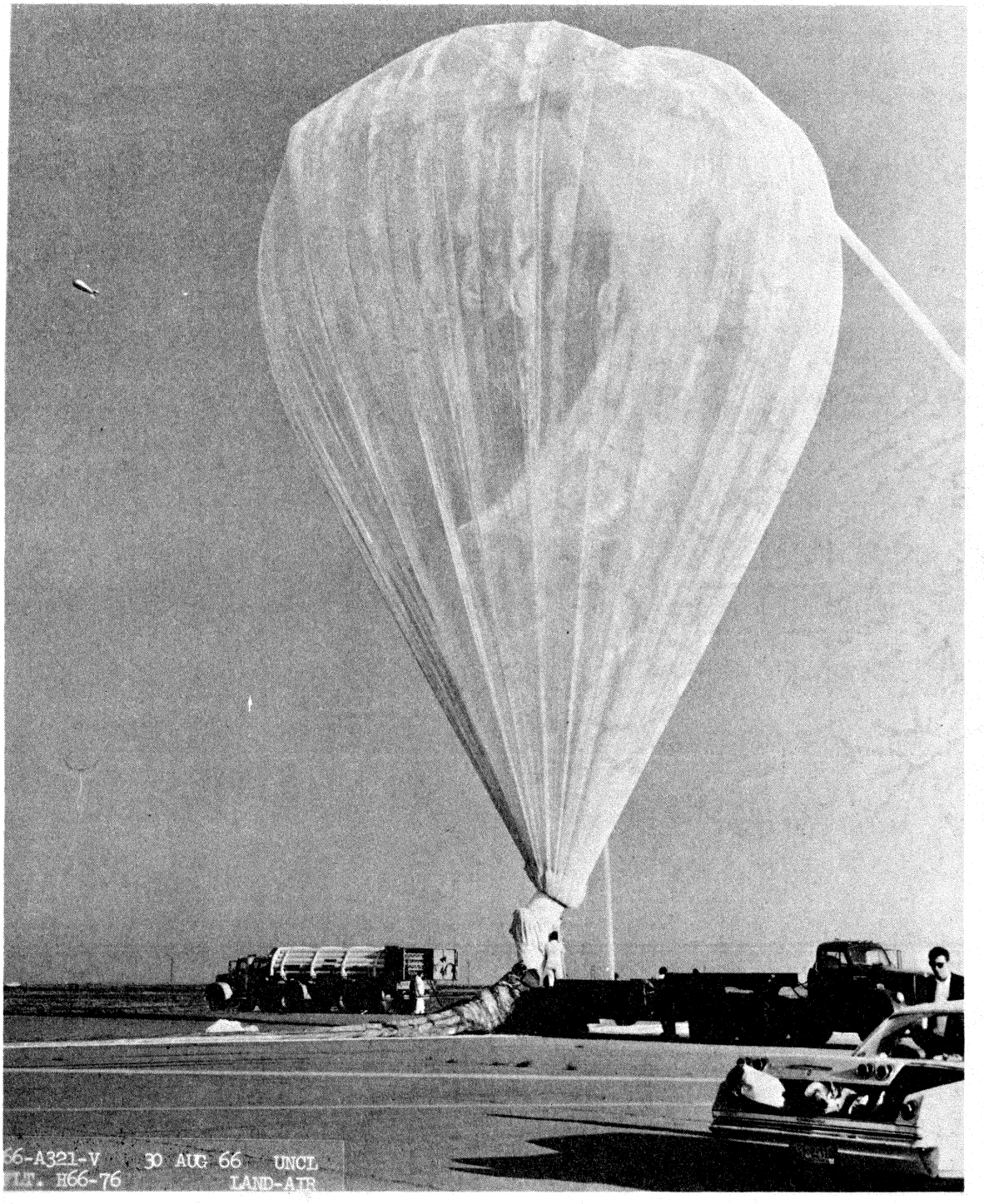

Figure 1.- Launching of a high-altitude helium-filled balloon.

is due to the fact that a doubly curved surface is not developable from a flat surface. As a load is applied to the membrane, the wrinkles in certain regions of the doubly curved surface will be removed due to stretching of the membrane. These two regions, the wrinkled and unwrinkled, must be analyzed separately and matched together.

A theory for the analysis of flat, partly wrinkled membranes was developed in reference 1 by Stein and Hedgepeth in 1961. As early as 1938, Reissner solved a flat wrinkled membrane problem using tension field theory, reference 2. References 3 and 4 present experimental work which verified the theory of reference 1. Although the analysis of references 1 and 2 are quite adequate for flat wrinkled membrane behavior, they are not suitable for extension to the analysis of flat membranes being deformed into doubly curved wrinkled membranes because of the small strain theory used. In 1919 G. I. Taylor wrote a paper on parachute shapes, reference 5. In that paper, Taylor analyzed a parachute which before flight was a flat circular disc of material. Taylor then theorized that during flight the doubly curved parachute had so much excess material in the circumferential direction that the circumferential hoop stress would have to be zero. He used this concept of zero hoop stress in conjunction with linear membrane shell theory to predict the now-famous Taylor parachute shape. Although this approach yields a good description of the parachute shape, the predicted stresses in the vicinity of the crown are not realistic. This shortcoming is due to the fact that linear membrane theory does not take into account stretching of the surface which is necessary

in the vicinity of the crown. An analysis of isotensoid membrane decelerators, which is an extension of Taylor's work, is presented in references 6 and 7. Again, stretching of the membrane surface was not considered.

In this thesis, a theory for the analysis of axisymmetric doubly curved membranes which are formed from an initially flat membrane is presented. In the theory, the doubly curved membrane is analyzed in two parts, then matched together. The first part is that region of the doubly curved membrane surface which is wrinkled due to excess material in the circumferential direction. This region will be analyzed as a zero hoop stress linear membrane, as was done by Taylor. The remaining part to be analyzed is that region of the membrane in which stretching of the surface has eliminated the wrinkles and the zero hoop stress assumption is no longer valid. In this unwrinkled region, nonlinear membrane theory is used to take into account the stretching of the membrane. The theory used in this region is that of Sanders (ref. 8) with the bending terms set equal to zero. An excellent application of Sanders' theory is presented in reference 9. In reference 9, asymptotic methods are used to determine where linear membrane theory is applicable, and where nonlinear membrane theory is necessary. The addition of stiffening to the isotropic membrane in this thesis is accomplished in the same fashion as that used in reference 10. References 11, 12, and 13 analyze flat circular membranes loaded with lateral pressure using a power series approach. Although

this approach is somewhat outdated in the age of high-speed computers and numerical techniques, it is pursued in this thesis as an alternate technique.

The theory developed in this thesis is used to solve three problems which demonstrate its applicability. An experimental investigation was conducted on one of the three problems, using models made of very thin Mylar. Measurements were made of deformations and the extent of the unwrinkled region, and the results are compared with theory.

FUNDAMENTAL EQUATIONS

In this section the nonlinear governing equations are derived for an axisymmetric membrane which is stiffened with cords in both the meridional and hoop directions. The stiffening elements are assumed to be closely spaced so that their effects may be "smeared out" or averaged over the membrane surface. The derivation will consist of setting up the energy for the isotropic membrane and for the unidirectional stiffening cords, adding them together, and using the principle of minimum potential energy to obtain the equilibrium equations. These general nonlinear equations are used for the analysis of the unwrinkled region, while the linear membrane equations to be used in the wrinkled region are found by setting the meridional rotation equal to zero.

Geometry and Kinematic Relations

The membrane surface shown in figure 2 is defined by r and z as

$$r = r(\xi) \quad \text{and} \quad z = z(\xi) \tag{1}$$

where

$$\frac{dr}{d\xi} = \cos \phi \quad \text{and} \quad \frac{dz}{d\xi} = \sin \phi \tag{2}$$

The arc length on the surface is given by

$$ds^2 = d\xi^2 + r^2 \, d\theta^2 \tag{3}$$

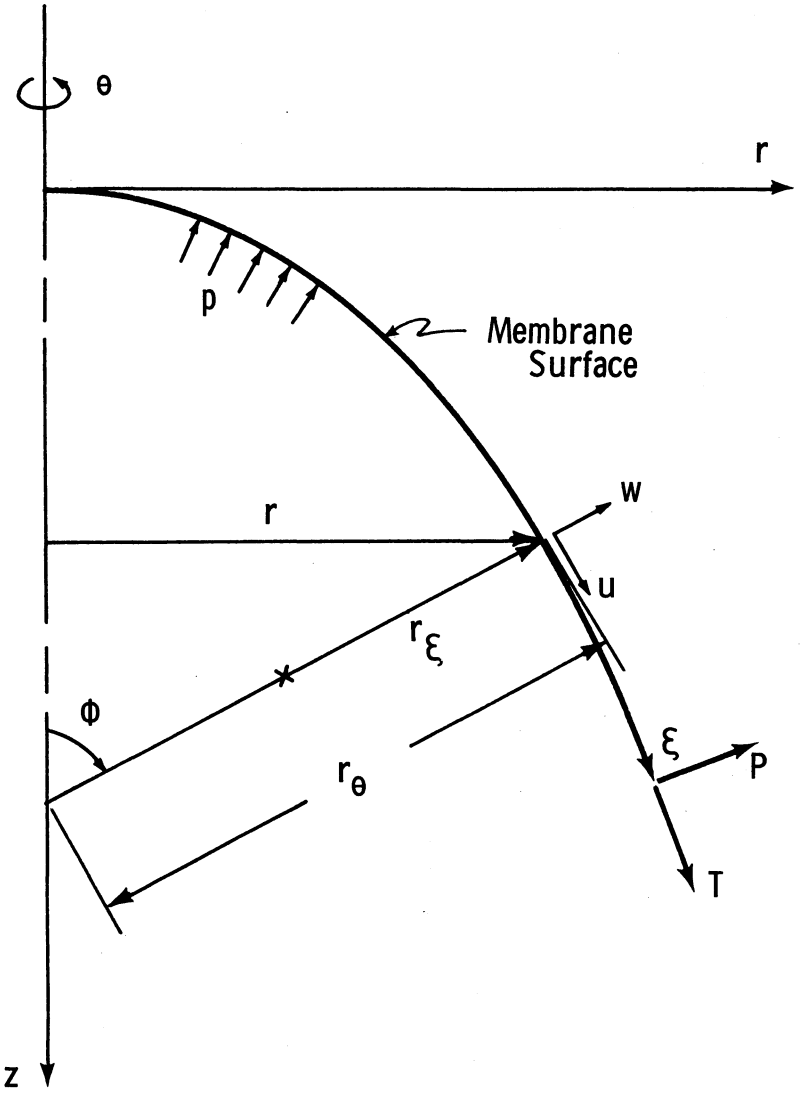

Figure 2.- Coordinate system and notation.

The principal radii of curvature r_ξ and r_θ on the surface are given by

$$\frac{1}{r_\xi} = \frac{d\phi}{d\xi} \quad \text{and} \quad \frac{1}{r_\theta} = \frac{\sin \phi}{r} \tag{4}$$

The kinematic relations to be used in this analysis are taken from Sanders (ref. 8). These relations involve moderately large rotations and are written as

$$\epsilon_\xi = \frac{du}{d\xi} + \frac{1}{2}\psi^2 + \frac{w}{r_\xi} \tag{5}$$

$$\epsilon_\theta = \frac{u}{r}\cos \phi + \frac{w}{r}\sin \phi \tag{6}$$

where ψ is the meridional rotation and is given by

$$\psi = \frac{dw}{d\xi} - \frac{u}{r_\xi} \tag{7}$$

Strain Energy

The strain energy Π_m of the isotropic membrane surface is

$$\Pi_m = \frac{Eh}{2(1 - \mu^2)} \int_{\xi_1}^{\xi_2} \int_0^{2\pi} \left[\epsilon_\xi^2 + \epsilon_\theta^2 + 2\mu\epsilon_\xi\epsilon_\theta\right] r \, d\theta \, d\xi \tag{8}$$

The strain energy Π_S of n unidirectional stiffening cords in the meridional direction of constant cross-sectional area A_S is

$$\Pi_S = \frac{n}{2}\int_V E_S \epsilon_\xi^2 \, dV \tag{9}$$

where the elemental volume is $dV = A_S \, d\xi$, so that equation (9) can be written

$$\Pi_S = \frac{n}{2}\int_{\xi_1}^{\xi_2} E_S A_S \epsilon_\xi^2 \, d\xi \tag{10}$$

Since ϵ_ξ is independent of θ, and if the effect of the stiffening is "smeared out" or averaged over the circumference, then this equation can be written in the same form as equation (8) as

$$\Pi_S = \frac{1}{2}\int_{\xi_1}^{\xi_2}\int_0^{2\pi} \frac{nE_S A_S}{2\pi r} \epsilon_\xi^2 r \, d\theta \, d\xi \tag{11}$$

The stiffening in the hoop direction is assumed to be spaced such that the hoop stiffening is some ratio η of the meridional stiffening. Thus, the strain energy Π_H of the hoop stiffening is written as

$$\Pi_H = \frac{1}{2}\int_{\xi_1}^{\xi_2}\int_0^{2\pi} \eta \frac{nE_S A_S}{2\pi r} \epsilon_\theta^2 r \, d\theta \, d\xi \tag{12}$$

The potential energy Π_L of the internal pressure p, the tangential edge load T, and the perpendicular edge load P is written as

$$\Pi_L = -\int_{\xi_1}^{\xi_2}\int_0^{2\pi} pwr\, d\theta\, d\xi - \int_0^{2\pi} rTu\Big|_{\xi_1}^{\xi_2} d\theta - \int_0^{2\pi} rPw\Big|_{\xi_1}^{\xi_2} d\theta \tag{13}$$

By combining equations (8), (11), (12), and (13), the total energy Π_T of the stiffened membrane is written as

$$\Pi_T = \frac{1}{2}\int_{\xi_1}^{\xi_2}\int_0^{2\pi}\left[\frac{Eh}{1-\mu^2}(\epsilon_\xi^2 + \epsilon_\theta^2 + 2\mu\epsilon_\xi\epsilon_\theta) + \frac{nE_sA_s}{2\pi r}\epsilon_\xi^2 + \eta\frac{nE_sA_s}{2\pi r}\epsilon_\theta^2 - 2pw\right] r\, d\theta\, d\xi - \int_0^{2\pi} rTu\Big|_{\xi_1}^{\xi_2} d\theta - \int_0^{2\pi} rPw\Big|_{\xi_1}^{\xi_2} d\theta \tag{14}$$

The first variation of the energy is

$$\delta\Pi_T = \int_{\xi_1}^{\xi_2}\int_0^{2\pi}\left[\frac{Eh}{1-\mu^2}(\epsilon_\xi\delta\epsilon_\xi + \epsilon_\theta\delta\epsilon_\theta + \mu\epsilon_\theta\delta\epsilon_\xi + \mu\epsilon_\xi\delta\epsilon_\theta) + \frac{nE_sA_s}{2\pi r}\epsilon_\xi\delta\epsilon_\xi + \eta\frac{nE_sA_s}{2\pi r}\epsilon_\theta\delta\epsilon_\theta - p\delta w\right] r\, d\theta\, d\xi - \int_0^{2\pi} rT\delta u\Big|_{\xi_1}^{\xi_2} d\theta - \int_0^{2\pi} rP\delta w\Big|_{\xi_1}^{\xi_2} d\theta \tag{15}$$

Or, in terms of the stress resultants N_ξ and N_θ, equation (15) is written as

$$\delta\Pi_T = \int_{\xi_1}^{\xi_2}\int_0^{2\pi}\left[N_\xi\delta\epsilon_\xi + N_\theta\delta\epsilon_\theta - p\delta w\right] r\, d\theta\, d\xi - \int_0^{2\pi} rTu\Big|_{\xi_1}^{\xi_2} d\theta - \int_0^{2\pi} rP\delta w\Big|_{\xi_1}^{\xi_2} d\theta \tag{16}$$

where N_ξ and N_θ are defined as

$$N_\xi = \frac{Eh}{1 - \mu^2}(\epsilon_\xi + \mu\epsilon_\theta) + \frac{nE_sA_s}{2\pi r}\epsilon_\xi \tag{17}$$

$$N_\theta = \frac{Eh}{1 - \mu^2}(\epsilon_\theta + \mu\epsilon_\xi) + \eta\frac{nE_sA_s}{2\pi r}\epsilon_\theta \tag{18}$$

The strains in equation (16) are now eliminated by using equations (5), (6), and (7) to yield

$$\delta\Pi_T = \int_{\xi_1}^{\xi_2}\int_0^{2\pi}\left[N_\xi\left\{\frac{d\delta u}{d\xi} + \psi\left(\frac{d\delta w}{d\xi} - \frac{\delta u}{r_\xi}\right) + \frac{\delta w}{r_\xi}\right\} + N_\theta\left\{\frac{\delta u}{r}\cos\phi + \frac{\delta w}{r}\sin\phi\right\}\right.$$
$$\left. - p\delta w\right] r\, d\theta\, d\xi - \int_0^{2\pi} rT\delta u\Big|_{\xi_1}^{\xi_2} d\theta - \int_0^{2\pi} rP\delta w\Big|_{\xi_1}^{\xi_2} d\theta \tag{19}$$

After integrating by parts and applying the principle of minimum potential energy ($\delta\Pi_T = 0$), there results

$$\delta\Pi_T = \int_{\xi_1}^{\xi_2}\int_0^{2\pi}\left[\left\{-\frac{d}{d\xi}(rN_\xi) - \frac{rN_\xi\psi}{r_\xi} + N_\theta\cos\phi\right\}\delta u\right.$$
$$\left. + \left\{-\frac{d}{d\xi}(rN_\xi\psi) + \frac{rN_\xi}{r_\xi} + N_\theta\sin\phi - pr\right\}\delta w\right] d\theta\, d\xi$$
$$+ \int_0^{2\pi} r(N_\xi - T)\delta u\Big|_{\xi_1}^{\xi_2} d\theta + \int_0^{2\pi} r(N_\xi\psi - P)\delta w\Big|_{\xi_1}^{\xi_2} d\theta = 0 \tag{20}$$

Equilibrium Equations and Boundary Conditions

In equation (20) the variation of the displacements δu and δw may be assumed to be arbitrary and independent, so that the following conditions of equilibrium must hold.

$$\frac{d}{d\xi}(rN_\xi) + \frac{rN_\xi\psi}{r_\xi} - N_\theta \cos\phi = 0 \tag{21}$$

$$\frac{N_\xi}{r_\xi} + \frac{N_\theta}{r_\theta} - \frac{1}{r}\frac{d}{d\xi}(rN_\xi\psi) - p = 0 \tag{22}$$

where the $\sin\phi$ in equation (20) was eliminated using the second of equations (4). The boundary conditions are obtained from the single integrals and may be stated as follows: on an edge ξ = const. specify

$$N_\xi = T \quad \text{or} \quad u \tag{23}$$

$$N_\xi\psi = P \quad \text{or} \quad w \tag{24}$$

GENERAL THEORY

A theory is presented in this section for the structural behavior of doubly curved axisymmetric membrane structures which are formed from an initially flat membrane. The membrane considered in this analysis is elastic, has no bending stiffness, and cannot carry compressive stress. The doubly curved membrane structure is considered as consisting of two regions. The first region is that part of the membrane structure which is doubly curved due to stretching in the initially flat membrane. The second region is that part of the doubly curved membrane which is wrinkled due to the very large deformations that must take place to form the desired doubly curved surface. These two regions can be seen in figure 3 which is a photograph of an initially flat circular membrane which has been pleated around its periphery and attached to a rigid circular boundary and pressurized. The crown of the membrane is completely smooth and unwrinkled, while the rest of the membrane has large meridional wrinkles in it. The extent of the smooth unwrinkled region increases with increasing internal pressure as more and more of the wrinkles are taken up by stretching of the membrane.

In the unwrinkled region, small strain, moderate rotation, nonlinear membrane theory will be utilized. In the wrinkled region, the wrinkles are always assumed to be in the meridional direction and the hoop stress perpendicular to the wrinkles is taken equal to zero. The meridional strain along the wrinkles is assumed to be small, while the average strain in the hoop direction is of unlimited size. It

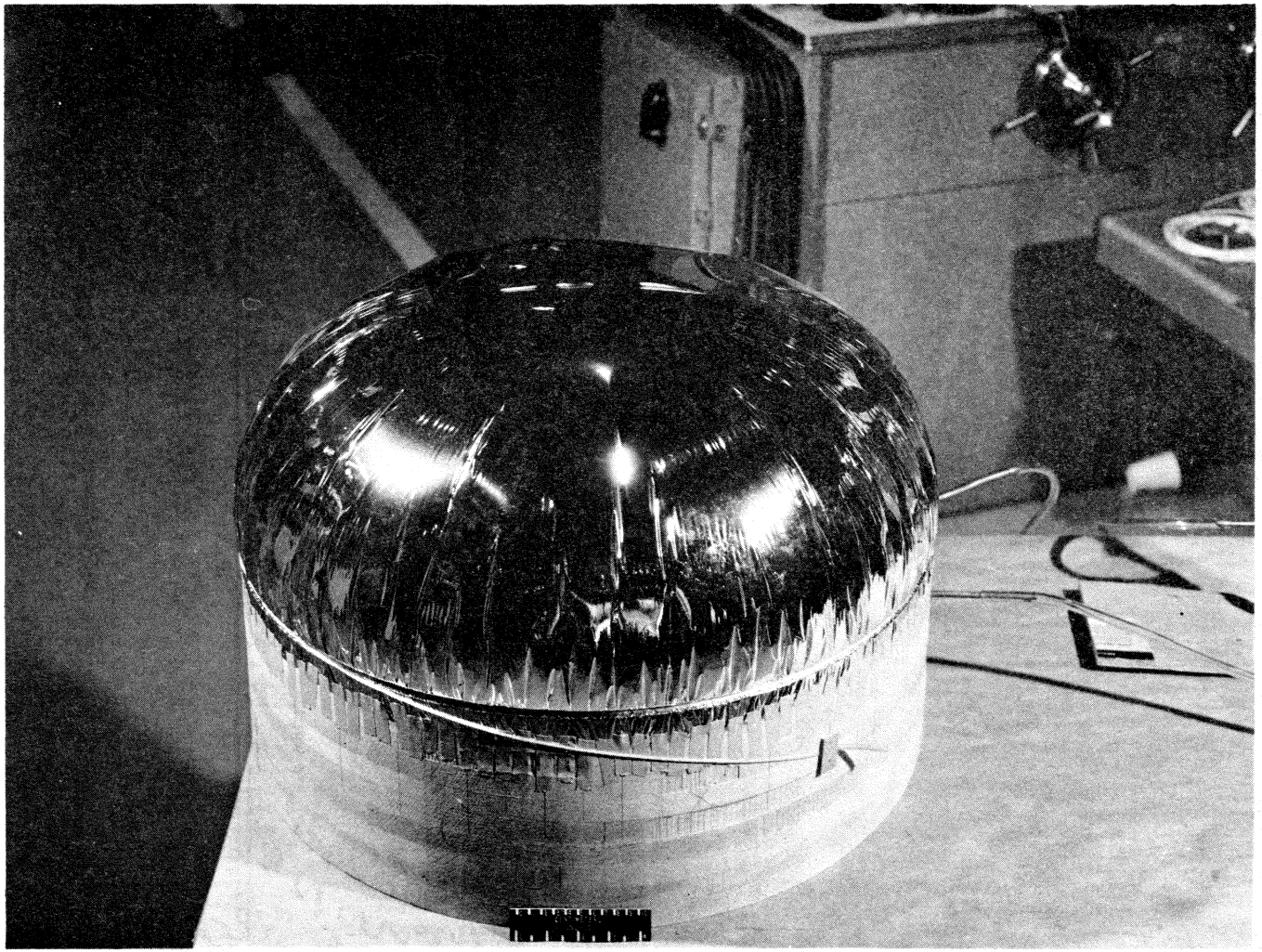

Figure 3.- An initially flat membrane which has been pleated around the outer circumference attached to a cylindrical boundary and pressurized.

should be noted that the present theory is quite different from that presented in reference 1 for flat wrinkled membranes where the strains in the wrinkled region had to be small compared with unity. In the present theory as in reference 1, however, the wrinkles are not studied in detail. Rather, the wrinkled region is considered as a smooth axisymmetric membrane shell unable to sustain hoop stresses, and equilibrium conditions are written accordingly.

Unwrinkled Region

The fundamental equations presented in the previous chapter are valid for any axisymmetric membrane shape. In this thesis, however, only two types of unwrinkled regions will be considered. One is a flat circular membrane and the other is a cylindrical membrane. For convenience, the governing equations for these two types of unwrinkled regions are now presented.

Flat circular membrane.- For a flat circular membrane, $r_\theta = \infty$, $r_\xi = \infty$, $\phi = 0$, $\xi = r$. Utilizing these quantities, equations (5), (6), (17), (18), (21), and (22) become

$$\epsilon_r = \frac{du}{dr} + \frac{1}{2}\left(\frac{dw}{dr}\right)^2 \tag{25}$$

$$\epsilon_\theta = \frac{u}{r} \tag{26}$$

$$N_r = \frac{Eh}{1 - \mu^2}(\epsilon_r + \mu\epsilon_\theta) + \frac{nE_sA_s}{2\pi r}\epsilon_r \tag{27}$$

$$N_\theta = \frac{Eh}{1 - \mu^2}(\epsilon_\theta + \mu\epsilon_r) + \eta \frac{nE_sA_s}{2\pi r} \epsilon_\theta \tag{28}$$

$$\frac{d(rN_r)}{dr} - N_\theta = 0 \tag{29}$$

$$-\frac{1}{r}\frac{d}{dr}\left(r \frac{dw}{dr} N_r\right) = p \tag{30}$$

where the rotation ψ has been eliminated using equation (7). The boundary conditions are stated as follows: on an edge r = const. specify

$$N_r = T \quad \text{or} \quad u \tag{31}$$

$$N_r \frac{dw}{dr} = p \quad \text{or} \quad w \tag{32}$$

Cylindrical membrane.- For a cylindrical membrane, $r_\xi = \infty$, $r_\theta = R$, $\phi = \frac{\pi}{2}$, and $\xi = x$. Utilizing these quantities, equations (5), (6), (17), (18), (21), and (22) become

$$\epsilon_x = \frac{du}{dx} + \frac{1}{2}\left(\frac{dw}{dx}\right)^2 \tag{33}$$

$$\epsilon_\theta = \frac{w}{R} \tag{34}$$

$$N_x = \frac{Eh}{1 - \mu^2}(\epsilon_x + \mu\epsilon_\theta) + \frac{nE_sA_s}{2\pi R} \epsilon_x \tag{35}$$

$$N_\theta = \frac{Eh}{1 - \mu^2}(\epsilon_\theta + \mu\epsilon_x) + \eta \frac{nE_sA_s}{2\pi r} \epsilon_\theta \tag{36}$$

$$\frac{dN_x}{dx} = 0 \tag{37}$$

$$\frac{N_\theta}{R} - \frac{d}{dx}\left(N_x \frac{dw}{dx}\right) = p \tag{38}$$

The boundary conditions are stated as follows: on an edge $x = \text{const.}$ specify

$$N_x = T \quad \text{or} \quad u \tag{39}$$

$$N_x \frac{dw}{dx} = P \quad \text{or} \quad w \tag{40}$$

Wrinkled Region

In the wrinkled region, linear membrane theory is used. This assumption will be discussed later in this section. The linear, axisymmetric membrane equilibrium equations are found from equations (21) and (22) by setting the rotation $\psi = 0$, and are written as

$$\frac{d(rN_\xi)}{d\xi} - \cos\phi\, N_\theta = 0 \tag{41}$$

$$\frac{N_\xi}{r_\xi} + \frac{N_\theta}{r_\theta} = p \tag{42}$$

In addition, the hoop stress resultant $N_\theta = 0$ in the wrinkled region so that equations (41) and (42) become

$$\frac{d(rN_\xi)}{d\xi} = 0 \tag{43}$$

and

$$\frac{N_\xi}{r_\xi} = p \tag{44}$$

Equation (43) can be integrated to obtain the meridional stress resultant in the wrinkled region as

$$rN_\xi = r_1 N_{\xi_1} = \text{const.} \tag{45}$$

It can be shown that equations (44) and (45) are the same equilibrium equations that would be obtained for an axisymmetric structure composed of many meridional strings which could somehow carry an internal pressure. Such a structure could not develop a boundary-layer region regardless of how it was loaded. For this reason the use of linear membrane theory in the wrinkled region is justified.

The equation for determining the shape of the wrinkled region is found from equations (44), (43), the first of equations (4), and the first of equations (2) as

$$d(rN_\xi \sin \phi) = pr\, dr \tag{46}$$

This equation can be integrated to obtain

$$rN_\xi \sin \phi - r_1 N_{\xi_1} \sin \phi_1 = \frac{p(r^2 - r_1^2)}{2} \tag{47}$$

Substituting for rN_ξ from equation (45), the sin ϕ from equation (47) is written as

$$\sin \phi = \frac{p(r^2 - r_1^2)}{2r_1 N_{\xi_1}} + \sin \phi_1 \tag{48}$$

The radial coordinate r which defines the wrinkled surface is found from equation (48) as

$$r = \left[\left(\sin \phi - \sin \phi_1 + \frac{pr_1}{2N_{\xi_1}}\right)\frac{2r_1 N_{\xi_1}}{p}\right]^{1/2} \tag{49}$$

An expression from which the axial coordinate z of the wrinkled surface can be obtained is found by eliminating $d\xi$ from equations (2) and then substituting for dr from equation (49) to yield

$$dz = \frac{1}{2}\left[\frac{\frac{2r_1 N_{\xi_1}}{p}}{\sin \phi - \sin \phi_1 + \frac{pr_1}{2N_{\xi_1}}}\right]^{1/2} \sin \phi \, d\phi \tag{50}$$

This equation is readily integrated numerically to obtain the axial coordinate z of the wrinkled surface.

Solutions to several problems will be presented in the subsequent sections using the theory developed in this section. For each of these problems a general solution is found for the stress resultants, first for the unwrinkled region, and then for the wrinkled region. The overall behavior of the structure is obtained by matching the two regions at their interface.

PRESSURIZATION OF AN INITIALLY FLAT CIRCULAR MEMBRANE INTO A DOUBLY CURVED SURFACE

A photograph of the doubly curved membrane configuration to be analyzed here is shown in figure 3. The membrane shown in that photograph was a flat circular membrane which was pleated around its periphery and attached to a rigid circular boundary. The line of attachment on the membrane was determined such that the slope of the membrane at the rigid boundary was vertical. This same configuration can be obtained by gluing two circular membranes together around their peripheries and pressurizing them. A photograph of such a configuration is shown in figure 4. In this photograph the highly stressed unwrinkled region at the crown of the membrane is readily seen. Although zero hoop stress linear membrane theory yields a very good description of the wrinkled region for this configuration, the zero hoop stress assumption is obviously violated in the vicinity of the crown. In this section, nonlinear membrane theory will be used to properly treat the unwrinkled region where stretching of the membrane surface is important, while the wrinkled region is considered to behave as a linear membrane. A free-body diagram of the configuration to be analyzed is shown in figure 5 where the unwrinkled region has been cut away from the wrinkled region.

Solution for Unwrinkled Region

The problem to be solved for the unwrinkled region is that of a flat circular membrane of radius a, loaded with lateral pressure p,

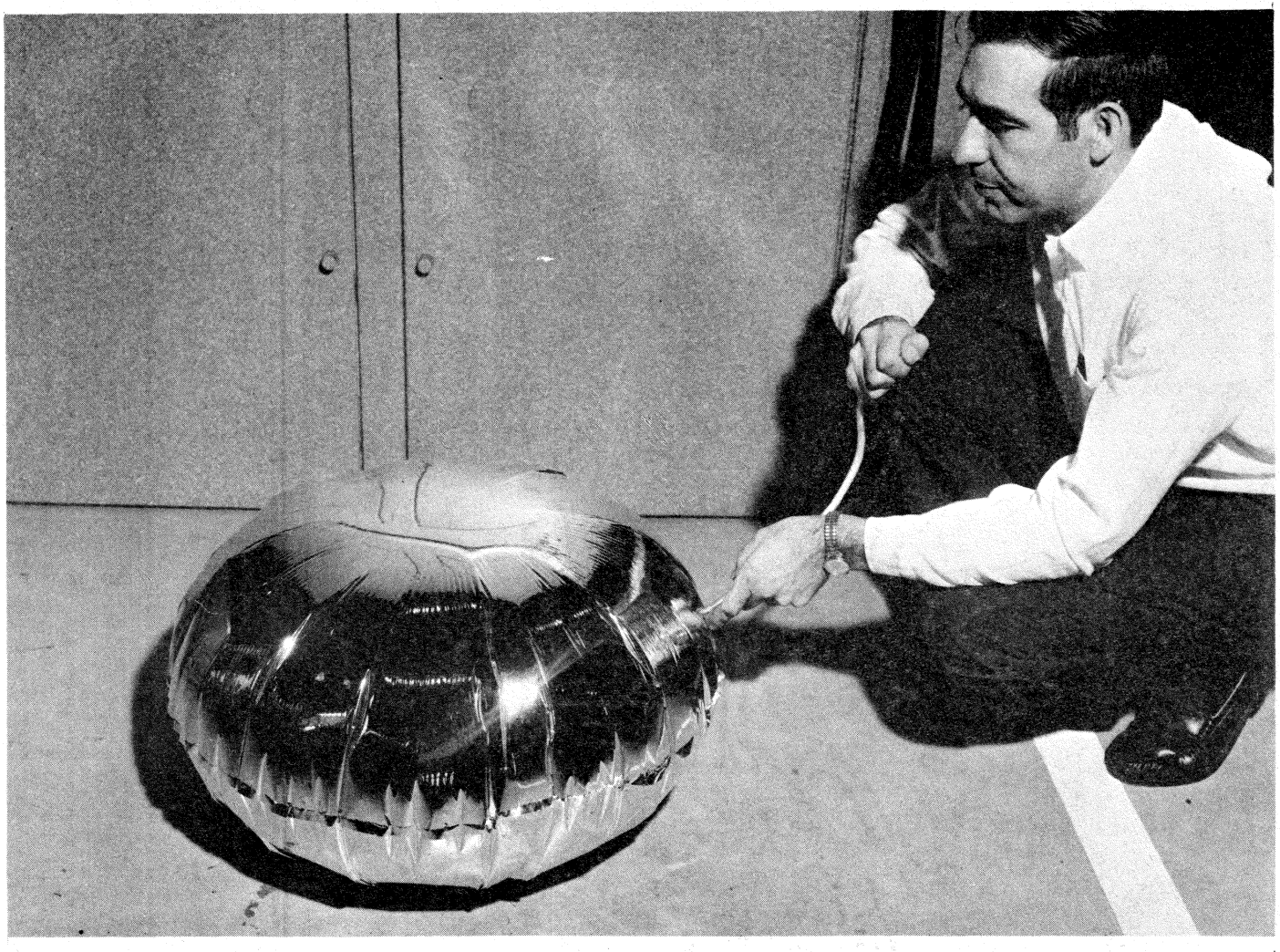

Figure 4.- Two initially flat circular membranes which have been glued together around their edges and pressurized.

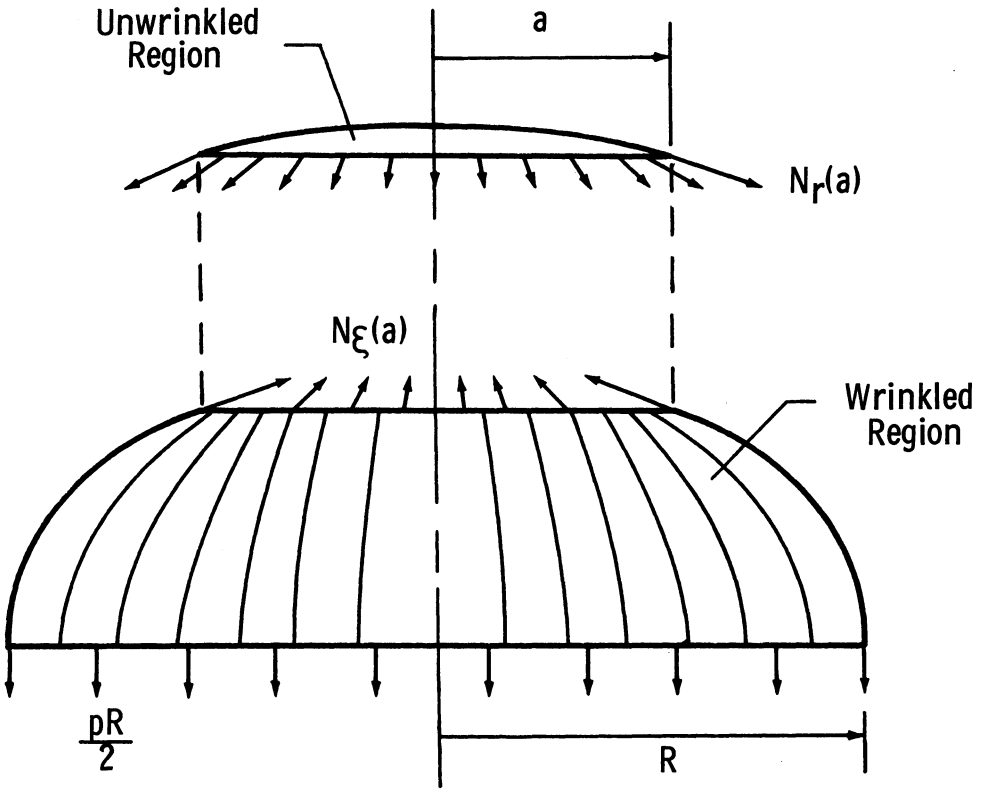

Figure 5.- Freebody diagram of wrinkled and unwrinkled regions of initially flat pressurized membrane.

and supported by a tangential edge load $N_r(a)$. In addition, the hoop stress at the edge of this membrane must drop to zero so that the transition from the unwrinkled region to the wrinkled region is continuous. The governing equation for this region is found by eliminating ϵ_θ, ϵ_r, u, w, and N_θ from equations (25) through (30) with $A_s = 0$. The resulting second-order nonlinear equation on N_r is

$$\bar{N}_r^2\left[\frac{d}{d\rho}\left(\rho^3 \frac{d\bar{N}_r}{d\rho}\right)\right] + 4\rho^3 = 0 \tag{51}$$

where N_r has been nondimensionalized as

$$\bar{N}_r = \left(\frac{32}{p^2 a^2 Eh}\right)^{1/3} N_r \tag{52}$$

and the nondimensional radius ρ is introduced as

$$\rho = \frac{r}{a} \tag{53}$$

The solution of equation (51) will be accomplished by the use of numerical techniques. An alternate power series solution is presented in appendix A as a check on the numerical solution.

Half-station central differences will be used to approximate the derivatives in equation (51). The choice of half-station instead of full-station central differences was governed by the fact that the first and second derivatives in equation (51) could be combined into one derivative. A discussion of the advantages afforded by half-station

central differences in cases such as this is given in reference 14. The first derivative approximation given by half-station central differences is

$$( )'_{i+1/2} = \frac{- ( )_i + ( )_{i+1}}{\epsilon} \tag{54}$$

where a prime denotes differentiation with respect to ρ. Applying this approximation to the derivative outside the parenthesis in equation (51) yields

$$\bar{N}^2_{r_{i+1/2}} \left[\frac{- \rho_i \bar{N}'_{r_i} + \rho_{i+1} \bar{N}'_{r_{i+1}}}{\epsilon} \right] + 4\rho^3_{i+1/2} = 0 \tag{55}$$

Applying the approximation from equation (54) to the remaining derivatives in equation (55) and combining terms yields the following difference equation for $\bar{N}_r$ at the half stations.

$$\frac{\bar{N}^2_{r_{i+1/2}}}{\epsilon^2} \left[\rho^3_i \bar{N}_{r_{i-1/2}} - (\rho^3_i + \rho^3_{i+1}) \bar{N}_{r_{i+1/2}} + \rho^3_{i+1} \bar{N}_{r_{i+3/2}} \right] + 4\rho^3_{i+1/2} = 0 \tag{56}$$

The region $\rho = 0$ to $\rho = 1$ is divided into I stations such that $\epsilon = \frac{1}{I}$. By writing equation (56) at the stations $i = 0$ through $i = I - 1$, yields I equations and the $I + 2$ unknowns $\bar{N}_{r-1/2}$ through $\bar{N}_{rI+1/2}$ which is what should be expected from the second-order

differential equation being solved. Equation (56) written at the first station $i = 0$ and $\rho_o = 0$ is

$$\frac{\bar{N}_{r\,1/2}^2}{\epsilon^2}\left[-\rho_1^3\bar{N}_{r\,1/2} + \rho_1^3\bar{N}_{r\,3/2}\right] + 4\rho_{1/2}^3 = 0 \tag{57}$$

It can be seen in equation (57) that the quantity $\bar{N}_{r-1/2} - \bar{N}_{r\,1/2}$ vanishes at the origin. This is an inherent symmetry condition on the stress $\bar{N}_r$ at the origin due to the half-station difference formulation used. This results in the elimination of the one unknown, $\bar{N}_{r-1/2}$, from these equations and leaves only one more condition, the applied inplane load $\bar{N}_r(1)$ at $\rho = 1$ to be prescribed. The boundary condition is written in numerical form as

$$\frac{\bar{N}_{rI-1/2} + \bar{N}_{rI+1/2}}{2} = \bar{N}_r(1) \tag{58}$$

The first step in solving this set of I nonlinear equations is to guess $\bar{N}_{r\,1/2}$ at the first station and solve for $\bar{N}_{r\,3/2}$ from equation (57). Using these two quantities, $\bar{N}_{r\,1/2}$ and $\bar{N}_{r\,3/2}$, the next unknown $\bar{N}_{r\,5/2}$ can be found from equation (56) written for the next station $i = 1$. This procedure is repeated until $\bar{N}_{rI+1/2}$ is found. A check is then made to see if the boundary condition given by equation (58) is satisfied. If it is not, another guess of $\bar{N}_{r\,1/2}$ is made and the procedure is repeated. A systematic method for determining subsequent guesses for $\bar{N}_{r\,1/2}$ is provided by the Newton-Raphson technique until an acceptable convergence is

found. A derivation and discussion of the Newton-Raphson technique is given by Scarborough in reference 15. The numerical solution of equation (51) just described was programed on a CDC 6600 computer. This program was used to generate the stress distribution in a flat circular membrane loaded with lateral pressure and supported by the tangential edge load $\bar{N}_r(1)$. A plot of the radial and circumferential stresses for three different values of the nondimensional edge load $\bar{N}_r(1)$ is presented in figure 6. The hoop stress N_θ in the unwrinkled region must drop to zero at the point where the unwrinkled region meets the zero hoop stress wrinkled region. The lower two curves in figure 6 represent the stress distribution for the unwrinkled region in which the circumferential stress $\bar{N}_\theta$ vanishes identically at its edge, $\frac{r}{a} = 1$. The value of the nondimensional radial edge load $\bar{N}_r(1)$ for this case is 0.9187, or in dimensional form

$$N_r(a) = 0.9187\left(\frac{p^2a^2Eh}{32}\right)^{1/3} \tag{59}$$

The corresponding maximum stresses at the center of the membrane are

$$N_r(0) = N_\theta(0) = 1.286\left(\frac{p^2a^2Eh}{32}\right)^{1/3} \tag{60}$$

A check on these numerical results is given in appendix A where a power series solution of equation (51) is presented.

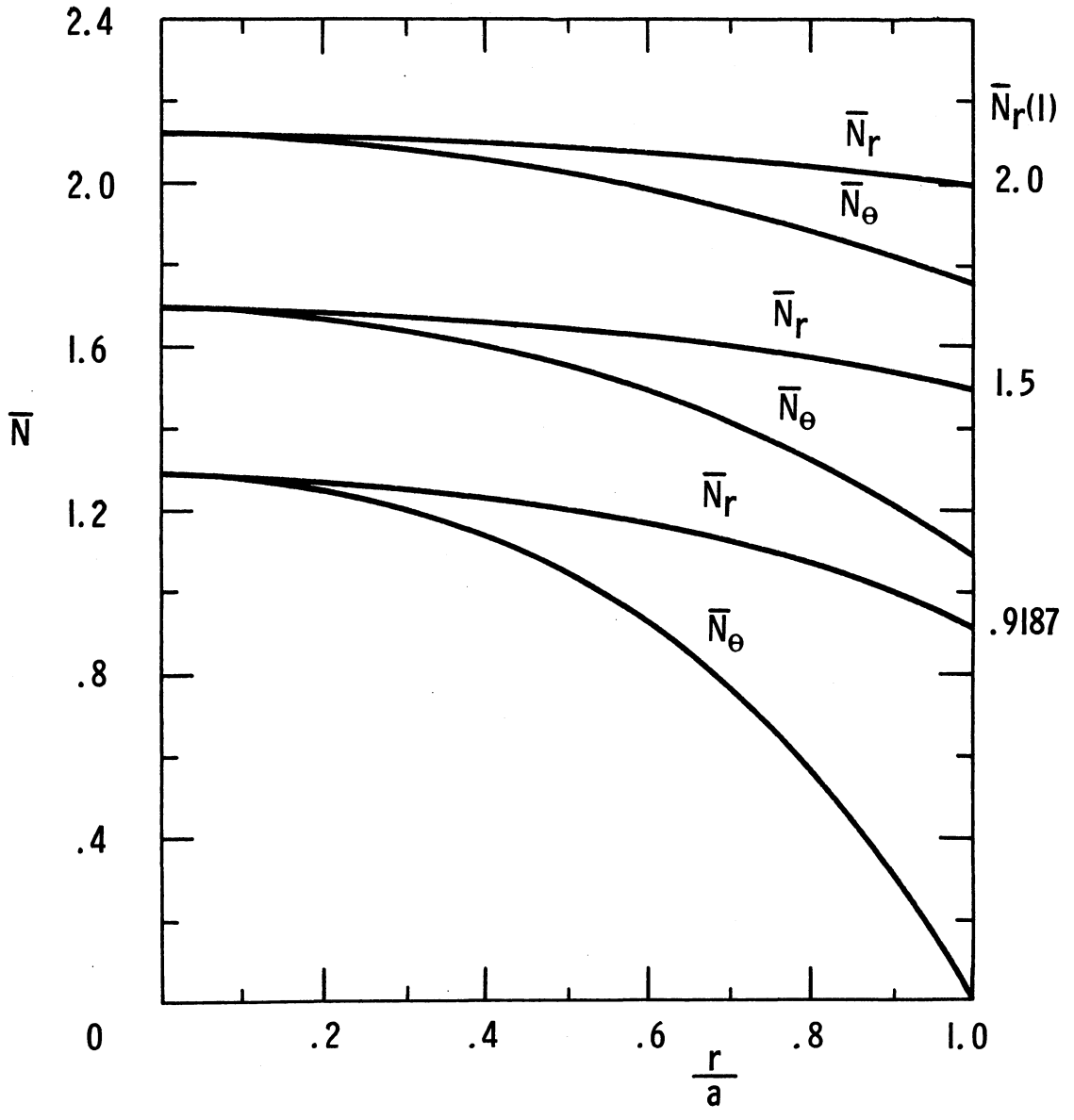

Figure 6.- Stresses in a flat membrane loaded with lateral pressure and supported by tangential edge loads.

The inplane radial displacement u can be written in terms of N_r by using equations (26), (27), (28), and (29). In nondimensional form this expression is written as

$$\frac{u}{a}\left(32\,\frac{E^2h^2}{p^2a^2}\right)^{1/3} = \rho\left[\rho\bar{N}_r' + \bar{N}_r(1 - \mu)\right] \tag{61}$$

This equation is now written in finite difference form as

$$\frac{u_i}{a}\left(32\,\frac{E^2h^2}{p^2a^2}\right)^{1/3} = \rho_i\left[\rho_i\,\frac{N_{ri+1/2} - N_{ri-1/2}}{\epsilon} + \frac{N_{ri+1/2} + N_{ri-1/2}}{2}(1 - \mu)\right] \tag{62}$$

The values of $\bar{N}_r$ found in the numerical solution of equation (56) were substituted into equation (62) at the various stations to produce the plot shown in figure 7. This nondimensional plot of u as a function of $\frac{r}{a}$ is for the unwrinkled region where the circumferential stress N_θ vanishes at the edge of the membrane and the corresponding stresses are given by the lower two curves of figure 6.

A relation between the slope $\frac{dw}{dr}$ and the radial stress resultant N_r is obtained by integration of equation (30). This relation is written in nondimensional form as

$$\frac{d\left(\frac{w}{a}\right)}{d\rho} = -\left(4\,\frac{pa}{Eh}\right)^{1/3}\frac{\rho}{\bar{N}_r} \tag{63}$$

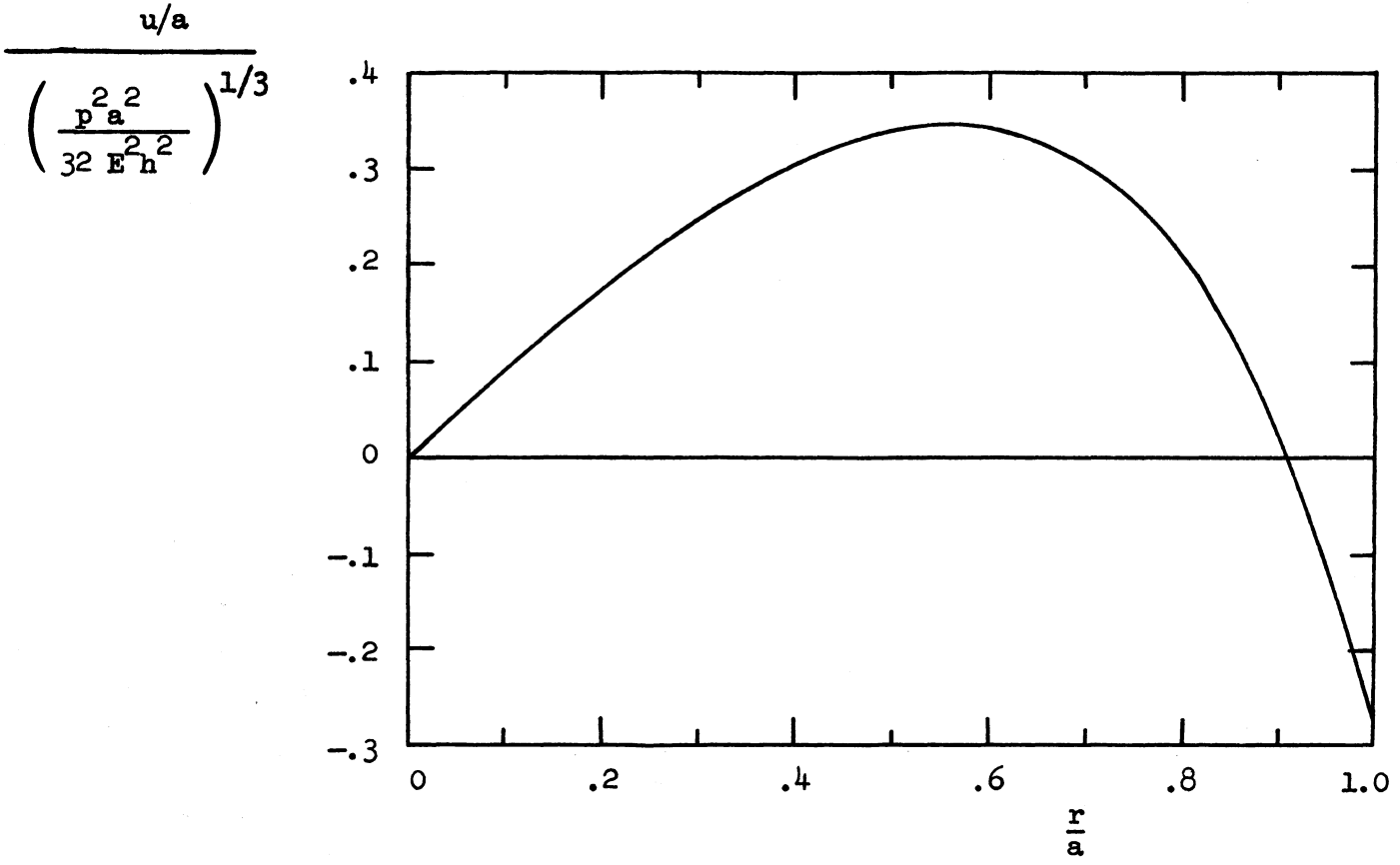

Figure 7.- Nondimensional radial displacement of unwrinkled region as a function of nondimensional radius.

The lateral displacement w can now be found by integration of this equation. The trapezoidal method was used to integrate equation (63) and is written as

$$\frac{w_i/a}{\left(4\,\frac{pa}{Eh}\right)^{1/3}} = -\epsilon \sum_{i=1}^{i} \frac{\rho_{i-1/2}}{\bar{N}_{ri-1/2}} \tag{64}$$

The constant of integration is determined by taking the lateral displacement equal to zero at the origin, $w_o = 0$. Equation (64) was programed using values for $\bar{N}_r$ found from the numerical solution of equation (56) to generate the plot shown in figure 8. In this plot the nondimensional lateral displacement for the unwrinkled region is presented as a function of $\frac{r}{a}$.

Solution for Wrinkled Region Matched With Unwrinkled Region

The general solution for the meridional stress resultant N_ξ in the wrinkled region is given by equation (45) as

$$rN_\xi = RN_\xi(R) \tag{65}$$

where the constant is evaluated at the maximum radius of the wrinkled region $r = R$. The meridional stress resultant $N_\xi(R)$ for the wrinkled region is seen from figure 4 to be

$$N_\xi(R) = \frac{pR}{2} \tag{66}$$

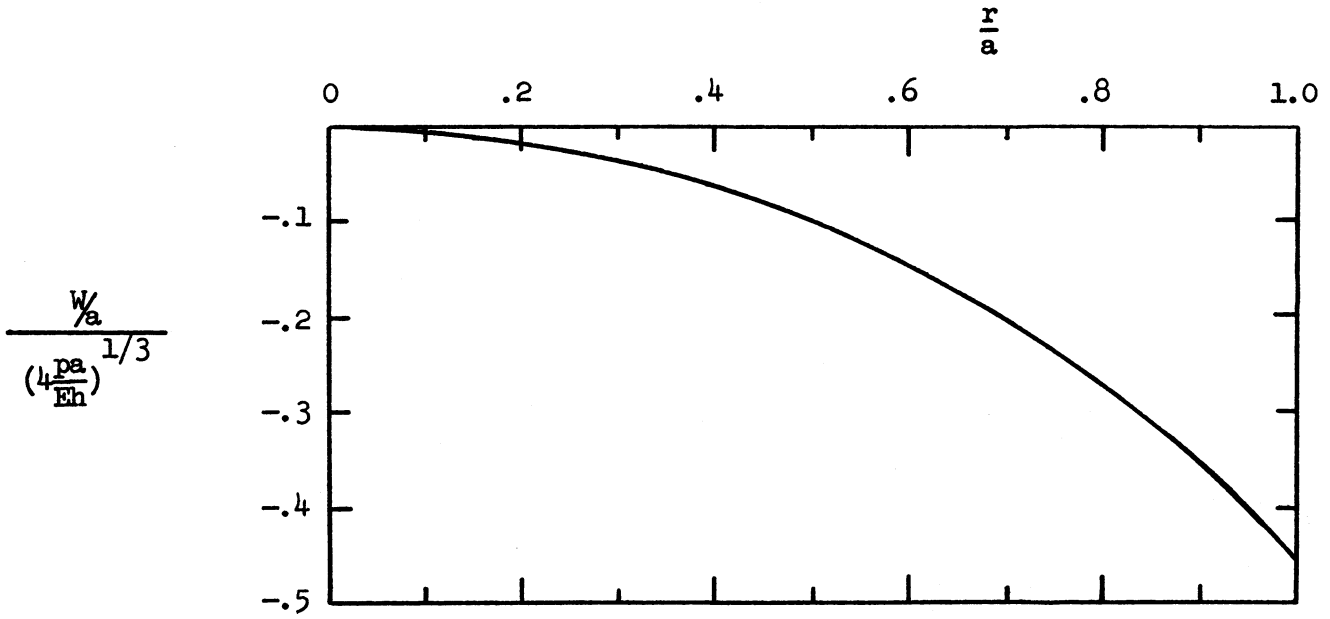

Figure 8.- Nondimensional lateral displacement of unwrinkled region as a function of nondimensional radius.

Substituting for $N_\xi(R)$ from equation (66) into equation (65) yields the solution for the meridional stress resultant in the wrinkled region as

$$N_\xi = \frac{pR^2}{2r} \tag{67}$$

To determine the extent of the unwrinkled region, a, the meridional stress resultant for the wrinkled and unwrinkled regions are equated at their interface r = a, using equations (59) and (67) to yield

$$\frac{pR^2}{2a} = 0.9187\left(\frac{p^2a^2Eh}{32}\right)^{1/3} \tag{68}$$

This equation is then solved for $\frac{a}{R}$ as

$$\frac{a}{R} = 1.388\left(\frac{pR}{Eh}\right)^{1/5} \tag{69}$$

It can be seen from equation (69) that, for a given membrane configuration, the extent of unwrinkled region $\frac{a}{R}$ grows as the one-fifth power of the pressure. This growth trend will be checked in a subsequent experimental section.

Results and Discussion

A plot of the meridional stress resultant as a function of $\frac{r}{R}$ for the entire membrane is shown in figure 9. In this figure the solid line is the linear membrane meridional stress resultant for the wrinkled region as given from equation (67). The radial stress

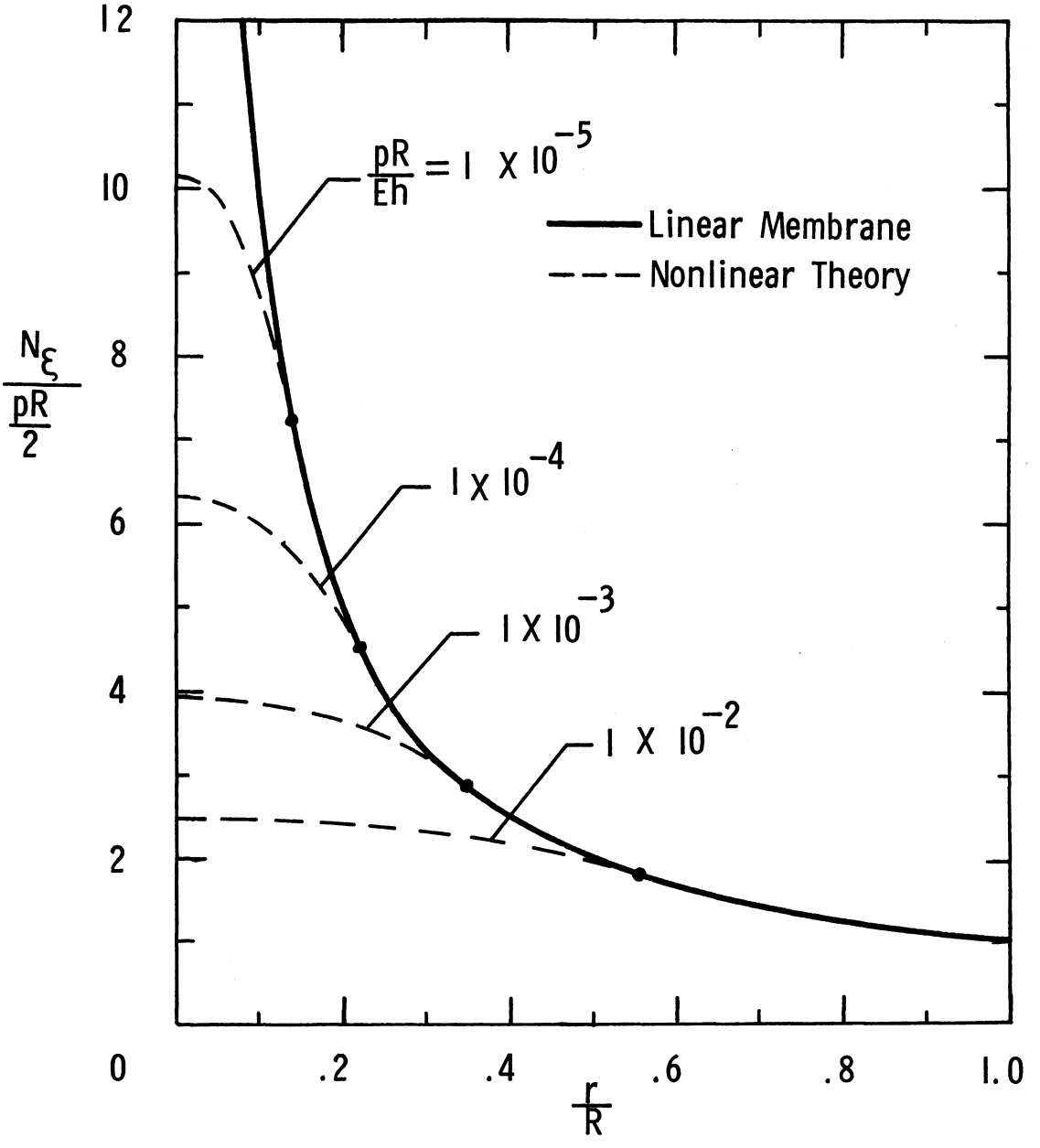

Figure 9.- Meridional stress resultant in an initially flat pressurized membrane.

resultant in the unwrinkled region as given by nonlinear theory is shown by the dashed lines for various values of the load parameter $\frac{pR}{Eh}$. The dashed lines are numerical results obtained from the computer program discussed previously. The intersection of the dashed lines with the solid line is the extent of the unwrinkled region for that particular value of the load parameter $\frac{pR}{Eh}$. The meridional stress N_ξ predicted by linear membrane theory (the solid line in fig. 9) becomes infinite at $r = 0$. This is due to the fact that linear membrane theory does not take into account stretching of the membrane surface and the radii of curvature in the vicinity of the crown remain infinite as was the case for the flat membrane from which the surface was formed. By using nonlinear membrane theory in the vicinity of the crown, however, stretching of the membrane surface is properly taken into account and realistic values of stresses in that region are obtained, as shown by the dashed lines.

In many inflatable structures, meridional and circumferential stiffening cords are added to the basic material to help carry loads in a more efficient fashion. In order to demonstrate the application of nonlinear membrane theory to such structures, meridional and circumferential stiffening cords are added to the problem solved in the present section and solutions to the unwrinkled region for sample cases of stiffening are presented in appendix B.

FLAT MEMBRANE STRETCHED OVER A RIGID DOUBLY CURVED MANDREL

General Mandrel Shape

In this problem an initially flat circular membrane is draped over a rigid axisymmetric mandrel and loaded with a load per unit length T at a radius R as shown in figure 10. The rigid mandrel shape is defined by the curve $W_m(r)$ which is rotated about the z-axis.

Since the doubly curved mandrel is not a developable surface, the only way an initially flat, unloaded membrane can conform to this surface is for the meridional wrinkles to develop over the entire membrane. However, as the load T is applied, an unwrinkled region of radius a develops at the crown of the membrane. As in the previous problem of a pressurized flat membrane, the main quantities to be determined are the extent of the unwrinkled region and the resulting stress distribution. In addition, for this problem which is a contact problem, the variable contact pressure $p(r)$ between the membrane and the mandrel is to be determined.

Unwrinkled region.- As in the previous problem, the unwrinkled region and the wrinkled region of the membrane will be analyzed separately, then matched together by equating the meridional stresses of the two regions at the wrinkled and unwrinkled interface $r = a$. The equations for the unwrinkled region are found by eliminating the strains from equations (25), (26), (27), (28), (29), and (30) with $A_s = 0$ and are written as

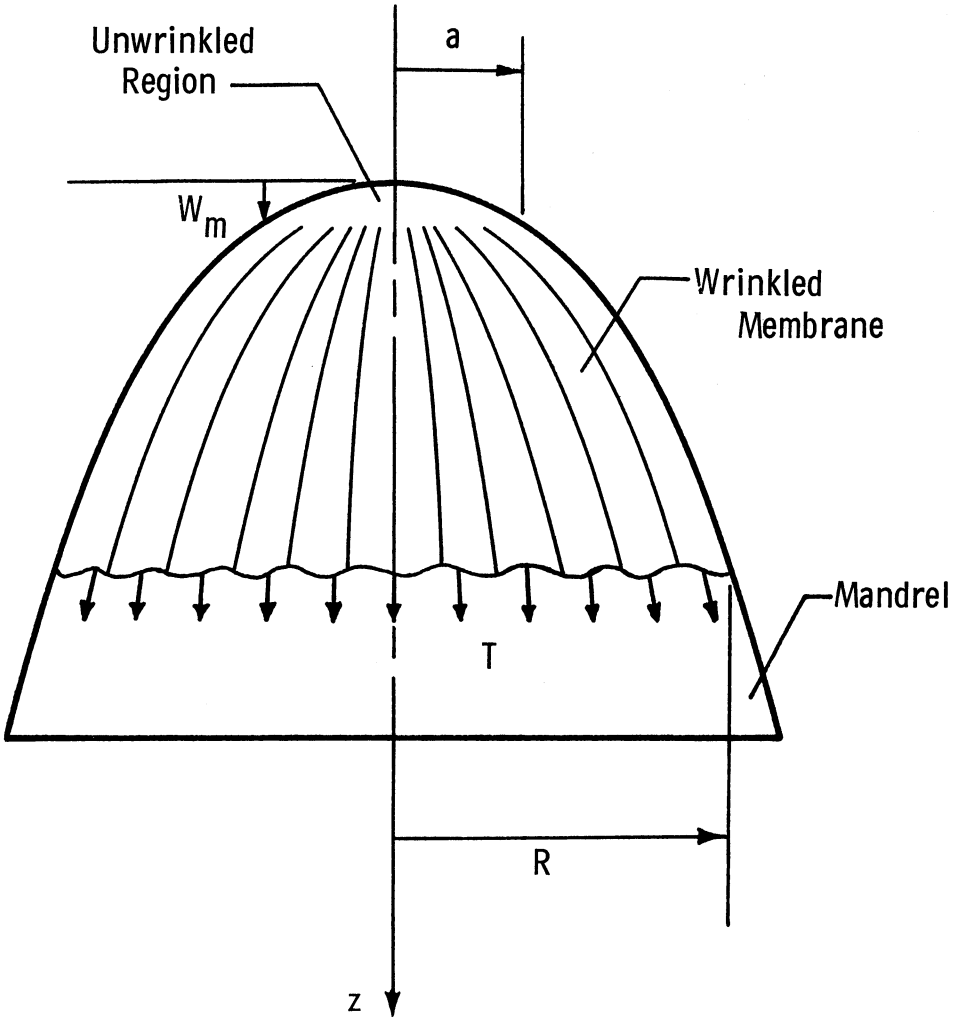

Figure 10.- Flat membrane stretched over a rigid mandrel.

$$\frac{1}{Eh}(N_r - \mu N_\theta) = \frac{du}{dr} + \frac{1}{2}\left(\frac{dW_m}{dr}\right)^2 \tag{70}$$

$$\frac{1}{Eh}(N_\theta - \mu N_r) = \frac{u}{r} \tag{71}$$

$$\frac{d(rN_r)}{dr} - N_\theta = 0 \tag{72}$$

$$\frac{1}{r}\frac{d}{dr}\left(r\frac{dW_m}{dr}N_r\right) = p \tag{73}$$

In these equations the lateral displacement w has been taken as $-W_m$ since the membrane must conform to the mandrel surface. Since W_m is not an unknown, this uncouples equation (73) from equations (70), (71), and (72), which are three equations for the three unknowns N_r, N_θ, and u. By eliminating N_θ and u from these equations, the following governing equation on N_r is obtained:

$$\frac{d}{dr}\left(r^3\frac{dN_r}{dr}\right) = -\frac{Eh}{2}r\left(\frac{dW_m}{dr}\right)^2 \tag{74}$$

For a given mandrel, which is defined by W_m, this equation is readily integrated twice to obtain N_r. After N_r is obtained for a given mandrel, N_θ is found from equation (72) and the contact pressure p is found from equation (73).

Wrinkled region.- The general solution for the meridional stress N_ξ in the wrinkled region is found by equating the total meridional load at r to the total meridional load at $r = R$. This can be done

since the mandrel is assumed to be friction free and the hoop stress N_θ in the wrinkled region is zero. This results in

$$2\pi r N_\xi = 2\pi R N_\xi(R) \tag{75}$$

The meridional stress at R, $N_\xi(R)$, is taken as T so that equation (75) is written as

$$N_\xi = \frac{R}{r} T \tag{76}$$

which is the general solution for the wrinkled region.

Special Cases

These equations for the unwrinkled and wrinkled regions will now be used to solve for the extent of the unwrinkled region, the membrane stresses, and the contact pressure of several different mandrel shapes.

Parabolic mandrel.- The mandrel shape for this case will be defined by the equation

$$\frac{W_m}{R} = \alpha\left(\frac{r}{R}\right)^2 \tag{77}$$

Substituting for W_m from equation (77) into equation (75) and integrating one time yields

$$\frac{dN_r}{dr} = -\frac{Eh\alpha^2}{2R^2} r + \frac{C_1}{r^3} \tag{78}$$

Since the stress N_r at $r = 0$ must be finite, $C_1 = 0$. Integrating equation (78) yields

$$N_r = - \frac{Eh\alpha^2}{4}\left(\frac{r}{R}\right)^2 + C_2 \tag{79}$$

By equating $N_r(a)$ from equation (79) to $N_\xi(a)$ from equation (76), the unwrinkled and wrinkled regions are matched yielding

$$N_r = \frac{Eh\alpha^2}{4}\left[\left(\frac{a}{R}\right)^2 - \left(\frac{r}{R}\right)^2\right] + \frac{R}{a}T \tag{80}$$

The hoop stress in the unwrinkled region is found by substituting for N_r from equation (80) into equation (72) as

$$N_\theta = \frac{Eh\alpha^2}{4}\left[\left(\frac{a}{R}\right)^2 - 3\left(\frac{r}{R}\right)^2\right] + \frac{R}{a}T \tag{81}$$

The extent of the unwrinkled region $\frac{a}{R}$ is now found by setting the hoop stress N_θ equal to zero at $r = a$. This yields

$$\frac{a}{R} = \left(\frac{2T}{Eh\alpha^2}\right)^{1/3} \tag{82}$$

The pressure p between the mandrel and the membrane in the unwrinkled region is found by substituting N_r from equation (80) into equation (73). This yields

$$pR = Eh\alpha^3\left[\left(\frac{a}{R}\right)^2 - 2\left(\frac{r}{R}\right)^2\right] + \frac{4\alpha T}{a} \tag{83}$$

The pressure between the mandrel and the membrane in the wrinkled region is found from equation (44) as

$$p = \frac{N_\xi}{r_\xi} \tag{84}$$

where r_ξ is the local radius of curvature of the mandrel and is given as

$$r_\xi = \frac{(1 + W_m'^2)^{3/2}}{W_m''} \tag{85}$$

Equations (84), (85), and (77) yield the pressure for the wrinkled region for the parabolic surface as

$$pR = \frac{2\alpha T}{\left[1 + 4\alpha^2\left(\frac{r}{R}\right)^2\right]^{3/2}\left(\frac{r}{R}\right)} \tag{86}$$

In the subsequent sections, the results will be given for several different mandrel shapes. The procedure used in obtaining these results was the same as that used in this section for the parabolic mandrel and will not be repeated.

Cubic mandrel.- The mandrel shape for this case will be defined by the curve

$$\frac{W_m}{R} = \gamma\left(\frac{r}{R}\right)^3 \tag{87}$$

Unwrinkled Region

$$N_r = \frac{3Eh\gamma^2}{16}\left[\left(\frac{a}{R}\right)^4 - \left(\frac{r}{R}\right)^4\right] + \frac{R}{a}T \tag{88}$$

$$N_\theta = \frac{3Eh\gamma^2}{16}\left[\left(\frac{a}{R}\right)^4 - 5\left(\frac{r}{R}\right)^4\right] + \frac{R}{a}T \tag{89}$$

$$\frac{a}{R} = \left(\frac{4T}{3Eh\gamma^2}\right)^{1/5} \tag{90}$$

$$pR = \left\{\frac{9Eh\gamma^3}{16}\left[3\left(\frac{a}{R}\right)^4 - 7\left(\frac{r}{R}\right)^4\right] + 9\gamma\,\frac{R}{a}T\right\}\frac{r}{R} \tag{91}$$

Wrinkled Region

$$N_\xi = \frac{R}{r}T \tag{92}$$

$$pR = \frac{6\gamma T}{\left[1 + 9\gamma^2\left(\frac{r}{R}\right)^4\right]^{3/2}} \tag{93}$$

Quartic mandrel.- The mandrel shape for this case will be defined by the equation

$$\frac{W_m}{R} = \Delta\left(\frac{r}{R}\right)^4 \tag{94}$$

Unwrinkled Region

$$N_r = \frac{Eh\Delta^2}{12}\left[\left(\frac{a}{R}\right)^6 - \left(\frac{r}{R}\right)^6\right] + \frac{R}{a}T \tag{95}$$

$$N_\theta = \frac{Eh\Delta^2}{12}\left[\left(\frac{a}{R}\right)^6 - 7\left(\frac{r}{R}\right)^6\right] + \frac{R}{a}T \tag{96}$$

$$\frac{a}{R} = \left(\frac{2T}{Eh\Delta^2}\right)^{1/7} \tag{97}$$

$$pR = \left[\frac{Eh\Delta^3}{3}\left\{4\left(\frac{a}{R}\right)^6 - 10\left(\frac{r}{R}\right)^6\right\} + 16\Delta\frac{R}{a}T\right]\left(\frac{r}{R}\right)^2 \tag{98}$$

Wrinkled Region

$$N_\xi = \frac{R}{r}T \tag{99}$$

$$pR = \frac{12\Delta T\left(\frac{r}{R}\right)}{\left[1 + 16\Delta^2\left(\frac{r}{R}\right)^6\right]^{3/2}} \tag{100}$$

Spherical mandrel.- For a spherical mandrel of radius R, a relation between the meridional coordinate ϕ and the radial coordinate r can be written as

$$\sin\phi = \frac{r}{R} \tag{101}$$

In the unwrinkled region, the nonlinear membrane theory used is only valid for small rotations so that

$$\sin \phi \approx \frac{dW_m}{dr} \tag{102}$$

Elimination of $\sin \phi$ from equations (101) and (102) yields

$$\frac{dW_m}{dr} = \frac{r}{R} \tag{103}$$

This equation can be integrated to yield

$$\frac{W_m}{R} = \frac{1}{2}\left(\frac{r}{R}\right)^2 \tag{104}$$

where the constant of integration has been set equal to zero to be consistent with the coordinate system for the mandrel shown in figure 10. The parabolic representation of a spherical surface, as given by equation (104), is a representation which is consistent with the nonlinear theory being used in the unwrinkled region. The solution for the unwrinkled region of the sphere is the same as that given for the parabolic mandrel with $\alpha = \frac{1}{2}$; therefore, the equations for that region will not be repeated. This same solution for a membrane in contact with a spherical surface was found in reference 16.

In the wrinkled region the meridional stress resultant is again given by equation (76) as

$$N_\xi = \frac{R}{r} T \tag{105}$$

The pressure between the mandrel and the membrane in the wrinkled region is found from equation (84) where N_ξ is eliminated using equation (105) and $r_\xi = R$. This pressure is written as

$$pR = \frac{T}{\frac{r}{R}} \tag{106}$$

Results and Discussion

In the previous sections, closed-form solutions are presented for the stress distributions in a membrane stretched over a parabolic mandrel, a cubic mandrel, a quartic mandrel, and a spherical mandrel. In the first three cases the solutions are given for a family of mandrel shapes represented by the constants α for the parabolic mandrel, γ for the cubic mandrel, and Δ for the quartic mandrel. For comparison purposes a particular value of these constants will now be chosen. In figure 11 a plot of these mandrel shapes is shown for the specific value of the constants, $\alpha = \gamma = \Delta = \frac{1}{2}$. In figure 12 the stress distribution for these particular shapes is presented along with the stress distribution for the pressurized membrane solved in the previous section. It should also be noted that the stress distribution for the particular parabolic mandrel chosen corresponds identically to the stress distribution for the spherical mandrel because of the choice of the constant $\alpha = \frac{1}{2}$. All of the stress distributions are shown for one value of the loading parameter $\frac{T}{Eh} = 0.001$. For the pressurized membrane, T was taken as $\frac{pR}{2}$. It can be seen in figure 12 that a membrane stretched over a parabolic

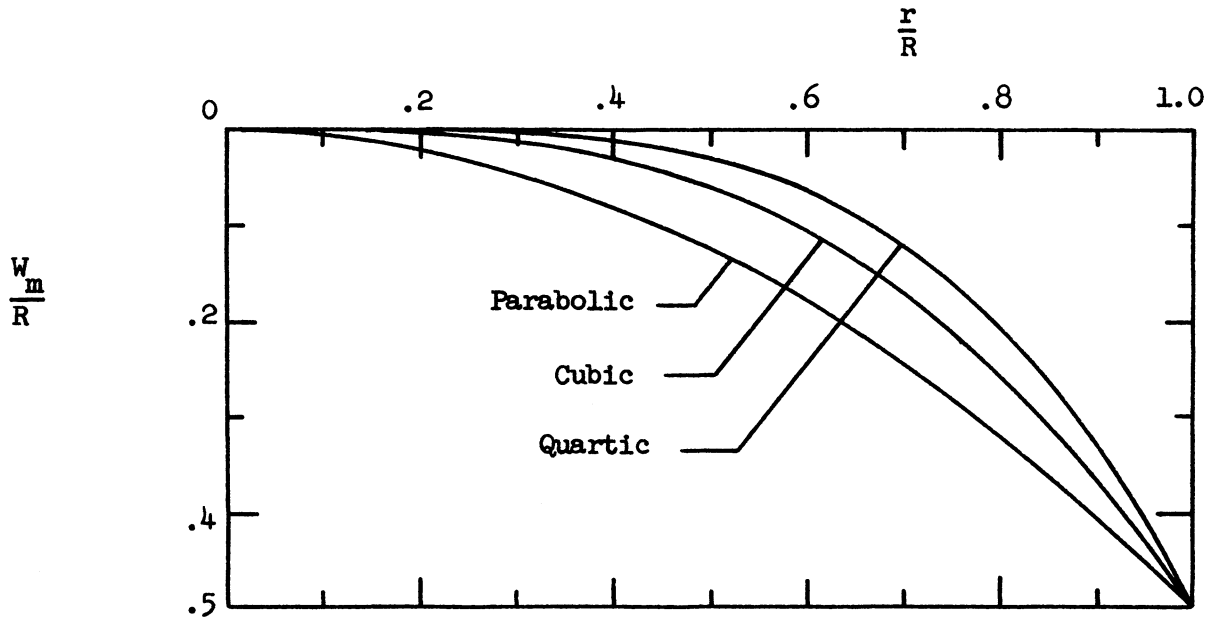

Figure 11.- Nondimensional mandrel profiles used to obtain the stress distributions shown in figure 12.

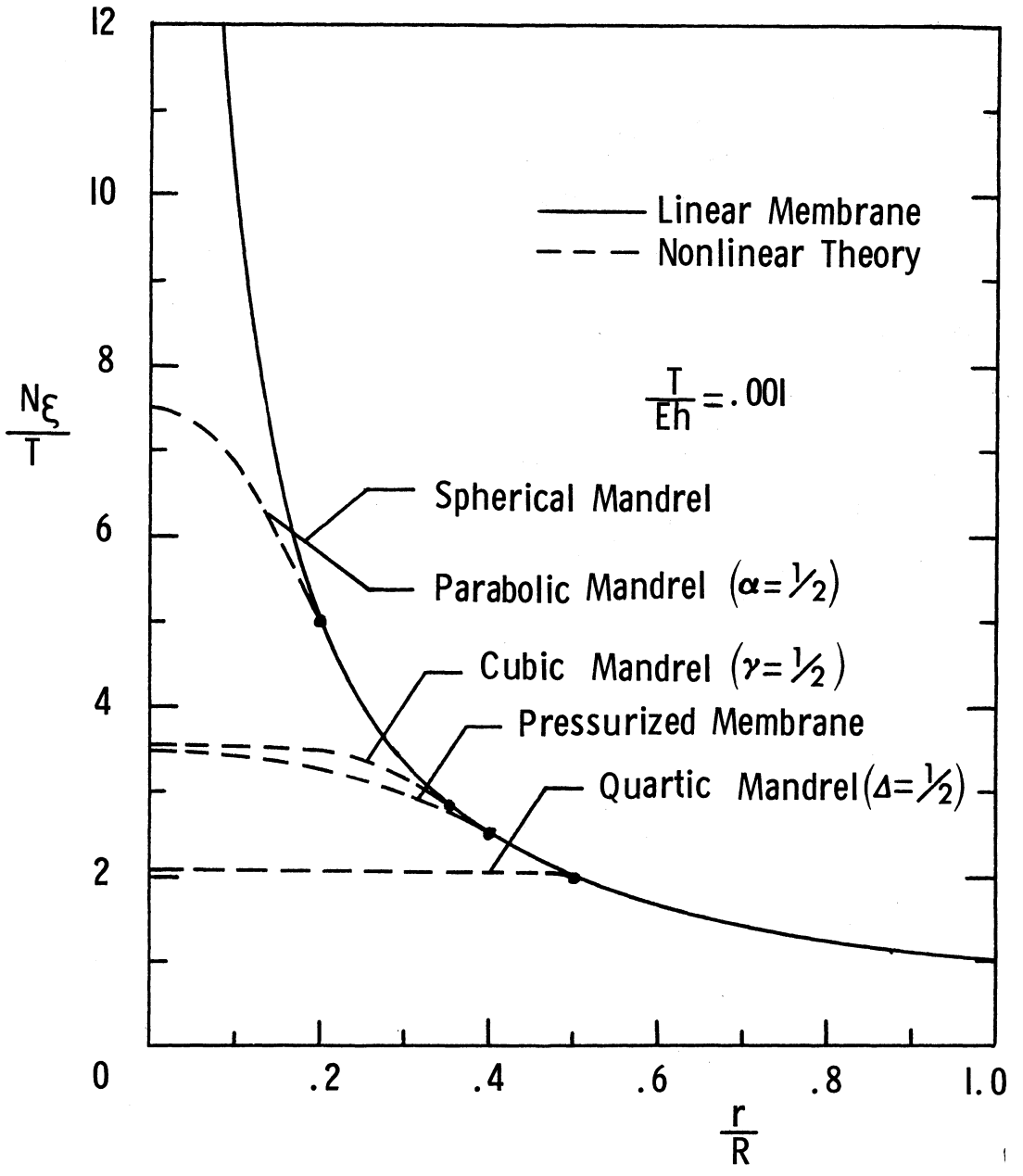

Figure 12.- Meridional stress distribution for the various mandrel shapes compared with results for pressurized membrane.

mandrel suffers higher stresses than the other cases considered. This is due to higher curvature of the parabolic mandrel in the vicinity of the crown. The relative characteristics of the various mandrel shapes can be seen in figure 11. In figure 12 the stress resultant at the center of the membrane for the parabolic mandrel is seen to be about 7-1/2 times the value at the edge $\frac{r}{R} = 1$. In fact, this characteristic of a higher stress at the center of the membrane, than at the edge, is true for all the cases shown. This feature could be utilized in the design of a biaxial testing fixture for membranes for which premature failures would not occur around the edges where the load is applied. A region of essentially constant stress in the center of the test specimen, as can be seen in figure 12, could be obtained by using a quartic mandrel. By using combinations of the mandrels presented here, or even higher degree mandrels, a biaxial testing fixture could be designed to produce almost any desired stress distribution.

RADIAL LINE LOAD ON AN INFINITELY LONG PRESSURIZED MEMBRANE CYLINDER

A schematic of the pressurized membrane cylinder to be analyzed in this section is shown in figure 13(a). This infinitely long membrane cylinder of undeformed radius R has an internal pressure p, is loaded with an axial load T, and is subjected to a radial line load 2P. Such a pressurized membrane cylinder can carry a certain amount of applied radial line load before wrinkling occurs. A solution to this prewrinkled loading range is presented first. As the value of the applied radial line load is increased, however, the hoop stress at the line of application of the radial line load will eventually drop to zero. For larger values of the applied radial load, a wrinkled region will develop and solutions must be obtained for both the wrinkled and unwrinkled regions, then matched together as in the previous problems. A freebody diagram of a membrane cylinder which has been deformed into the wrinkled range is shown in figure 13(b).

Prewrinkled Solution

The governing equations for an unwrinkled membrane are given by equations (33), (34), (35), (36), (37), and (38). Equation (37) is integrated to obtain

$$N_x = \text{const.} = T \tag{107}$$

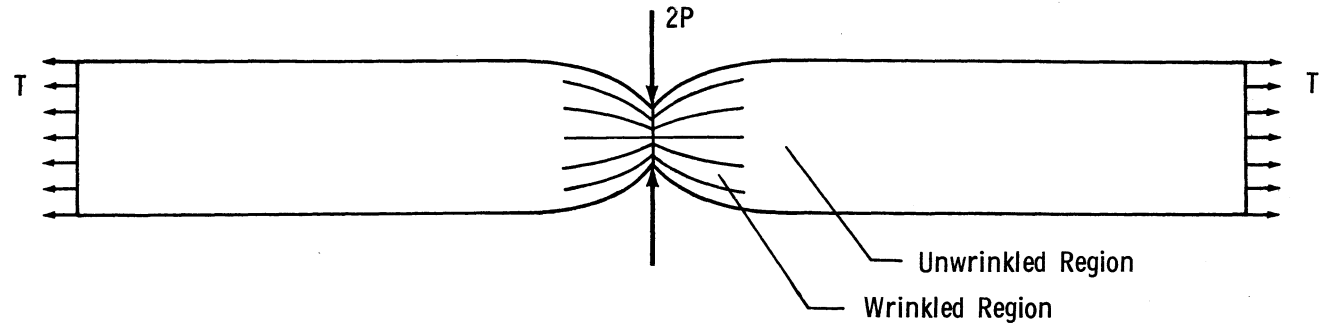

Figure 13(a).- Infinitely long pressurized membrane cylinder with radial line load.

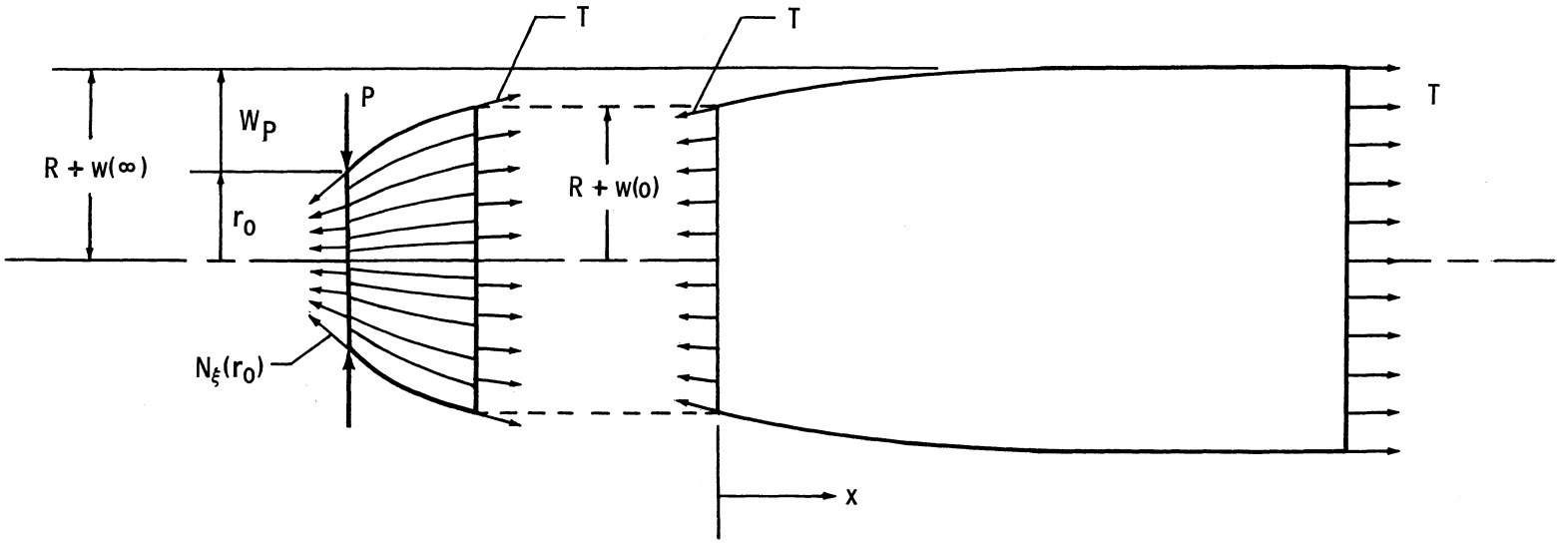

Figure 13(b).- Freebody diagram of wrinkled and unwrinkled regions.

Substituting this into equation (38) yields

$$\frac{N_\theta}{R} - T\frac{d^2w}{dx^2} = p \tag{108}$$

Eliminating ϵ_θ from equations (35) and (36) with $A_s = 0$, and substituting for N_x from equation (107) and for ϵ_θ from equation (34) yields

$$N_\theta = \frac{Eh}{R}w + \mu T \tag{109}$$

This expression for N_θ is now substituted into equation (108) to obtain the governing equation on w as

$$\frac{d^2w}{dx^2} - \frac{Eh}{TR^2}w - \frac{\mu}{R} + \frac{p}{T} = 0 \tag{110}$$

The general solution to this equation is

$$w = Ae^{\sqrt{\frac{Eh}{T}}\frac{x}{R}} + Be^{-\sqrt{\frac{Eh}{T}}\frac{x}{R}} - \mu\frac{TR}{Eh} + \frac{pR^2}{Eh} \tag{111}$$

By applying the condition that the slope is zero at $x = \infty$, $\left(\left.\frac{dw}{dx}\right|_{x=\infty} = 0\right)$, equation (111) is written as

$$w = Be^{-\sqrt{\frac{Eh}{T}}\frac{x}{R}} - \mu\frac{TR}{Eh} + \frac{pR^2}{Eh} \tag{112}$$

The slope is found from equation (112) as

$$\frac{dw}{dx} = - B\sqrt{\frac{Eh}{TR^2}}\, e^{-\sqrt{\frac{Eh}{T}}\frac{x}{R}} \tag{113}$$

The condition to be applied at $x = 0$ is that the radial component of the inplane stress resultant equal the applied radial line load. This condition is expressed as

$$T \left.\frac{dw}{dx}\right|_{x=0} = P \tag{114}$$

Applying this condition to equation (113) yields

$$B = - \frac{P}{T}\sqrt{\frac{T}{Eh}}\, R \tag{115}$$

Substituting for B into equation (112) gives the expression for w in the prewinkled loading range as

$$\frac{w}{R} = - \frac{P}{T}\sqrt{\frac{T}{Eh}}\, e^{-\sqrt{\frac{Eh}{T}}\frac{x}{R}} + \frac{pR}{Eh} - \mu\frac{T}{Eh} \tag{116}$$

The slope is found from equation (113) as

$$\frac{dw}{dx} = \frac{P}{T}\, e^{-\sqrt{\frac{Eh}{T}}\frac{x}{R}} \tag{117}$$

The hoop stress N_θ is found by substituting for w from equation (116) into equation (109). This yields

$$N_\theta = pR - P\sqrt{\frac{Eh}{T}}\, e^{-\sqrt{\frac{Eh}{T}}\frac{x}{R}} \tag{118}$$

Post-Wrinkled Solution

Unwrinkled region.- The value of radial line load for which wrinkling begins is found by setting $N_\theta = 0$ at $x = 0$ in equation (118). This yields

$$P = pR\sqrt{\frac{T}{Eh}} \tag{119}$$

The expressions for w, $\frac{dw}{dx}$, and N_θ, in the unwrinkled region are found by substituting for P from equation (119) into equations (116), (117), and (118). This yields

$$\frac{w}{R} = -\mu\frac{T}{Eh} + \frac{pR}{Eh}\left(1 - e^{-\sqrt{\frac{Eh}{T}}\frac{x}{R}}\right) \tag{120}$$

$$\frac{dw}{dx} = \frac{pR}{T}\sqrt{\frac{T}{Eh}}\, e^{-\sqrt{\frac{Eh}{T}}\frac{x}{R}} \tag{121}$$

$$N_\theta = pR\left(1 - e^{-\sqrt{\frac{Eh}{T}}\frac{x}{R}}\right) \tag{122}$$

Wrinkled region.- From equation (45), the meridional stress in the wrinkled region is found as

$$N_\xi = \frac{\text{const.}}{r} \tag{123}$$

The const. is evaluated at $r = R + w(0)$ and yields

$$N_\xi = \frac{T\left[R + w(0)\right]}{r} \tag{124}$$

At the line of application of the radial line load P, the meridional stress resultant is found from equation (124) to be

$$N_\xi(r_o) = \frac{T\left[R + w(0)\right]}{r_o} \tag{125}$$

Summation of forces in the radial direction at $r = r_o$ yields

$$2\pi r_o P = 2\pi r_o N_\xi(r_o)\cos \phi_o \tag{126}$$

or

$$\cos \phi_o = \frac{P}{N_\xi(r_o)} \tag{127}$$

Substituting for $N_\xi(r_o)$ from equation (125) into equation (127) yields

$$\cos \phi_o = \frac{Pr_o}{T\left[R + w(0)\right]} \tag{128}$$

From equation (48) the expression for the $\sin \phi$ in the wrinkled region is found as

$$\sin \phi = \sin \phi_o + \frac{p(r^2 - r_o^2)}{2r_o N_\xi(r_o)} \tag{129}$$

Substituting for $N_\xi(r_o)$ from equation (125) and for $\sin \phi_o$ from equation (128) into equation (129) yields

$$\sin \phi = \sqrt{1 - \frac{P^2 r_o^2}{T^2\left[R + w(0)\right]^2}} + \frac{p(r^2 - r_o^2)}{2T\left[R + w(0)\right]} \tag{130}$$

In order to match the wrinkled and unwrinkled regions to determine the unknown r_o, the slopes of the two regions are matched at their interface. The relation between the slope in the unwrinkled region, $\frac{dw}{dx}$, and the angle in the wrinkled region, ϕ, is

$$\sin \phi = \frac{1}{\sqrt{1 + \left(\frac{dw}{dx}\right)^2}} \approx 1 - \frac{1}{2}\left(\frac{dw}{dx}\right)^2 \tag{131}$$

By evaluating $\frac{dw}{dx}$ and w at $x = 0$ in equations (121) and (120), and $\sin \phi$ at $r = R + w(0)$ in equation (130), then substituting into equation (131) yields the following relation between the radial line load P and the deformed radius r_o.

$$\left(\frac{2P}{T}\right)^2 \frac{\left(\frac{r_o}{R}\right)^2}{\left[1 - \mu \frac{T}{pR} \frac{pR}{Eh}\right]^2} = 4 \frac{pR}{Eh} \frac{pR}{T} + \left[1 - \frac{1}{2} \frac{pR}{Eh} \frac{pR}{T}\right] \frac{\left(1 - \mu \frac{T}{pR} \frac{pR}{Eh}\right)^2 - \left(\frac{r_o}{R}\right)^2}{\frac{T}{pR}\left(1 - \mu \frac{T}{pR} \frac{pR}{Eh}\right)}$$

$$- \frac{\left[\left(1 - \mu \frac{T}{pR} \frac{pR}{Eh}\right)^2 - \left(\frac{r_o}{R}\right)^2\right]^2}{\left(\frac{T}{pR}\right)^2 \left(1 - \mu \frac{T}{pR} \frac{pR}{Eh}\right)^2} \tag{132}$$

Results and Discussion

The behavior of a pressurized membrane cylinder under the application of a radial line load will now be investigated by plotting the radial line load as a function of the deflection at the line of application of the line load as shown in figure 14. In this figure the radial line load P has been normalized with respect to the value of the line load at initial wrinkling P_{wr}. The deflection W_p, which is defined in figure 13(b), is the deflection away from the pressurized state and has been nondimensionalized with respect to the pressurized radius of the cylinder R_p. An expression for this radius is written as

$$R_p = R + w(\infty) = R\left(1 + \frac{pR}{Eh} - \mu \frac{T}{Eh}\right) \tag{133}$$

The linear behavior in the prewrinkled range is found from equation (116), while the behavior after wrinkling is found from equation (132).

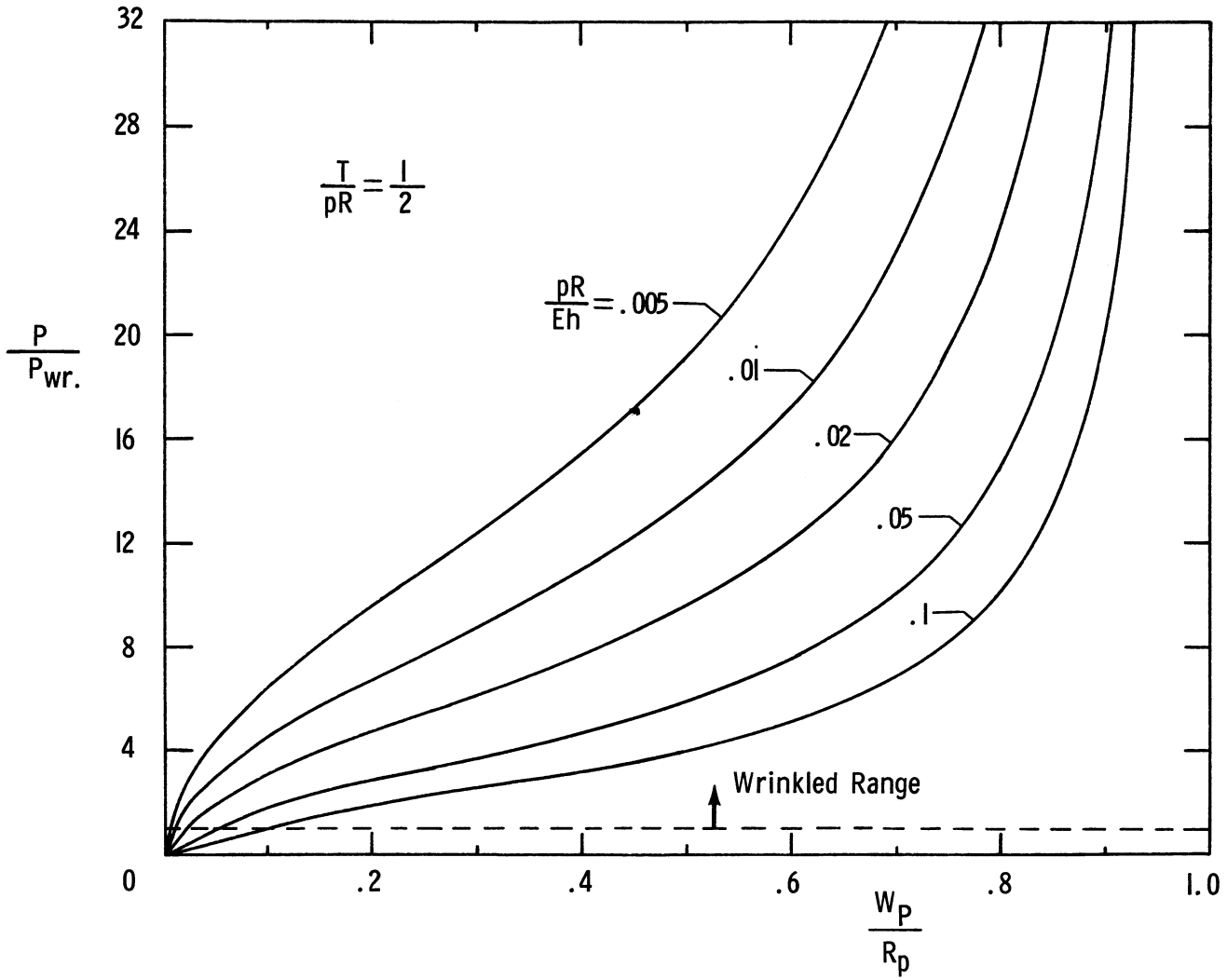

Figure 14.- Nondimensional radial line load as a function of its lateral displacement.

The curves shown in figure 14 are for different values of the pressure parameter $\frac{pR}{Eh}$ and for the one value of the axial loading parameter $\frac{T}{pR} = \frac{1}{2}$. This value of the axial loading parameter corresponds to the case of a pressurized cylinder with closed ends and no other applied axial load.

As can be seen in figure 14, the radial line load is a linear function of the deflection until wrinkling occurs at a value of $\frac{P}{P_{wr}} = 1$ which is indicated by the dashed line. Immediately after wrinkling occurs, the capacity of the cylinder for carrying further increases in the radial line load decreases. For very large deflections $\frac{W_P}{R_p} > 0.4$, however, the radial line load begins to increase rapidly with increases in the deflection. This rapid increase in the line load is due to the fact that P is a line load per unit length of radius r_o and that for very large deflections where $\frac{W_P}{R_p}$ is approaching 1, r_o is approaching zero. The total load $2\pi r_o P$ required to deform the cylinder all the way to the axis remains finite, however.

EXPERIMENTAL INVESTIGATION

In this section an experimental investigation which was conducted to check the validity of the theory developed in this thesis is presented. The model used in this investigation was made of a very thin plastic film and the configuration was chosen to represent the theoretical problem which was solved in the section beginning on page 22. A photograph of a model tested is shown in figure 3. Measurements were made on these models of the depth and extent of the unwrinkled region for various levels of internal pressure, and the results are compared with theory.

Test Specimens

Tests were performed on circular sheets of Mylar which were pleated around the circumference and attached to the vertical end of a wooden cylinder, as can be seen in figure 3. The shape of the membrane was chosen to be the same as that given by zero hoop stress linear membrane theory. One-half of this shape and its coordinates are presented in figure 15. The coordinates used in plotting this shape were obtained by numerical integration of equation (50). The radius of the wooden cylinder to which the Mylar disc was attached for the experiments was 12.75 inches. From figure 15 it can be seen that the meridional length from the center of the pressurized membrane to the point of attachment is 1.312 times the maximum radius, which in this case is 12.75 inches. This yields a radius for the flat disc from which the model is made of 16.72 inches. An additional

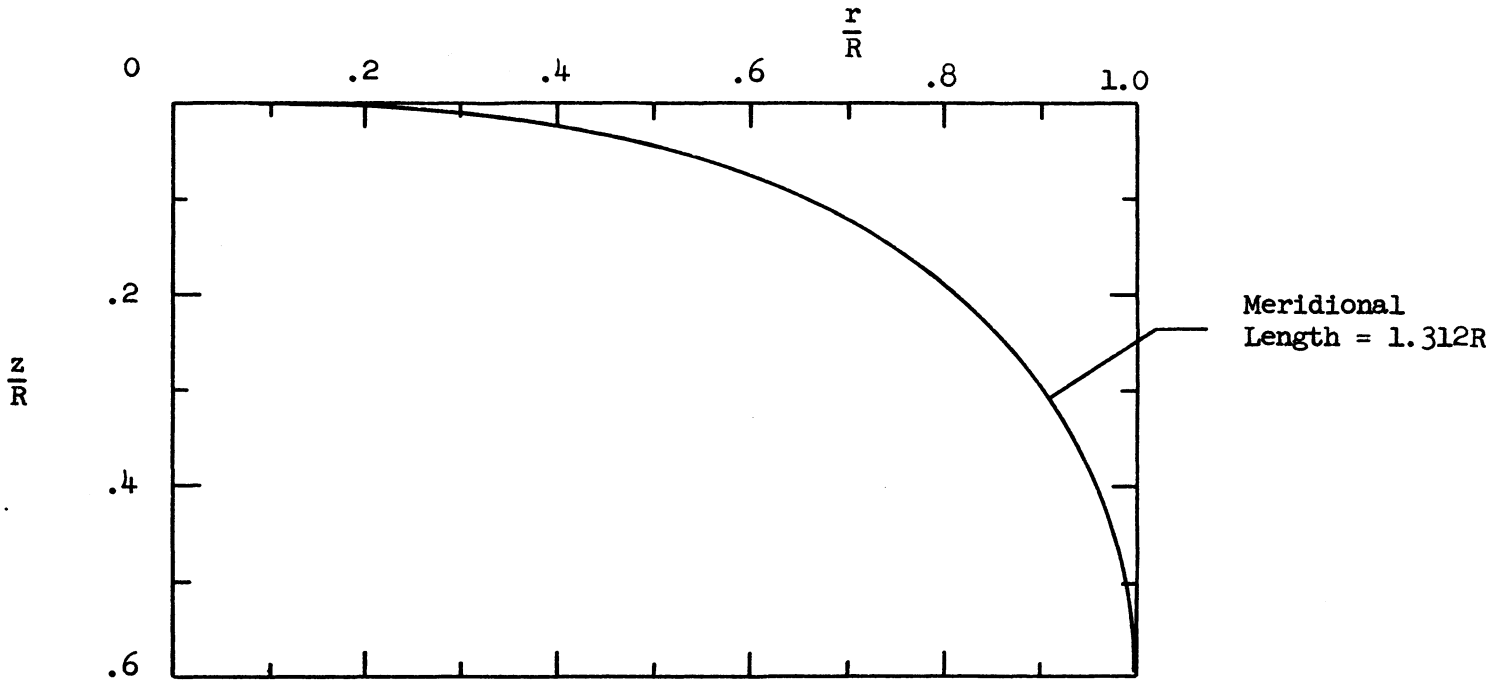

Figure 15.- Zero hoop stress shape as given by linear membrane theory.

3 inches of material was allowed around the edge for attachment. A side photograph of the specimen mounted in place on the cylinder with just enough internal pressure to hold its shape is shown in figure 16. A qualitative comparison of the theoretical zero hoop stress shape with the profile shown in figure 16 indicated very good agreement.

Young's modulus for the material used in this investigation was obtained from dead-weight loading uni-axial tests conducted on three 1-inch-wide strips of Mylar 15 inches long. The strain in the Mylar for these tests was determined by measuring the relative displacements of two marks put on the strips a known distance apart. The gage length used in these tests was 3 inches, and measurements were made with two optical extensometers. The smallest reading possible on the extensometers was 0.0002 inch, with a total reading range of 0.2 inch. A typical stress-strain curve obtained in these tests is shown in figure 17. The average modulus obtained from the three tests was 660,000 psi with a variation of ± 4 percent. This value of the modulus agrees very well with the 670,000 psi reported in reference 16. It can be seen in figure 17 that the Mylar starts yielding at a stress level a little higher than 10,000 psi. For further increases in the load, the behavior is very time dependent. No attempt was made in these tests to accurately define the time-dependent behavior of Mylar at stress levels above 10,000 psi; however, it should be pointed out that the last five readings were taken at about 2-minute intervals, and at the last reading the material was flowing rapidly. At stress

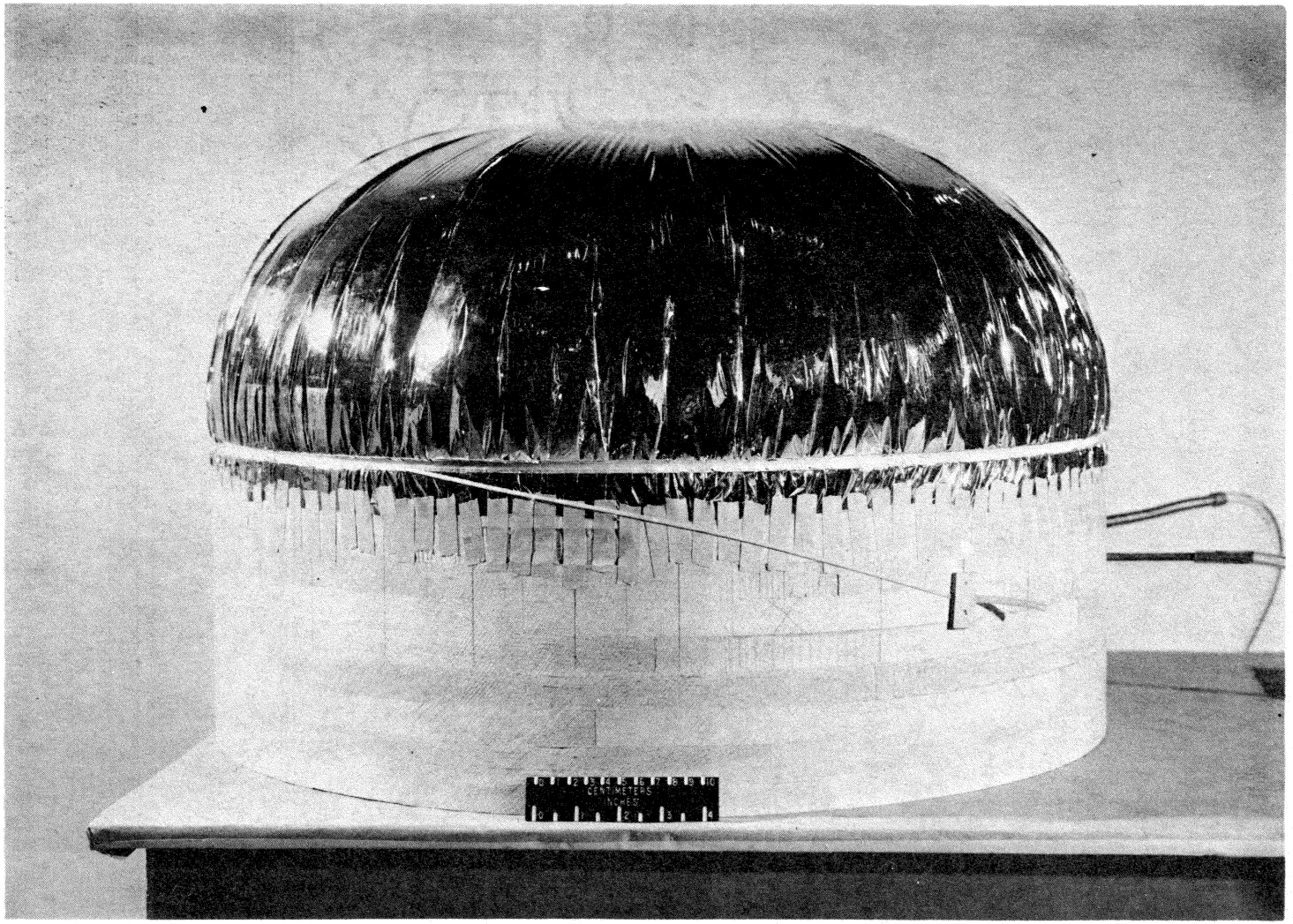

Figure 16.- Profile view of lightly pressurized membrane.

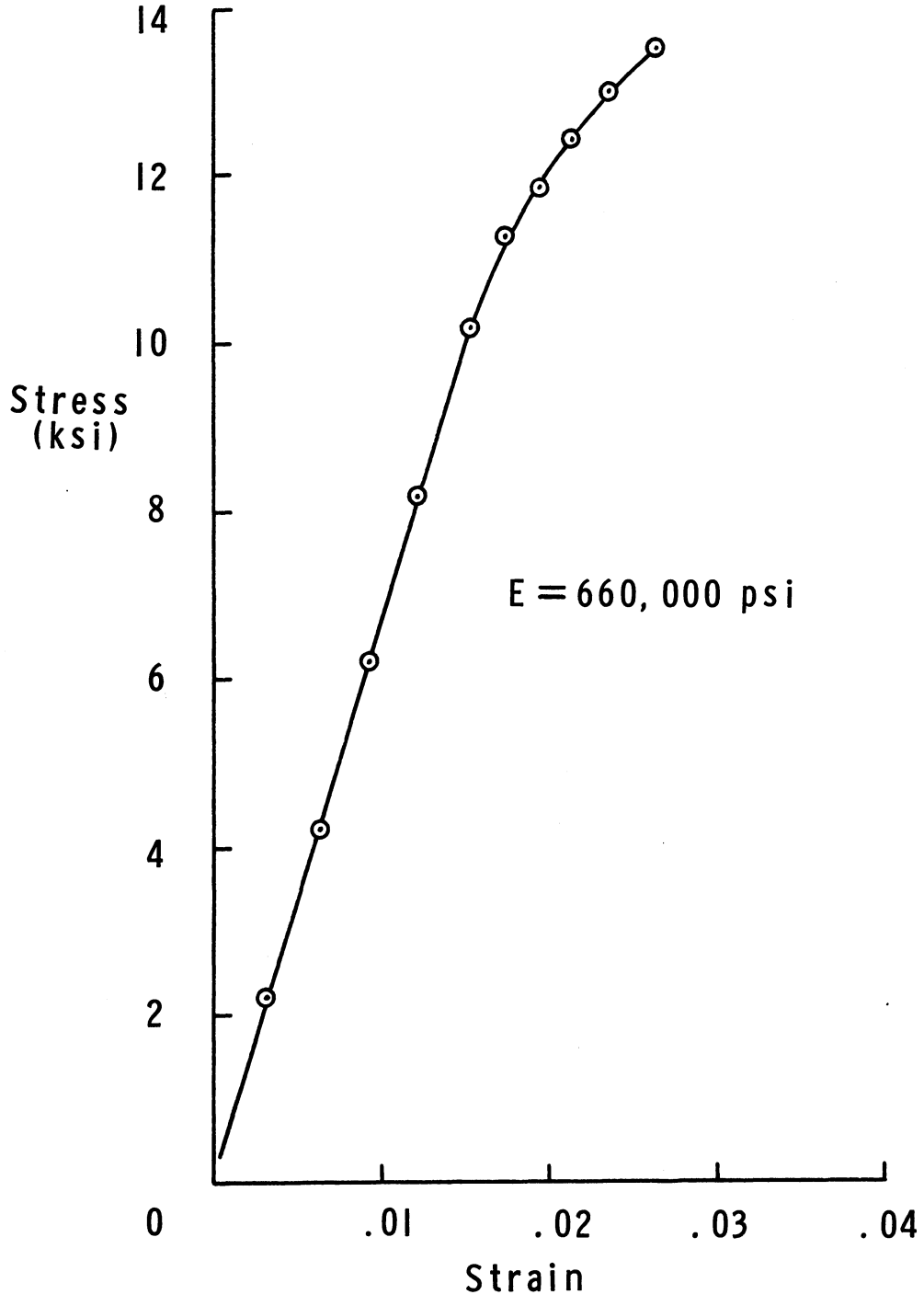

Figure 17.- Stress-strain curve for a 1-inch-wide strip of 1/2-mil Mylar.

levels slightly below 10,000 psi, the Mylar was left loaded for 10 minutes and no noticeable creep was observed.

Results and Discussion

In the photograph of figure 16, it can be seen that the very lightly pressurized membrane is quite flat in the vicinity of the crown as predicted by linear membrane theory. As the internal pressure is increased to a substantial level, however, this highly stressed region undergoes large deformations, due to stretching of the surface, that are not taken into account by linear membrane theory. In the theoretical analysis of this problem, nonlinear membrane theory is used to properly take into account stretching of the surface and the resulting large deformations. Nondimensional plots of the stress distribution, the radial displacement, and the lateral displacement of this unwrinkled region are presented in figures 6, 7, and 8, respectively.

As a check on these theoretical results, the depth of the unwrinkled region was measured on a model such as that shown in figure 16 and the results were compared with theory. A sketch of the unwrinkled region is shown in figure 18(a). The theoretical prediction for the depth d of the unwrinkled region is found from figure 8 where $d = - w\Big|_{\rho=1}$. The depth of the unwrinkled region can then be written as

$$d = 0.4525a\left(\frac{4pa}{Eh}\right)^{1/3} \tag{134}$$

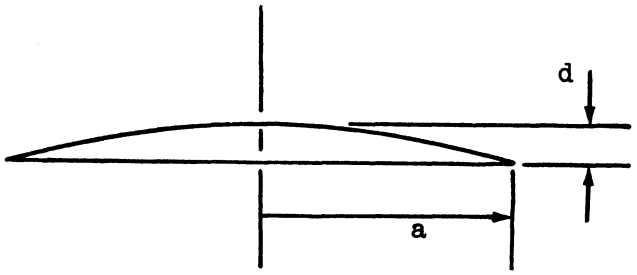

Figure 18(a).- Sketch of unwrinkled region.

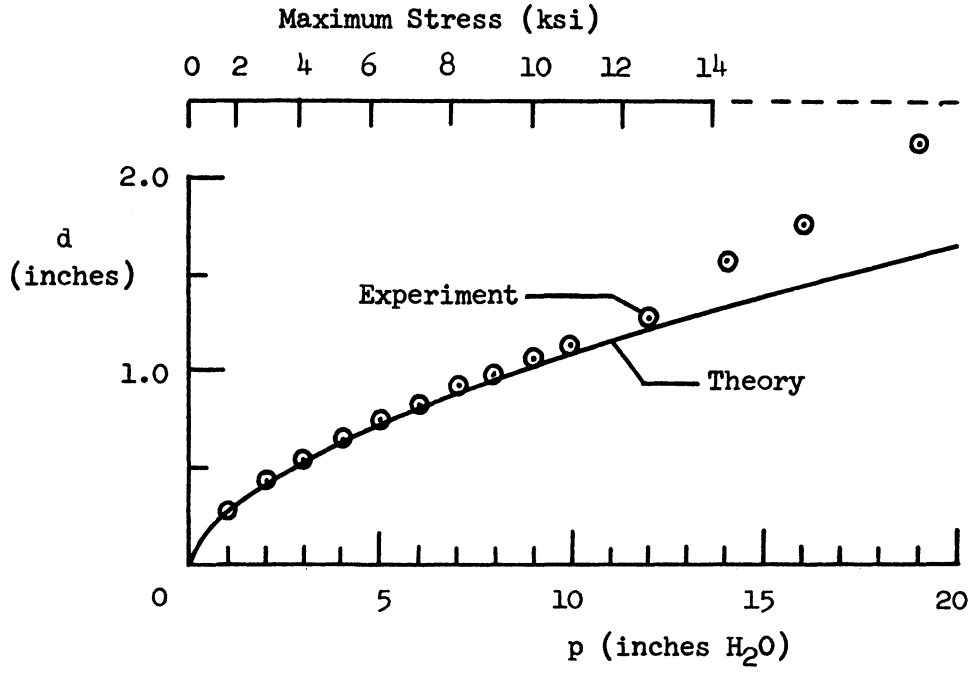

Figure 18(b).- Comparison of experiment with theory for depth of the unwrinkled region.

where a, the radius of the unwrinkled region is found from equation (68) as

$$a = 1.388R\left(\frac{pR}{Eh}\right)^{1/5} \tag{135}$$

By substituting for a from equation (135) into equation (134) yields the depth of the unwrinkled region d as a function of pressure as

$$d = 1.112R\left(\frac{pR}{Eh}\right)^{3/5} \tag{136}$$

A plot of d as a function of pressure as calculated from equation (136) is presented in figure 18(b) for the following values of R, E, and h:

$$R = 12.75 \text{ inches}$$

$$E = 660{,}000 \text{ psi}$$

$$h = 0.0005 \text{ inch}$$

In this same figure the results of the experimental investigation as represented by the circles are shown for comparison. The experimental data were obtained from measurements on a model such as shown in figure 16. The measurements were made with a depth gage which was free to slide along a metal straight edge which was clamped securely in place horizontally above the model. At each level of pressure, the depth of the unwrinkled region was determined by measuring the distance

from the straight edge to the crown of the membrane and the distance from the straight edge to the edge of the unwrinkled region and taking the difference. Since it is very difficult to place the straight edge exactly perpendicular to the membrane axis, measurements to the edge of the unwrinkled region were taken at two diametrically opposite points and averaged. It can be seen in figure 18(b) that the experimental results agree very well with theory until yielding of the Mylar occurs at the higher levels of pressure. A scale of the maximum theoretical stress which occurs at the crown of the unwrinkled region is provided above the figure. By comparing these stresses with those obtained from the uni-axial tests as shown in figure 17, it can be determined that yielding of the pressurized model begins around an internal pressure of 8.5 in. H_2O. By the time the internal pressure reaches 12 in. H_2O, the Mylar is stressed well into its yielded range and very large deviations from the elastic theory begin to occur.

In making the measurements of the depth of the unwrinkled region, the edge of the unwrinkled region was determined from equation (135). The radius a of the unwrinkled region as determined from this equation is plotted in figure 19 as a function of internal pressure. From this figure it can be seen that the extent of the unwrinkled region grows very rapidly as the internal pressure is initially applied and that this growth rate decreases with increasing values of internal pressure. The extent of the unwrinkled region is difficult to obtain by observation, as the transition between the wrinkled and unwrinkled region is gradual. In addition, there is a slight nonaxisymmetric

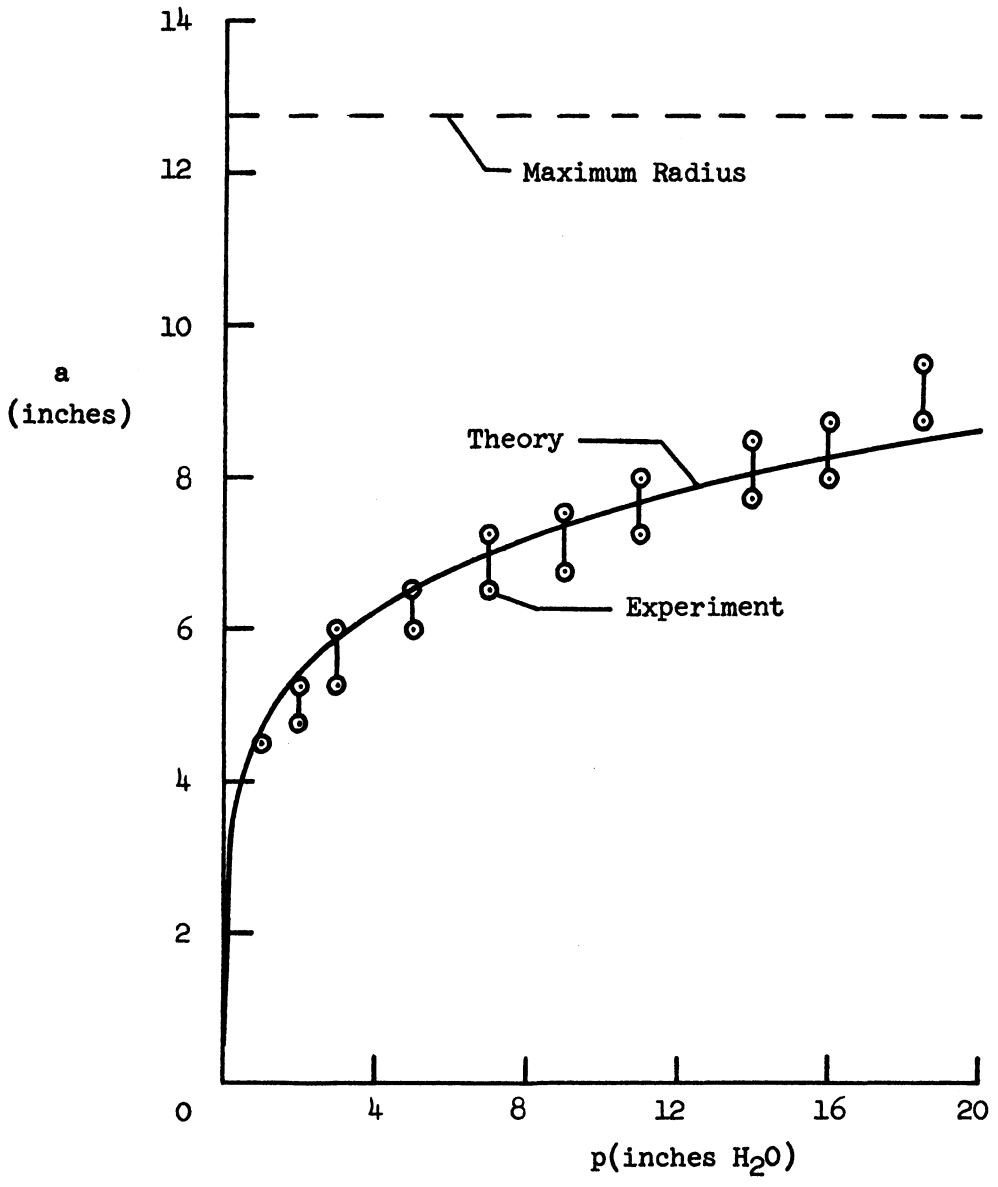

Figure 19.- Comparison of experiment with theory for the extent of the unwrinkled region.

pattern which develops in the wrinkled region which is probably due to the small bending stiffness which exists in the Mylar. Taking these difficulties into account, however, measurements of the extent of the unwrinkled region were made using the best judgment possible. These results are indicated by the circles in figure 19. The upper and lower circle at each level of pressure indicates the maximum and minimum observed radius of the unwrinkled region. Although these particular measurements are quite rough, it is believed that this comparison with theory along with the more accurate comparison of the depth of the unwrinkled region does lend credence to the validity of the proposed theory.

CONCLUSIONS

A theory has been presented for the elastic analysis of deep doubly curved, axisymmetric, partly wrinkled membranes which are formed from an initially flat sheet. The doubly curved membrane surface is analyzed separately in the wrinkled and unwrinkled regions and then properly matched together. The wrinkled region is considered as a zero hoop stress linear membrane, while in the unwrinkled region where stretching of the membrane surface is important, small strain nonlinear membrane theory is used. In addition, meridional and circumferential stiffening cords which are closely spaced so that their effects may be "smeared out" or averaged over the surface are included.

In order to demonstrate the application of the proposed theory, three illustrative sample problems are solved. The first problem is an initially flat circular membrane which has been pleated around its outer circumference to form a deep doubly curved axisymmetric surface which is then attached to a rigid boundary and pressurized. Sir Geoffrey Ingram Taylor, in his famous paper "On the Shapes of Parachutes,"[5] solved this problem in 1919 using zero hoop stress linear membrane theory for the entire surface. His analysis yielded a very good description of the overall shape; however, due to the inextensional nature of the linear membrane theory used, unrealistic stresses were obtained in the vicinity of the crown where stretching of the surface is important. In the present thesis, stretching of the surface in the vicinity of the crown, where an unwrinkled region forms, is

properly taken into account using nonlinear membrane theory. Away from the crown in the wrinkled region, linear membrane theory as was used by Taylor is employed. The stress distribution throughout the membrane as predicted by the present analysis is given in the form of a plot, and a comparison is made with linear membrane theory. In appendix B the effects of adding meridional stiffening cords to the doubly curved membrane considered in this problem are investigated. For the stiffened case, the effects of a small circular cutout with a rigid ring insert at the crown are also studied.

The second problem solved is the stretching of an initially flat circular membrane over a doubly curved, axisymmetric mandrel. As in the previous problem, an unwrinkled region develops in the vicinity of the crown, while the remainder of the membrane remains wrinkled. A simplification is afforded in this problem, however, in that the membrane must conform to the surface of the mandrel so that the lateral displacement of the membrane is known everywhere. This results in linear equations for the unwrinkled region which are subsequently solved in closed form for four specific mandrel shapes. Three of the mandrel shapes considered are a parabolic, a cubic, and a quartic surface of revolution. The fourth is a spherical mandrel. It was found that the solution for the stresses for the unwrinkled region in the spherical mandrel problem were the same as those obtained for the contact region in reference 16 where the indentation of an initially flat stretched membrane by a spherical indenter was solved. The meridional stress distributions obtained for the various mandrels of

the present thesis are presented in the form of a plot, and a comparison is made with results obtained from the pressurized membrane discussed previously. It was found that a membrane stretched over a cubic mandrel has a behavior very similar to that of the pressurized membrane.

The last problem solved was the very large deformation behavior of a pressurized membrane cylinder subjected to a radial line load. In this problem the pressurized membrane cylinder can withstand a certain value of the radial line load before wrinkling occurs. When the hoop stress at the line of application of the line load drops to zero, however, wrinkling will occur and further increases in the loading will result in a growth of the wrinkled region. A closed-form solution is obtained for this problem and a plot of the radial line load as a function of its lateral displacement is presented for displacements as large as the radius of the cylinder.

In order to assess the validity of the theory presented herein, an experimental investigation of the first problem was conducted. The specimens used in the experiments were circular sheets of 1/2-mil Mylar, 33 inches in diameter. These circular sheets were pleated around the circumference, attached to a rigid circular boundary 25.5 inches in diameter and then pressurized. Measurements were made for different levels of internal pressure of the depth af the resulting unwrinkled region at the crown.

The results were compared with theoretical predictions and the correlation between experiment and theory was very good until yielding

of the Mylar occurred. After yielding occurred, the depth of the unwrinkled region grew much faster than predicted by the elastic theory; however, the correlation obtained in elastic range does verify the proposed elastic theory.

REFERENCES

1. Stein, Manuel; and Hedgepeth, John M.: Analysis of Partly Wrinkled Membranes. NASA TN D-813, 1961.

2. Reissner, Eric: On Tension Field Theory. Proc. Fifth Int. Cong. Appl. Mech., John Wiley and Sons, Inc., 1938, pp. 88-92.

3. Mikulas, Martin M., Jr.: Behavior of a Flat Stretched Membrane Wrinkled by the Rotation of an Attached Hub. NASA TN D-2456, 1964.

4. McComb, Harvey G.; Zender, George W.; and Mikulas, Martin M., Jr.: The Membrane Approach to Bending Instability of Pressurized Cylindrical Shells. NASA TN D-1510, 1962, pp. 229-237.

5. Taylor, Sir Geoffrey Ingram: On the Shapes of Parachutes. The Scientific Papers of Sir Geoffrey Ingram Taylor, vol. III, 1963.

6. Houtz, N. E.: Optimization of Inflatable Drag Devices by Isotensoid Design. AIAA Paper 64-437, 1964.

7. Mikulas, Martin M., Jr.; and Bohon, Herman L.: Development Status of Attached Inflatable Decelerators. Journal of Spacecraft and Rockets, vol. 6, no. 6, 1969, pp. 654-660.

8. Sanders, J. Lyell, Jr.: Nonlinear Theories for Thin Shells. Quart. Appl. Math., vol. XXI, no. 1, April 1963, pp. 21-36.

9. Rossettos, John N.: Nonlinear Membrane Solutions for Symmetrically Loaded Deep Membranes of Revolution. NASA TN D-3297, 1966.

10. Mikulas, Martin M., Jr.; and McElman, John A.: On Free Vibrations of Eccentrically Stiffened Cylindrical Shells and Flat Plates. NASA TN D-3010, 1965.

11. Hencky, H.: Über den Spannungszustand in Kreisrunden Platten mit Verschwindender Biegungssteifigkeit. Zeitschr. f. Math. U. Phys. 63 (1915) s. 311.

12. Schwerin E.: Über Spannungen und Formanderungen Kreisringförmiger Membranen. AEG-Berlin Z Tech. Phys. No. 12, 1929.

13. Campbell, J. D.: On the Theory of Initially Tensioned Circular Membranes Subjected to Uniform Pressure. Quart. Jour. Mech. and Appl. Math., vol. IX, Part 1, 1956.

14. Cyrus, Nancy Jane; and Fulton, Robert E.: Accuracy Study of the Finite Difference Methods. NASA TN D-4372, 1968.

15. Scarborough, J. B.: Numerical Mathematical Analysis. The Johns Hopkins Press, 2nd Edition, 1950.

16. Bhatia, N. M.; and Nachbar, W.: Finite Indentation of an Elastic Membrane by a Spherical Indenter. Int. J. Non-Linear Mechanics, vol. 3, Pergamon Press, 1968, pp. 307-324.

APPENDIX A

POWER SERIES SOLUTION FOR A FLAT MEMBRANE LOADED WITH LATERAL PRESSURE AND SUPPORTED BY TANGENTIAL EDGE LOADS

A power series solution to equation (51) is presented in this appendix as a check on the numerical solution presented in the text. Equation (51) is repeated here and is written as

$$\bar{N}_r^2\left[\frac{d}{d\rho}\left(\rho^3\,\frac{d\bar{N}_r}{d\rho}\right)\right] + 4\rho^3 = 0 \qquad \text{(A-1)}$$

Due to the symmetry of $\bar{N}_r$ in this problem, a power series is chosen with only even powers of ρ as

$$\bar{N}_r = A_o + A_2\rho^2 + A_4\rho^4 + A_6\rho^6 + A_8\rho^8 + A_{10}\rho^{10} + A_{12}\rho^{12} + \ldots \qquad \text{(A-2)}$$

Using this expression for $\bar{N}_r$, the quantity inside the brackets of equation (A-1) becomes

$$\frac{d}{d\rho}\left(\rho^3\,\frac{d\bar{N}_r}{d\rho}\right) = 8A_2\rho^3 + 24A_4\rho^5 + 48A_6\rho^7 + 80A_8\rho^9 + 120A_{10}\rho^{11} + 168A_{12}\rho^{13} + \ldots \qquad \text{(A-3)}$$

Squaring equation (A-2) yields $\bar{N}_r^2$ as

$$\bar{N}_r^2 = A_o^2 + 2A_oA_2\rho^2 + (2A_oA_4 + A_2^2)\rho^4 + 2(A_oA_6 + A_2A_4)\rho^6 + (2A_oA_8 + 2A_2A_6 + A_4^2)\rho^8 + 2(A_oA_{10} + A_2A_8 + A_4A_6)\rho^{10} + \ldots \qquad \text{(A-4)}$$

These quantities from equations (A-3) and (A-4) are substituted into the governing equation (A-1) to yield

$$\bar{N}_r^2\left[\frac{d}{d\rho}\left(\rho^3\,\frac{d\bar{N}_r}{d\rho}\right)\right] + 4\rho^3 = 4(2A_2A_o^2 + 1)\rho^3 + 16A_oA_2^2\rho^5 + 8A_2(2A_oA_4 + A_2^2)\rho^7 + 16A_2(A_oA_6 + A_2A_4)\rho^9$$
$$+ 8A_2(2A_oA_8 + 2A_2A_6 + A_4^2)\rho^{11} + 16A_2(A_oA_{10} + A_2A_8 + A_4A_6)\rho^{13} + 24A_4A_o^2\rho^5$$
$$+ 48A_4\,A_oA_2\rho^7 + 24A_4(2A_oA_4 + A_2^2)\rho^9 + 48A_4(A_oA_6 + A_2A_4)\rho^{11}$$
$$+ 24A_4(2A_oA_8 + 2A_2A_6 + A_4^2)\rho^{13} + 48A_6A_o^2\rho^7 + 96A_oA_2A_6\rho^9$$
$$+ 48A_6(2A_oA_4 + A_2^2)\rho^{11} + 96A_6(A_oA_6 + A_2A_4)\rho^{13} + 80A_8A_o^2\rho^9$$
$$+ 160A_oA_2A_8\rho^{11} + 80A_8(2A_oA_4 + A_2^2)\rho^{13} + 120A_{10}A_o^2\rho^{11}$$
$$+ (240A_{10}A_oA_2 + 168A_{12}A_o^2)\rho^{13} + \ldots \qquad \text{(A-5)}$$

By equating to zero, the sum of the coefficients of like powers of ρ in equation (A-5) yields the following relations between the constants of the power series:

$$
\left.
\begin{aligned}
&2A_2A_o^2 + 1 = 0 \\
&2A_oA_2^2 + 3A_4A_o^2 = 0 \\
&A_2(2A_oA_4 + A_2^2) + 6(A_4A_oA_2 + A_6A_o^2) = 0 \\
&2A_2(A_oA_6 + A_2A_4) + 3A_4(2A_oA_4 + A_2^2) + 12A_oA_2A_6 + 10A_8A_o^2 = 0 \\
&A_2(2A_oA_8 + 2A_2A_6 + A_4^2) + 6(3A_oA_4A_6 + A_2A_4^2 + A_2^2A_6) + 20A_oA_2A_8 + 15A_{10}A_o^2 = 0 \\
&8A_2(A_oA_{10} + A_2A_8 + A_4A_6) + 12A_4(2A_oA_8 + 2A_2A_6 + A_4^2) + 48A_6(A_oA_6 + A_2A_4) + 40A_8(2A_oA_4 + A_2^2) \\
&\qquad + 120A_{10}A_oA_2 + 84A_{12}A_o^2 = 0
\end{aligned}
\right\} \quad (A\text{-}6)
$$

By solving the first of equations (A-6) for A_2 in terms of A_o, then substituting into the second equation and solving for A_4 and so on, all of the constants can be written in terms of the one constant A_o as

$$\left.\begin{aligned} A_2 &= -\frac{1}{2A_o^2} & A_8 &= -\frac{17}{288\,A_o^{11}} \\ A_4 &= -\frac{1}{6A_o^5} & A_{10} &= -\frac{37}{864\,A_o^{14}} \\ A_6 &= -\frac{13}{144\,A_o^8} & A_{12} &= -\frac{1205}{36{,}288\,A_o^{17}} \end{aligned}\right\} \qquad \text{(A-7)}$$

These quantities are substituted back into the original power series to yield

$$\bar{N}_r = A_o - \frac{1}{2\,A_o^2}\rho^2 - \frac{1}{6\,A_o^5}\rho^4 - \frac{13}{144\,A_o^8}\rho^6 - \frac{17}{288\,A_o^{11}}\rho^8 - \frac{37}{864\,A_o^{14}}\rho^{10} - \frac{1{,}205}{36{,}288\,A_o^{17}}\rho^{12} - \ldots \qquad \text{(A-8)}$$

The hoop stress resultant $\bar{N}_\theta$ is found by substituting $\bar{N}_r$ from equation (A-8) into equation (29) to yield

$$\bar{N}_\theta = A_o - \frac{3}{2\,A_o^2}\rho^2 - \frac{5}{6\,A_o^5}\rho^4 - \frac{91}{144\,A_o^8}\rho^6 - \frac{17}{32\,A_o^{11}}\rho^8 - \frac{407}{864\,A_o^{14}}\rho^{10} - \frac{15{,}665}{36{,}288\,A_o^{17}}\rho^{12} - \ldots \qquad \text{(A-9)}$$

As in the numerical solution in the text, the particular solution of interest for the unwrinkled region is the case where the value of the tangential edge load $\bar{N}_\rho(1)$ is such that the hoop stress at the edge

of the membrane is zero. Thus, the condition to be used in determining A_o is

$$N_\theta(1) = 0 \tag{A-10}$$

Applying this condition to equation (A-9) yields the following successive approximations to the solution

$$\left.\begin{aligned}
&A_o^3 - \frac{3}{2} = 0 \\
&A_o^6 - \frac{3}{2} A_o^3 - \frac{5}{6} = 0 \\
&A_o^9 - \frac{3}{2} A_o^6 - \frac{5}{6} A_o^3 - \frac{91}{144} = 0 \\
&A_o^{12} - \frac{3}{2} A_o^9 - \frac{5}{6} A_o^6 - \frac{91}{144} A_o^3 - \frac{17}{32} A_o^3 - \frac{407}{864} = 0 \\
&A_o^{18} - \frac{3}{2} A_o^{15} - \frac{5}{6} A_o^{12} - \frac{91}{144} A_o^3 - \frac{17}{32} A_o^6 - \frac{407}{864} A_o^3 - \frac{15,665}{36,288} = 0
\end{aligned}\right\} \tag{A-11}$$

The solutions of the successive approximations given by equations (A-11) are

$$\left.\begin{aligned}
A_o &= 1.1447 \\
A_o &= 1.2453 \\
A_o &= 1.2714 \\
A_o &= 1.2802 \\
A_o &= 1.2836 \\
A_o &= 1.2850
\end{aligned}\right\} \tag{A-12}$$

A plot of A_o as a function of the number of terms taken in the power series is shown in figure 20 to give an indication of the convergence. The power series solution gives a value for the nondimensional stress resultant at the center of the membrane as

$$\bar{N}_r(0) = 1.2850 \quad \text{(Power series solution)}$$

The numerical solution presented in the text gave a value for the stress resultant at the center of the membrane as

$$\bar{N}_r(0) = 1.2861 \quad \text{(Numerical solution)}$$

The power series solution for the radial stress resultant at the edge of the membrane is found by substituting A_o into equation (A-2) evaluated at $\rho = 1$. This yields

$$\bar{N}_r(1) = 0.9170 \quad \text{(Power series solution)}$$

The corresponding stress resultant is given by the numerical solution as

$$\bar{N}_r(1) = 0.9187 \quad \text{(Numerical solution)}$$

The numerical results shown, where obtained using 500 stations, and a check which revealed no change to the number of places shown was made using 1,000 stations. Although the seven-term power series solution has not quite converged to the numerical results, it is felt that it does represent a verification of the numerical solution.

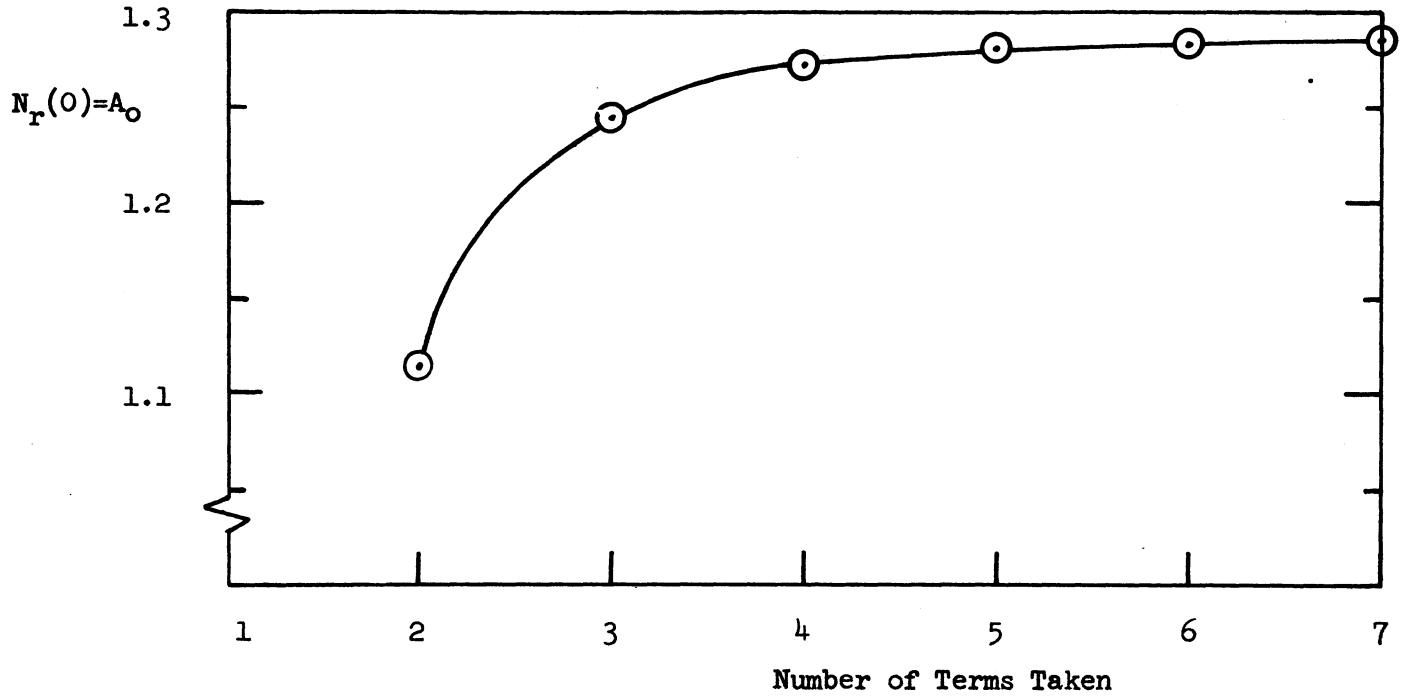

Figure 20.- Power series solution as a function of the number of terms taken.

APPENDIX B

ANALYSIS OF AN INITIALLY FLAT CIRCULAR MEMBRANE STIFFENED WITH CORDS IN THE MERIDIONAL AND CIRCUMFERENTIAL DIRECTIONS

In this appendix, an analytical technique for handling initially flat membranes stiffened with cords in the meridional and circumferential directions is demonstrated. The stiffening elements placed on the membrane are assumed to be closely spaced so that their effects may be "smeared out" or averaged over the surface. The particular problem to be investigated here is the stiffened counterpart of the one which is solved in the section beginning on page 22. The free-body diagram in figure 5, which was used for the isotropic case, will be referred to for notation in the present problem. The emphasis in this appendix will be on the nonlinear analysis of the stiffened unwrinkled region. The wrinkled region will not be considered here, since the solution and matching techniques are identical to the isotropic case. In the construction of meridional stiffened membranes, the convergence of the many stiffening cords at the crown presents a difficulty in both attachment of the cords to the membrane surface and in extreme bulkiness that is often eliminated by cutting a hole at the crown and inserting a stiff ring. To demonstrate the analysis of such a problem, a rigid ring insert is included in this appendix as well as the closed crown.

Governing Equations and Numerical Solution

The governing equations for the unwrinkled region shown in figure 5 are provided by equations (25) through (30). The difference between this problem and the isotropic case is the retention of the stiffening term $nE_sA_s/2\pi r$ in the constitutive equations (27) and (28). Due to the anisotropy of this problem, the stresses N_r and N_θ are not equal to the crown, which eliminates the classic symmetry condition $N_r'(0) = 0$. Since no other condition exists on the stresses at the origin, this problem is formulated in terms of the inplane displacement u, and the meridional rotation $\beta = \frac{dw}{dr}$. The nondimensional governing equations for this problem in terms of u and β are found from equations (25) through (30) as

$$(\rho + S)(\bar{u}'' + \bar{\beta}\bar{\beta}') + \bar{u}' + \frac{1 - \mu}{2}\beta^2 - \frac{\bar{u}}{\rho^2}(\rho + \eta S) = 0 \qquad \text{(B-1)}$$

and

$$\left[(\rho + S)(\bar{u}' + \frac{1}{2}\bar{\beta}^2) + \mu\bar{u}\right]\bar{\beta} = -\,8^{1/2}\,(1 - \mu^2)\rho^2 \qquad \text{(B-2)}$$

where

$$\rho = \frac{r}{a}, \quad S = \frac{nE_sA_s}{2\pi aEh}(1 - \mu^2) \qquad \text{(B-3)}$$

and

$$\bar{u} = \frac{u}{a}\left(32\,\frac{E^2h^2}{p^2a^2}\right)^{1/3}, \quad \bar{\beta} = \beta\left(32\,\frac{E^2h^2}{p^2a^2}\right)^{1/6} \tag{B-4}$$

The governing equations (B-1) and (B-2) are a pair of simultaneous, nonlinear differential equations which are second order in $\bar{u}$ and first order in $\bar{\beta}$. In half-station central differences, using the same notation as for the isotropic case, equations (B-1) and (B-2) become

$$(\rho_{i+1/2} + S)\left[\frac{\bar{u}_{i-1/2} - 2\bar{u}_{i+1/2} + \bar{u}_{i+3/2}}{\epsilon^2} + \left(\frac{\bar{\beta}_i + \bar{\beta}_{i+1}}{2}\right)\left(\frac{-\bar{\beta}_i + \bar{\beta}_{i+1}}{\epsilon}\right)\right]$$
$$+ \frac{-\bar{u}_{i-1/2} + \bar{u}_{i+3/2}}{2\epsilon} + \frac{1-\mu}{2}\left(\frac{\bar{\beta}_i + \bar{\beta}_{i+1}}{2}\right)^2 - \frac{\bar{u}_{i+1/2}}{\rho^2_{i+1/2}}(\rho_{i+1/2} + \eta S) = 0 \tag{B-5}$$

and

$$\left[(\rho_{i+1} + S)\left(\frac{-\bar{u}_{i+1/2} + \bar{u}_{i+3/2}}{\epsilon}\right) + \frac{1}{2}\bar{\beta}^2_{i+1}\right) + \mu\,\frac{\bar{u}_{i+1/2} + \bar{u}_{i+3/2}}{2}\right]\bar{\beta}_{i+1}$$
$$= -8^{1/2}(1-\mu^2)\rho^2_{i+1} \tag{B-6}$$

At the center of the membrane, two different sets of boundary conditions are considered. The first set corresponds to a membrane which is closed at the center and is written as

$$\bar{u}\Big|_{\rho=0} = 0 \tag{B-7}$$

and

$$\bar{\beta}\Big|_{\rho=0} = 0 \tag{B-8}$$

The second set corresponds to a membrane with a rigid ring insert at $r = b$ and is written as

$$\bar{u}\Big|_{\rho=b/a} = 0 \tag{B-9}$$

and

$$\bar{\beta}\Big|_{\rho=b/a} = 0 \tag{B-10}$$

In half-station central differences, equations (B-9) and (B-10) are written as

$$\frac{\bar{u}_{m-1/2} + \bar{u}_{m+1/2}}{2} = 0 \tag{B-11}$$

and

$$\bar{\beta}_m = 0 \tag{B-12}$$

where m is the station number which corresponds to the radius of rigid ring or

$$\frac{b}{a} = m\epsilon \tag{B-13}$$

For $m = 0$ the boundary conditions given by equations (B-11) and (B-12) reduce to those for a closed membrane with no hole at the center so that only the second set of boundary conditions needs to be programed. The boundary condition at the edge of membrane at $\rho = 1$ is

$$\bar{N}_r\Big|_{\rho=1} = \bar{N}_r(1) \tag{B-14}$$

where $\bar{N}_r(1)$ is the applied tangential edge load. As was the case for the unwrinkled region of the isotropic membrane problem, the solution of interest is the one for which the applied tangential edge load, $\bar{N}_r(1)$, is of such a value that the hoop stress drops at the edge of the membrane. This condition is written as

$$N_\theta\Big|_{\rho=1} = 0 \tag{B-15}$$

In central difference form, this condition is written in terms of $\bar{u}$ and $\bar{\beta}$ as

$$\bar{N}_\theta\Big|_{i=I} = \left[\left(1 + \eta\,\frac{s}{\rho_I}\right)\frac{\bar{u}_{I-1/2} + \bar{u}_{I+1/2}}{2\rho_I} + \mu\left(\frac{-\bar{u}_{I-1/2} + \bar{u}_{I+1/2}}{\epsilon} + \frac{1}{2}\bar{\beta}_I^2\right)\right]\frac{1}{1-\mu^2} = 0 \tag{B-16}$$

The procedure used in solving equations (B-5) and (B-6) subject to the boundary conditions given by equations (B-11) and (B-12) and the condition given by equation (B-16) is similar to that described in the text for the isotropic case. The primary difference is that for this problem a pair of simultaneous transcendental equations must be solved at each station before proceeding to the next. The solution of this pair of transcendental equations at each station was solved using a subroutine developed at Langley and presented no problem. Briefly then, the procedure was as follows:

(1) Apply boundary conditions (B-11) and (B-12) to equations (B-5) and (B-6) at the first station $i = m$.

(2) Guess $\bar{u}_{m+1/2}$ and solve equations (B-5) and (B-6) for $\bar{\beta}_{m+1}$ and $\bar{u}_{m+3/2}$.

(3) Substitute these values into equations (B-5) and (B-6) evaluated at second station $i = m + 1$ and solve for $\bar{\beta}_{m+2}$ and $\bar{u}_{m+5/2}$.

(4) Continue this procedure to station $i = I - 1$ and then check to see if condition (B-16) is satisfied.

(5) If not, make another guess for $u_{m+1/2}$ and repeat procedure.

(6) After first two guesses, use Newton-Raphson technique to determine subsequent guesses until condition (B-16) is satisfied to an acceptable degree of accuracy.

The procedure just described was programed on a CDC 6600 computer and a program listing along with two sample runs is presented in appendix C.

Results and Discussion

Unlike the isotropic case solved in the text where a universal solution to the problem was obtained, a stiffened membrane must be solved for the particular combination of skin thickness and stiffener geometry of interest. However, to demonstrate the application of the analysis, solutions from the computer program for sample cases of stiffener geometries will be presented. Specifically, the two problems investigated are the addition of meridional stiffening cords to an isotropic membrane with a closed crown, and the addition of meridional stiffening cords to an isotropic membrane with a rigid ring insert at the crown.

The results for these two problems will be presented in the form of plots of the meridional and circumferential stress resultants as a function of the radial coordinate. The meridional stress resultant including the effects of the smeared out stiffening cords is found from equation (27) as

$$N_r = \frac{Eh}{1 - \mu^2}\left[\frac{du}{dr} + \frac{1}{2}\beta^2 + \mu\frac{u}{r}\right] + \frac{nE_sA_s}{2\pi r}\left(\frac{du}{dr} + \frac{1}{2}\beta^2\right) \qquad \text{(B-17)}$$

where the strains have been eliminated using equations (25) and (26). In order to properly stress analyze a stiffened membrane, it is necessary to separate the stress in the isotropic face sheet from the load in the cords. This is accomplished by observing that the first term on the right-hand side of equation (B-17) is the stress resultant in the isotropic face sheet portion of the surface, while the second

term is the "smeared out" cord load so that equation (B-17) can be rewritten as

$$N_r = N_{r_f} + \frac{nL}{2\pi r} \tag{B-18}$$

where N_{r_f} is defined as the stress resultant in the isotropic membrane face sheet, and L is the load in each cord. In nondimensional form, N_{r_f} is written in terms of the nondimensional displacement $\bar{u}$ and the nondimensional rotation $\bar{\beta}$ as

$$\bar{N}_{r_f} = \frac{1}{1 - \mu^2}\left[\left(1 + \frac{S}{\rho}\right)\left(\bar{u}' + \frac{1}{2}\bar{\beta}^2\right) + \mu\frac{\bar{u}}{\rho}\right] \tag{B-19}$$

where

$$\bar{N}_{r_f} = \left(\frac{32}{p^2a^2Eh}\right)^{1/3} N_{r_f} \tag{B-20}$$

and ρ, S, $\bar{u}$, and $\bar{U}$ are defined as in equations (B-3) and (B-4). The nondimensional cord load is defined as

$$\bar{L} = \frac{2\pi}{1 - \mu^2} S\left(\bar{u}' + \frac{1}{2}\bar{\beta}^2\right) \tag{B-21}$$

where

$$\bar{L} = \frac{n}{a}\left(\frac{32}{p^2a^2Eh}\right)^{1/3} L \tag{B-22}$$

Similarly, the hoop stress resultant in the isotropic face sheet is found from equation (28) and is written in nondimensional form as

$$N_{\theta_f} = \frac{1}{1 - \mu^2}\left[\frac{\bar{u}}{\rho} + \mu\left(\bar{u}' + \frac{1}{2}\bar{\beta}^2\right)\right] \qquad \text{(B-23)}$$

In the computer program discussed previously, the governing equations are written and solved at each station in terms of the inplane displacement $\bar{u}$ and the meridional rotation $\bar{\beta}$. By writing equations (B-19), (B-22), and (B-23) in half-station central difference form and using the numerical results for $\bar{u}$ and $\bar{\beta}$ from the computer program, $\bar{N}_{r_f}$, $\bar{L}$, and $\bar{N}_{\theta_f}$ can be determined at each station. This was done and these quantities are included as part of the output of the program.

In figures 21 and 22 the effects on the meridional and circumferential stress resultants in the isotropic face sheet of adding meridional stiffening to an isotropic membrane with a closed crown are shown. The top curve in both figures is for the case with no stiffening and these two curves are the same as the bottom two curves of figure 6. The other curves, for various values of the nondimensional stiffening parameter S, demonstrate how the stresses in an isotropic membrane are lowered by the addition of meridional stiffening.

In figures 23 and 24 the effects on the meridional and circumferential stress results in the isotropic face sheet of adding meridional stiffening to an isotropic membrane with a rigid ring insert at the crown are shown. The top curve in both figures is for the case

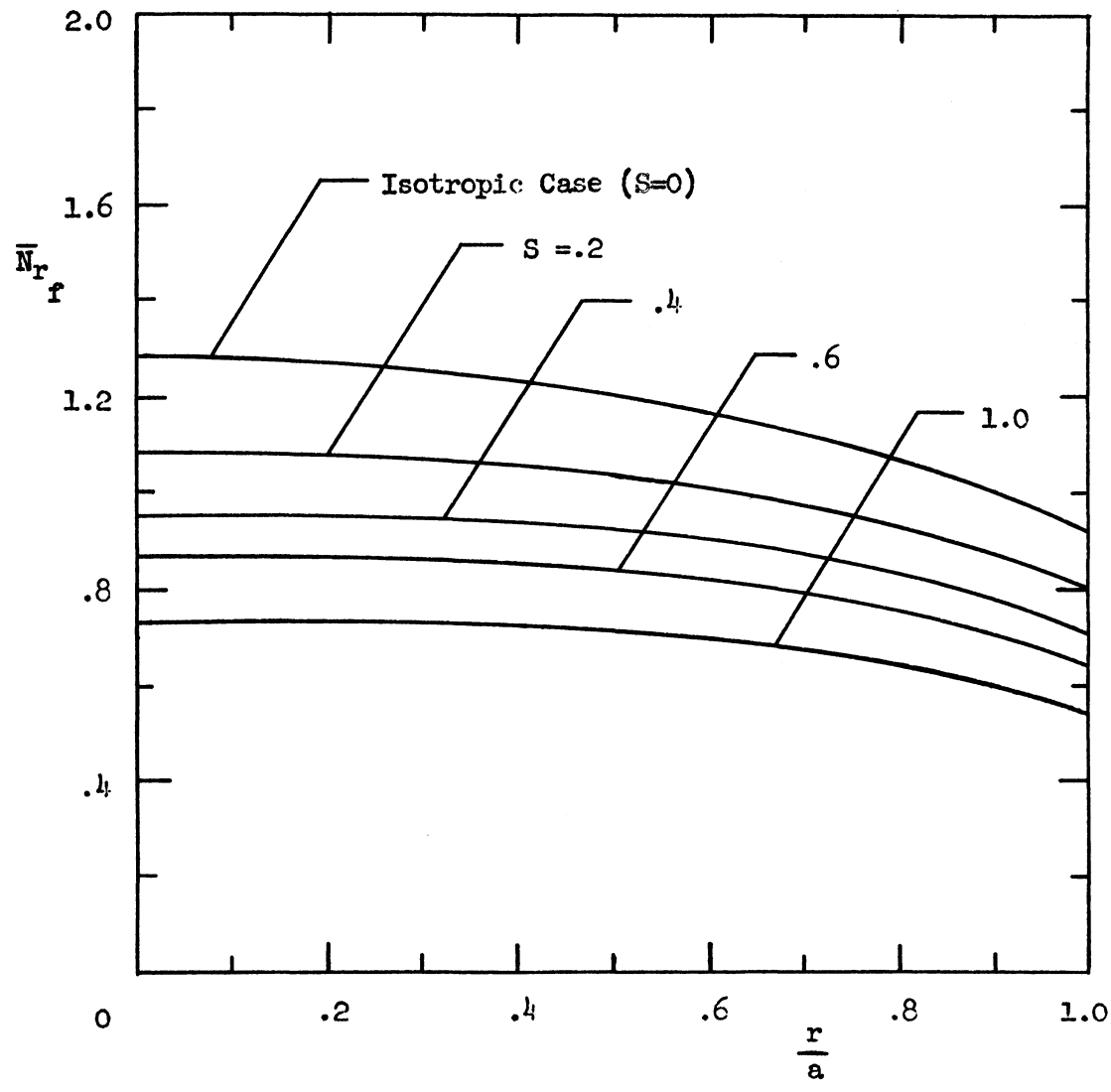

Figure 21.- Effect on meridional stress resultant of adding meridional stiffening cords to pressurized membrane.

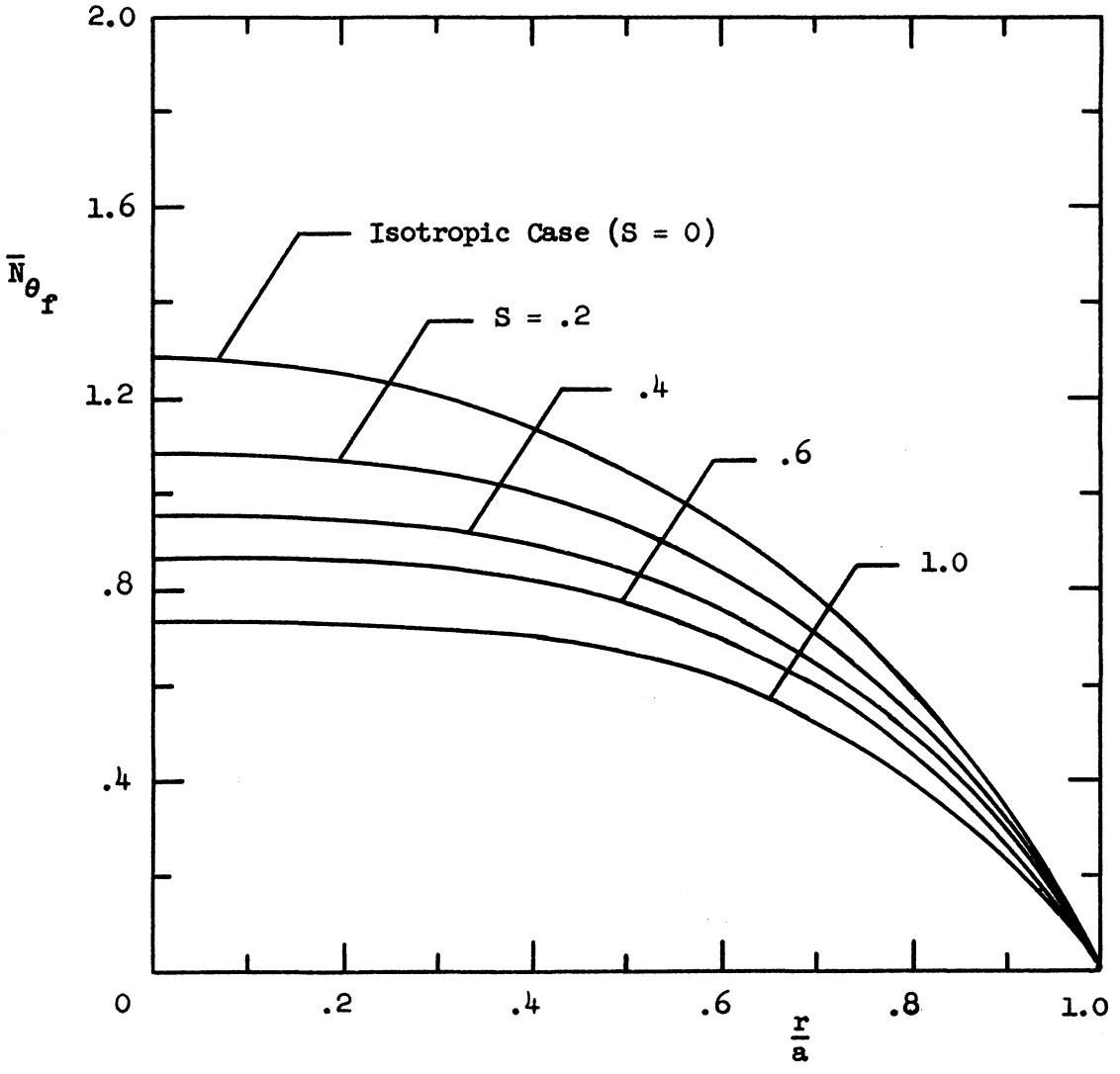

Figure 22.- Effect on circumferential stress resultant of adding meridional stiffening cords to pressurized membrane.

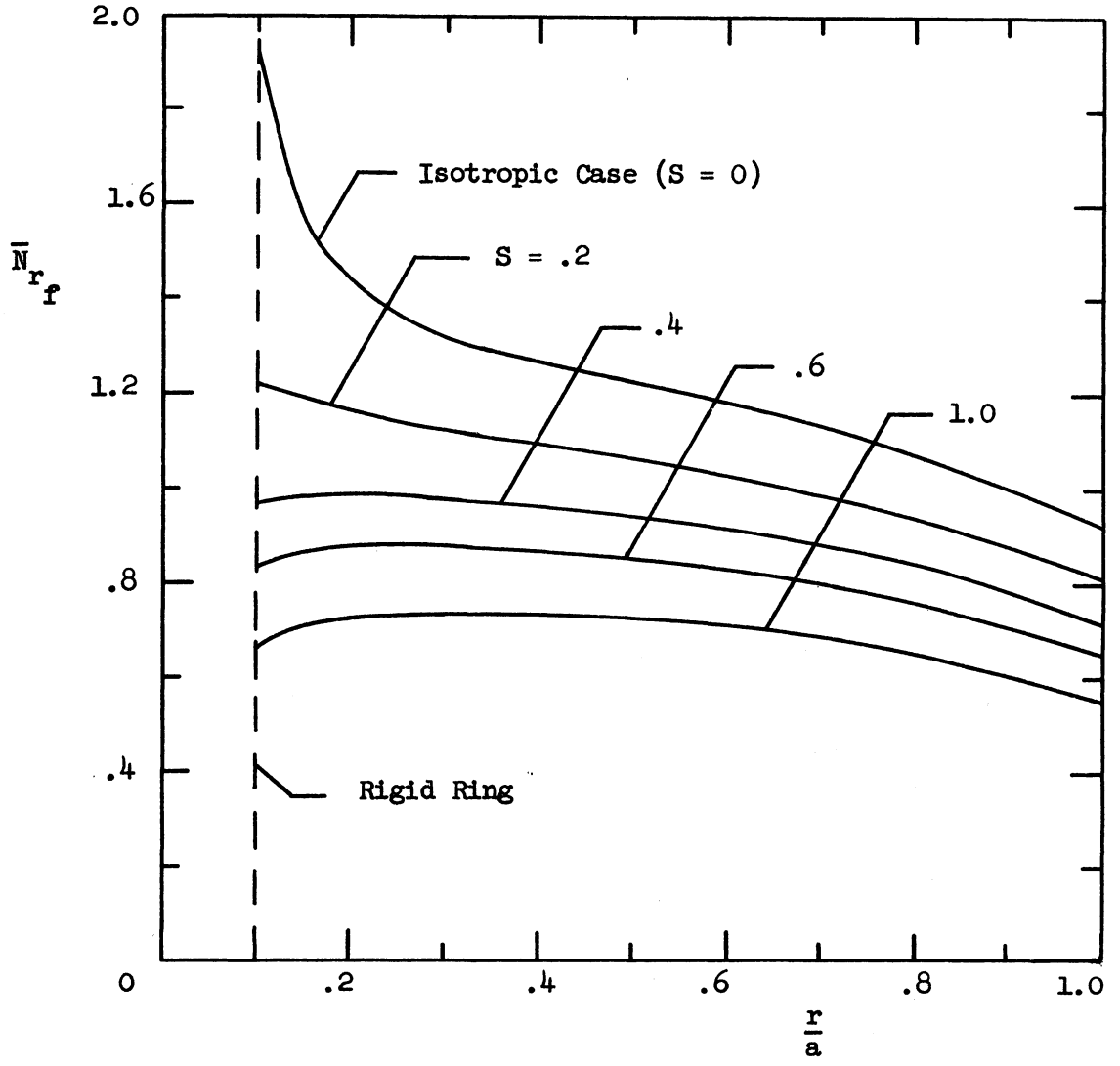

Figure 23.- Effect on meridional stress resultant of adding meridional stiffening cords to a pressurized membrane with a rigid ring insert.

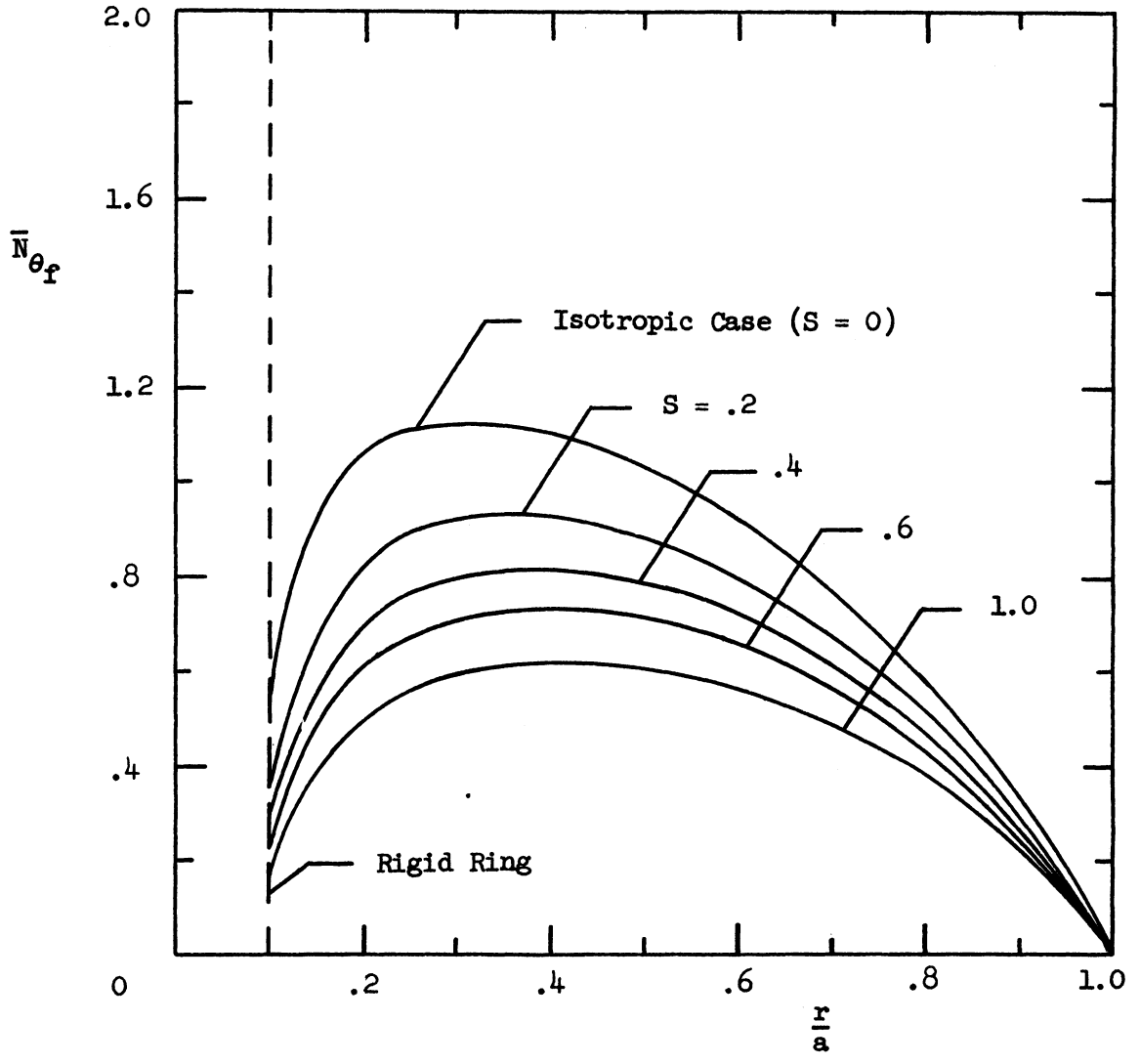

Figure 24.- Effect on circumferential stress resultant of adding meridional stiffening cords to a pressurized membrane with a rigid ring insert.

with no stiffening. It can be seen that a considerable stress concentration, as should be expected around a rigid insert, results. As meridional stiffening is added, however, the stress concentration is completely eliminated, as well as the stresses being lowered everywhere.

The two sample cases just presented demonstrate the application of the present analysis to membrane structures with closely spaced stiffening. The computer program which is presented in appendix C could be readily exercised for specific stiffened membrane configurations and it would be of considerable assistance in arriving at the optimum stiffening geometry.

APPENDIX C

COMPUTER PROGRAM FOR STIFFENED MEMBRANE

The listing for the Fortran IV program used in the analysis of a circular membrane stiffened with meridional and circumferential stiffening cords is presented in this appendix.

```
*    PROGRAM MESS2 (STIFFENED MEMBRANE ANALYSIS)

       PROGRAM MESS2(INPUT,OUTPUT,TAPE5=INPUT)

     1 FORMAT(1H1/////* DEXTER-MIKULAS      RDX124      FEBRUARY,1970.*/
      1///* INPUT DATA*//
      2* UGUESS(1) =*E16.8/* UGUESS(2) =*E16.8/*        NN =*I5/
      3*        ETA =*E16.8/*          S =*E16.8/*        MU =*E16.8/
      4*         E1 =*E16.8/*         E2 =*E16.8/*         M =*I5/)
     2 FORMAT(//*     I*,7X*N*,7X*RHO(I)*,14X*B(I)*,16X*NTHETA(I)*,11X*NR(
      1I)*,15X*L(I)*,16X*U(I)*/)
     3 FORMAT(/I5,F9.1,E20.8)
     4 FORMAT(34XE20.8)
     9 FORMAT(54X4E20.8//)
    10 FORMAT(114XE20.8)
     5 FORMAT(/* F(1) =*E16.8,5X*F(2) =*E16.8,5X*DEL =*E16.8,
      15X*UGUESS(2) =*E16.8)
     6 FORMAT(/* CONVERGENCE MET*)
     7 FORMAT(//* LIMIT REACHED WITHOUT CONVERGENCE*)
   500 FORMAT(I5,F9.1,5E20.8)
   503 FORMAT(I5,F9.1,E20.8,80X,E20.8)

       DIMENSION NTHETA(2002),NR(2002),UGUESS(2),F(2),ELL(2002)
       REAL N,NR,MU,NTHETA
       EXTERNAL FOFX
       COMMON/BLK1/I,U(2002),B(2002),RHO(2002),MU,EPS,S,ETA
       NAMELIST/INPUT/UGUESS,NN,IPRINT,ETA,S,MU,E1,E2,M

*    INPUT VARIABLES

*       UGUESS(1) - INITIAL GUESS FOR NEWTON-RAPHSON TECHNIQJE
*       UGUESS(2) - SECOND GUESS FOR NEWTON-RAPHSON TECHNIQUE
*               M - INITIAL STATION
*              NN - FINAL STATION
*             ETA - RATIO OF HOOP STIFFENING TO MERIDIONAL STIFFENING
*               S - NONDIMENSIONAL CORD STIFFNESS
*              MU - POISSONS RATIO
*           E1,E2 - CONVERGENCE CRITERIA FOR SUBROUTINE ITR2 (E2 LESS THAN E1)
*          IPRINT - OUTPUT CODE
*                   0 - PRINT RESULTS ONLY
*                   1 - PRINT INTERMEDIATE INFORMATION
```

```
 5000 READ INPUT
      IF(EOF,5)5500,5600
 5500 STOP
 5600 CONTINUE
      KOUNT = 0
 5001 KOUNT = KOUNT+1
      PRINT 1, UGUESS,NN,ETA,S,MU,E1,E2,M
      IF(IPRINT.EQ.1) PRINT 2
      LIMIT = 2*(NN-M)+2
      EPS = 1./FLOAT(NN)
      K = 1
 1000 CONTINUE
      N = FLOAT(M)

C    I = 1 TO LIMIT    (LIMIT=2*(NN-M)+2)
C     ODD I - WHOLE STATIONS, CALCULATE B
C    EVEN I - HALF STATIONS, CALCULATE U
C    EVEN AND ODD - CALCULATE RHO

      DO 100 I=1,LIMIT
      RHO(I) = N*EPS
      IF(IPRINT.EQ.1) PRINT 3, I,N,RHO(I)
      N = N+1./2.
      IF(I.GT.2) GO TO 150
      GO TO(101,102),I
  101 B(1) = 0.
      IF(IPRINT.EQ.1) PRINT 4, B(I)
      GO TO 100
  102 U(2) = UGUESS(K)
      IF(IPRINT.EQ.1) PRINT 10, U(I)
      GO TO 100
  150 IF(MOD(I,2).NE.0) GO TO 155
      IF(I.NE.4) GO TO 275
      U(I) = 2.*EPS**2/(2.*(RHO(I-2)+S)+EPS)*(-(RHO(I-2)+S)*
     1(-3.*U(I-2)/EPS**2+B(I-1)**2/(2.*EPS))-U(I-2)/(2.*EPS)-(1.-MU)/8.*
     2B(I-1)**2+U(I-2)/RHO(I-2)**2*(RHO(I-2)+ETA*S))
      GO TO 250
  275 CONTINUE
      U(I) = 2.*EPS**2/(2.*(RHO(I-2)+S)+EPS)*(-(RHO(I-2)+S)*
     1((U(I-4)-2.*U(I-2))/EPS**2+(B(I-3)+B(I-1))*(-B(I-3)+B(I-1))/
     2(2.*EPS))+U(I-4)/(2.*EPS)-(1.-MU)/2.*((B(I-3)+B(I-1))/2.)**2+
     3U(I-2)/RHO(I-2)**2*(RHO(I-2)+ETA*S))
```

```
  250 CONTINUE
      NTHETA(I-1) =                    ((U(I-2)+U(I))/(2.*RHO(I-1))+
     1MU*((-U(I-2)+U(I))/EPS+.5*B(I-1)**2))*1./(1.-MU**2)
      NR(I-1) =                       ((-U(I-2)+U(I))/EPS+.5*B(I-1)**2+
     1MU*(U(I-2)+U(I))/(2.*RHO(I-1)))*1./(1.-MU**2)
      ELL(I-1) = 2.*3.14159265359*S/(1.-MU**2)*((-U(I-2)+U(I))/EPS+
     1.5*B(I-1)**2)
      IF(IPRINT.EQ.1) PRINT 9, NTHETA(I-1),NR(I-1),ELL(I-1),U(I)
      GO TO 100
  155 CONTINUE
      B1 = -40.
      B2 = 40.
      MAXI = 1000
      DEL = (B2-B1)/1000.

*   LIBRARY SUBROUTINE ITR2
*      TO FIND X FOR GIVEN F(X)=0 WITHIN A GIVEN EPSILON
*      OF RELATIVE ERROR (E1,E2) IN A GIVEN INTERVAL (B1,B2)

      CALL ITR2(B(I),B1,B2,DEL,FOFX,E1,E2,MAXI,ICODE)
      IF(ICODE.NE.0) GO TO 2000
      IF(IPRINT.EQ.1) PRINT 4, B(I)
  100 CONTINUE

C   CONDITION TO BE SATISFIED AT EDGE OF MEMBRANE, HOOP STRESS MUST EQUAL ZERO

      F(K) =((1.+ETA*S/RHO(LIMIT-1))/(2.*RHO(LIMIT-1))*(U(LIMIT-2)+
     1U(LIMIT))+MU/EPS*(-U(LIMIT-2)+U(LIMIT))+MU/2.*B(LIMIT-1)**2)*
     21./(1.-MU**2)
      IF(K.NE.1) GO TO 200
      K = 2
      GO TO 1000
  200 CONTINUE
      IF(ABS(F(K)).LT.1.E-5) GO TO 300

C   NEWTON-RAPHSON TECHNIQUE TO DETERMINE NEXT GUESS

      DEL = -F(2)/((F(2)-F(1))/(UGUESS(2)-UGUESS(1)))
      PRINT 5, F,DEL,UGUESS(2)
      F(1) = F(2)
      UGUESS(1) = UGUESS(2)
      UGUESS(2) = UGUESS(2)+DEL
      PRINT 7
```

```
      GO TO 1000
  300 CONTINUE
      PRINT 6
      PRINT 5, F,DEL,UGUESS(2)
      PRINT 2
      N = FLOAT(M)
      DO 550 I=1,LIMIT
      IF(MOD(I,2).EQ.0) GO TO 501
      PRINT 500, I,N,RHO(I),B(I),NTHETA(I),VR(I),ELL(I)
      GO TO 502
  501 PRINT 503, I,N,RHO(I),U(I)
  502 N = N+.5
  550 CONTINUE
      GO TO 5000
 2000 PRINT 8, ICODE
    8 FORMAT(//* ERROR RETURN FROM ITR2    ICODE =*I3)
      STOP
      END
```

```
      FUNCTION FOFX(BB)

C    USER WRITTEN FUNCTION SUBPROGRAM FOR LIBRARY SUBROUTINE ITR2
C       ESTABLISHES FUNCTION F(X)=0

    1 FORMAT(* BB =*E16.8,*   UU =*E16.8,*   FOFX =*E16.8)
      REAL MU
      COMMON/BLK1/I,U(2002),B(2002),RHO(2002),MU,EPS,S,ETA
      IF(I.NE.3) GO TO 100
      UU = 2.*EPS**2/(2.*(RHO(I-1)+S)+EPS)*(-(RHO(I-1)+S)*
     1(-3.*U(I-1)/EPS**2+    BB**2/(2.*EPS))-U(I-1)/(2.*EPS)-(1.-MU)/8.*
     1BB**2+
     2U(I-1)/RHO(I-1)**2*(RHO(I-1)+ETA*S))
      GO TO 150
  100 CONTINUE
      UU = 2.*EPS**2/(2.*(RHO(I-1)+S)+EPS)*
     1(-(RHO(I-1)+S)*((U(I-3)-2.*U(I-1))/EPS**2+(B(I-2)+BB)*
     2(-B(I-2)+BB)/(2.*EPS))+U(I-3)/(2.*EPS)-(1.-MU)/2.*((B(I-2)+BB)/
     32.)**2+U(I-1)/RHO(I-1)**2*(RHO(I-1)+ETA*S))
  150 CONTINUE
      FOFX = -SQRT(8.)*RHO(I)**2*(1.-MU**2)-((RHO(I)+S)*(-U(I-1)/EPS
     1+UU/EPS+.5*BB**2)+MU/2.*(U(I-1)+UU))*BB
      RETURN
      END
```

DEXTER-MIKULAS RDX124 FEBRUARY,1970.

INPUT DATA

UGUESS(1) = 3.70000000E-03
UGUESS(2) = 3.60000000E-03
NN = 100
ETA = 0.
S = 2.00000000E-01
MU = 3.00000000E-01
E1 = 1.00000000E-09
E2 = 1.00000000E-10
M = 0

F(1) = -1.03396919E-01 F(2) = -2.37264022E-01 DEL = 1.77238483E-04 UGUESS(2) = 3.60000000E-03

LIMIT REACHED WITHOUT CONVERGENCE

F(1) = -2.37264022E-01 F(2) = -1.07355279E-02 DEL = 8.39959975E-06 UGUESS(2) = 3.77723848E-03

LIMIT REACHED WITHOUT CONVERGENCE

F(1) = -1.07355279E-02 F(2) = -1.14090862E-03 DEL = 9.98807294E-07 UGUESS(2) = 3.78563808E-03

LIMIT REACHED WITHOUT CONVERGENCE

CONVERGENCE MET

F(1) = -1.14090862E-03 F(2) = -5.87079914E-06 DEL = 8.00000000E-02 UGUESS(2) = 3.78663689E-03

I	N	RHO(I)	B(I)	NTHETA(I)	NR(I)	L(I)	U(I)
1	0.0	0.	0.	IIIII	IIIII	IIIII	
2	.5	5.00000000E-03					3.78663689E-0
3	1.0	1.00000000E-02	-1.59559666E-03	1.08189557E+00	1.08189607E+00	1.04580843E+00	
4	1.5	1.50000000E-02					1.13598981E-0
5	2.0	2.00000000E-02	-6.01525790E-03	1.08189071E+00	1.08189478E+00	1.04580867E+00	
6	2.5	2.50000000E-02					1.89329929E-0

7	3.0	3.00000000E-02	-1.27981558E-02	1.08187459E+00	1.08189043E+00	1.04580934E+00	
8	3.5	3.50000000E-02					2.65054545E-0
9	4.0	4.00000000E-02	-2.15785727E-02	1.08183749E+00	1.08188033E+00	1.04581076E+00	
10	4.5	4.50000000E-02					3.40764171E-0
11	5.0	5.00000000E-02	-3.20626010E-02	1.08176848E+00	1.08186147E+00	1.04581331E+00	
12	5.5	5.50000000E-02					4.16445864E-0
13	6.0	6.00000000E-02	-4.40113916E-02	1.08165613E+00	1.08183078E+00	1.04581747E+00	
14	6.5	6.50000000E-02					4.92082407E-0
15	7.0	7.00000000E-02	-5.72288995E-02	1.08148906E+00	1.08178518E+00	1.04582371E+00	
16	7.5	7.50000000E-02					5.67652496E-0
17	8.0	8.00000000E-02	-7.15527769E-02	1.08125620E+00	1.08172172E+00	1.04583255E+00	
18	8.5	8.50000000E-02					6.43130992E-0
19	9.0	9.00000000E-02	-8.68475098E-02	1.08094694E+00	1.08163756E+00	1.04584445E+00	
20	9.5	9.50000000E-02					7.18489215E-0
21	10.0	1.00000000E-01	-1.02999176E-01	1.08055123E+00	1.08153002E+00	1.04585988E+00	
22	10.5	1.05000000E-01					7.93695239E-0
23	11.0	1.10000000E-01	-1.19911396E-01	1.08005961E+00	1.08139655E+00	1.04587924E+00	
24	11.5	1.15000000E-01					8.68714169E-0
25	12.0	1.20000000E-01	-1.37502168E-01	1.07946317E+00	1.08123476E+00	1.04590291E+00	
26	12.5	1.25000000E-01					9.43508408E-0
27	13.0	1.30000000E-01	-1.55701369E-01	1.07875360E+00	1.08104238E+00	1.04593120E+00	
28	13.5	1.35000000E-01					1.01803789E-0
29	14.0	1.40000000E-01	-1.74448772E-01	1.07792311E+00	1.08081727E+00	1.04596439E+00	
30	14.5	1.45000000E-01					1.09226031E-0
31	15.0	1.50000000E-01	-1.93692441E-01	1.07696442E+00	1.08055741E+00	1.04600271E+00	
32	15.5	1.55000000E-01					1.16613128E-0
33	16.0	1.60000000E-01	-2.13387443E-01	1.07587071E+00	1.08026089E+00	1.04604634E+00	
34	16.5	1.65000000E-01					1.23960454E-0
35	17.0	1.70000000E-01	-2.33494790E-01	1.07463560E+00	1.07992591E+00	1.04609543E+00	
36	17.5	1.75000000E-01					1.31263207E-0
37	18.0	1.80000000E-01	-2.53980574E-01	1.07325308E+00	1.07955073E+00	1.04615008E+00	
38	18.5	1.85000000E-01					1.38516424E-0
39	19.0	1.90000000E-01	-2.74815245E-01	1.07171753E+00	1.07913372E+00	1.04621038E+00	
40	19.5	1.95000000E-01					1.45714992E-0
41	20.0	2.00000000E-01	-2.95973022E-01	1.07002361E+00	1.07867333E+00	1.04627636E+00	
42	20.5	2.05000000E-01					1.52853654E-0
43	21.0	2.10000000E-01	-3.17431390E-01	1.06816632E+00	1.07816807E+00	1.04634806E+00	
44	21.5	2.15000000E-01					1.59927022E-0
45	22.0	2.20000000E-01	-3.39170682E-01	1.06614087E+00	1.07761650E+00	1.04642548E+00	
46	22.5	2.25000000E-01					1.66929581E-0
47	23.0	2.30000000E-01	-3.61173722E-01	1.06394273E+00	1.07701726E+00	1.04650862E+00	
48	23.5	2.35000000E-01					1.73855693E-0
49	24.0	2.40000000E-01	-3.83425533E-01	1.06156758E+00	1.07636903E+00	1.04659743E+00	
50	24.5	2.45000000E-01					1.80699605E-0
51	25.0	2.50000000E-01	-4.05913070E-01	1.05901127E+00	1.07567055E+00	1.04669190E+00	
52	25.5	2.55000000E-01					1.87455449E-0
53	26.0	2.60000000E-01	-4.28625008E-01	1.05626983E+00	1.07492059E+00	1.04679198E+00	
54	26.5	2.65000000E-01					1.94117249E-0
55	27.0	2.70000000E-01	-4.51551551E-01	1.05333940E+00	1.07411796E+00	1.04689762E+00	
56	27.5	2.75000000E-01					2.00678916E-0
57	28.0	2.80000000E-01	-4.74684273E-01	1.05021626E+00	1.07326152E+00	1.04700879E+00	

58	28.5	2.85000000E-01					2.07134257E-0
59	29.0	2.90000000E-01	-4.98015973E-01	1.04689681E+00	1.07235015E+00	1.04712543E+00	
60	29.5	2.95000000E-01					2.13476968E-0
61	30.0	3.00000000E-01	-5.21540560E-01	1.04337751E+00	1.07138275E+00	1.04724750E+00	
62	30.5	3.05000000E-01					2.19700640E-0
63	31.0	3.10000000E-01	-5.45252944E-01	1.03965489E+00	1.07035828E+00	1.04737496E+00	
64	31.5	3.15000000E-01					2.25798755E-0
65	32.0	3.20000000E-01	-5.69148943E-01	1.03572557E+00	1.06927567E+00	1.04750780E+00	
66	32.5	3.25000000E-01					2.31764682E-0
67	33.0	3.30000000E-01	-5.93225208E-01	1.03158618E+00	1.06813392E+00	1.04764597E+00	
68	33.5	3.35000000E-01					2.37591682E-0
69	34.0	3.40000000E-01	-6.17479150E-01	1.02723340E+00	1.06693201E+00	1.04778949E+00	
70	34.5	3.45000000E-01					2.43272899E-0
71	35.0	3.50000000E-01	-6.41908880E-01	1.02266392E+00	1.06566896E+00	1.04793834E+00	
72	35.5	3.55000000E-01					2.48801362E-0
73	36.0	3.60000000E-01	-6.66513156E-01	1.01787444E+00	1.06434379E+00	1.04809255E+00	
74	36.5	3.65000000E-01					2.54169978E-0
75	37.0	3.70000000E-01	-6.91291339E-01	1.01286167E+00	1.06295553E+00	1.04825215E+00	
76	37.5	3.75000000E-01					2.59371529E-0
77	38.0	3.80000000E-01	-7.16243349E-01	1.00762228E+00	1.06150322E+00	1.04841718E+00	
78	38.5	3.85000000E-01					2.64398672E-0
79	39.0	3.90000000E-01	-7.41369631E-01	1.00215295E+00	1.05998591E+00	1.04858771E+00	
80	39.5	3.95000000E-01					2.69243928E-0
81	40.0	4.00000000E-01	-7.66671126E-01	9.96450306E-01	1.05840265E+00	1.04876383E+00	
82	40.5	4.05000000E-01					2.73899680E-0
83	41.0	4.10000000E-01	-7.92149247E-01	9.90510934E-01	1.05675250E+00	1.04894564E+00	
84	41.5	4.15000000E-01					2.78358170E-0
85	42.0	4.20000000E-01	-8.17805847E-01	9.84331374E-01	1.05503450E+00	1.04913327E+00	
86	42.5	4.25000000E-01					2.82611489E-0
87	43.0	4.30000000E-01	-8.43643211E-01	9.77908107E-01	1.05324771E+00	1.04932686E+00	
88	43.5	4.35000000E-01					2.86651573E-0
89	44.0	4.40000000E-01	-8.69664029E-01	9.71237544E-01	1.05139118E+00	1.04952659E+00	
90	44.5	4.45000000E-01					2.90470194E-0
91	45.0	4.50000000E-01	-8.95871395E-01	9.64316022E-01	1.04946395E+00	1.04973266E+00	
92	45.5	4.55000000E-01					2.94058958E-0
93	46.0	4.60000000E-01	-9.22268785E-01	9.57139789E-01	1.04746506E+00	1.04994530E+00	
94	46.5	4.65000000E-01					2.97409291E-0
95	47.0	4.70000000E-01	-9.48860047E-01	9.49705003E-01	1.04539354E+00	1.05016474E+00	
96	47.5	4.75000000E-01					3.00512434E-0
97	48.0	4.80000000E-01	-9.75649410E-01	9.42007721E-01	1.04324841E+00	1.05039129E+00	
98	48.5	4.85000000E-01					3.03359436E-0
99	49.0	4.90000000E-01	-1.00264146E+00	9.34043885E-01	1.04102867E+00	1.05062524E+00	
100	49.5	4.95000000E-01					3.05941142E-0
101	50.0	5.00000000E-01	-1.02984115E+00	9.25809324E-01	1.03873333E+00	1.05086693E+00	
102	50.5	5.05000000E-01					3.08248183E-0
103	51.0	5.10000000E-01	-1.05725379E+00	9.17299735E-01	1.03636136E+00	1.05111675E+00	
104	51.5	5.15000000E-01					3.10270970E-0
105	52.0	5.20000000E-01	-1.08488505E+00	9.08510681E-01	1.03391174E+00	1.05137511E+00	
106	52.5	5.25000000E-01					3.11999677E-0
107	53.0	5.30000000E-01	-1.11274099E+00	8.99437578E-01	1.03138339E+00	1.05164244E+00	
108	53.5	5.35000000E-01					3.13424236E-0

109	54.0	5.40000000E-01	-1.14082800E+00	8.90075687E-01	1.02877527E+00	1.05191923E+00	
110	54.5	5.45000000E-01					3.14534319E-0
111	55.0	5.50000000E-01	-1.16915287E+00	8.80420105E-01	1.02608627E+00	1.05220601E+00	
112	55.5	5.55000000E-01					3.15319329E-0
113	56.0	5.60000000E-01	-1.19772277E+00	8.70465754E-01	1.02331527E+00	1.05250334E+00	
114	56.5	5.65000000E-01					3.15768385E-0
115	57.0	5.70000000E-01	-1.22654524E+00	8.60207372E-01	1.02046114E+00	1.05281181E+00	
116	57.5	5.75000000E-01					3.15870308E-0
117	58.0	5.80000000E-01	-1.25562825E+00	8.49639498E-01	1.01752271E+00	1.05313210E+00	
118	58.5	5.85000000E-01					3.15613605E-0
119	59.0	5.90000000E-01	-1.28498016E+00	8.38756468E-01	1.01449879E+00	1.05346488E+00	
120	59.5	5.95000000E-01					3.14986454E-0
121	60.0	6.00000000E-01	-1.31460976E+00	8.27552396E-01	1.01138816E+00	1.05381092E+00	
122	60.5	6.05000000E-01					3.13976684E-0
123	61.0	6.10000000E-01	-1.34452628E+00	8.16021166E-01	1.00818955E+00	1.05417102E+00	
124	61.5	6.15000000E-01					3.12571762E-0
125	62.0	6.20000000E-01	-1.37473941E+00	8.04156417E-01	1.00490169E+00	1.05454602E+00	
126	62.5	6.25000000E-01					3.10758767E-0
127	63.0	6.30000000E-01	-1.40525932E+00	7.91951530E-01	1.00152324E+00	1.05493684E+00	
128	63.5	6.35000000E-01					3.08524376E-0
129	64.0	6.40000000E-01	-1.43609667E+00	7.79399614E-01	9.98052845E-01	1.05534446E+00	
130	64.5	6.45000000E-01					3.05854838E-0
131	65.0	6.50000000E-01	-1.46726263E+00	7.66493491E-01	9.94489103E-01	1.05576992E+00	
132	65.5	6.55000000E-01					3.02735950E-0
133	66.0	6.60000000E-01	-1.49876893E+00	7.53225676E-01	9.90830569E-01	1.05621431E+00	
134	66.5	6.65000000E-01					2.99153037E-0
135	67.0	6.70000000E-01	-1.53062786E+00	7.39588367E-01	9.87075754E-01	1.05667882E+00	
136	67.5	6.75000000E-01					2.95090921E-0
137	68.0	6.80000000E-01	-1.56285232E+00	7.25573420E-01	9.83223122E-01	1.05716470E+00	
138	68.5	6.85000000E-01					2.90533895E-0
139	69.0	6.90000000E-01	-1.59545583E+00	7.11172332E-01	9.79271088E-01	1.05767329E+00	
140	69.5	6.95000000E-01					2.85465693E-0
141	70.0	7.00000000E-01	-1.62845258E+00	6.96376224E-01	9.75218013E-01	1.05820599E+00	
142	70.5	7.05000000E-01					2.79869455E-0
143	71.0	7.10000000E-01	-1.66185746E+00	6.81175811E-01	9.71062203E-01	1.05876431E+00	
144	71.5	7.15000000E-01					2.73727699E-0
145	72.0	7.20000000E-01	-1.69568611E+00	6.65561388E-01	9.66801906E-01	1.05934986E+00	
146	72.5	7.25000000E-01					2.67022277E-0
147	73.0	7.30000000E-01	-1.72995495E+00	6.49522796E-01	9.62435307E-01	1.05996434E+00	
148	73.5	7.35000000E-01					2.59734341E-0
149	74.0	7.40000000E-01	-1.76468125E+00	6.33049400E-01	9.57960527E-01	1.06060956E+00	
150	74.5	7.45000000E-01					2.51844298E-0
151	75.0	7.50000000E-01	-1.79988316E+00	6.16130062E-01	9.53375617E-01	1.06128744E+00	
152	75.5	7.55000000E-01					2.43331767E-0
153	76.0	7.60000000E-01	-1.83557977E+00	5.98753103E-01	9.48678556E-01	1.06200003E+00	
154	76.5	7.65000000E-01					2.34175528E-0
155	77.0	7.70000000E-01	-1.87179119E+00	5.80906277E-01	9.43867246E-01	1.06274951E+00	
156	77.5	7.75000000E-01					2.24353470E-0
157	78.0	7.80000000E-01	-1.90853858E+00	5.62576729E-01	9.38939507E-01	1.06353819E+00	
158	78.5	7.85000000E-01					2.13842538E-0
159	79.0	7.90000000E-01	-1.94584428E+00	5.43750962E-01	9.33893073E-01	1.06436853E+00	

160	79.5	7.95000000E-01					2.02618666E-0
161	80.0	8.00000000E-01	-1.98373184E+00	5.24414791E-01	9.28725589E-01	1.06524316E+00	
162	80.5	8.05000000E-01					1.90656717E-0
163	81.0	8.10000000E-01	-2.02222610E+00	5.04553299E-01	9.23434601E-01	1.06616487E+00	
164	81.5	8.15000000E-01					1.77930411E-0
165	82.0	8.20000000E-01	-2.06135333E+00	4.84150790E-01	9.18017555E-01	1.06713663E+00	
166	82.5	8.25000000E-01					1.64412247E-0
167	83.0	8.30000000E-01	-2.10114131E+00	4.63190732E-01	9.12471787E-01	1.06816162E+00	
168	83.5	8.35000000E-01					1.50073418E-0
169	84.0	8.40000000E-01	-2.14161943E+00	4.41655705E-01	9.06794520E-01	1.06924321E+00	
170	84.5	8.45000000E-01					1.34883728E-0
171	85.0	8.50000000E-01	-2.18281882E+00	4.19527334E-01	9.00982855E-01	1.07038502E+00	
172	85.5	8.55000000E-01					1.18811484E-0
173	86.0	8.60000000E-01	-2.22477251E+00	3.96786224E-01	8.95033762E-01	1.07159089E+00	
174	86.5	8.65000000E-01					1.01823399E-0
175	87.0	8.70000000E-01	-2.26751554E+00	3.73411884E-01	8.88944075E-01	1.07286495E+00	
176	87.5	8.75000000E-01					8.38844708E-0
177	88.0	8.80000000E-01	-2.31108514E+00	3.49382648E-01	8.82710482E-01	1.07421159E+00	
178	88.5	8.85000000E-01					6.49578551E-0
179	89.0	8.90000000E-01	-2.35552091E+00	3.24675587E-01	8.76329513E-01	1.07563553E+00	
180	89.5	8.95000000E-01					4.50047297E-0
181	90.0	9.00000000E-01	-2.40086501E+00	2.99266411E-01	8.69797533E-01	1.07714180E+00	
182	90.5	9.05000000E-01					2.39841418E-0
183	91.0	9.10000000E-01	-2.44716241E+00	2.73129364E-01	8.63110730E-01	1.07873581E+00	
184	91.5	9.15000000E-01					1.85284164E-0
185	92.0	9.20000000E-01	-2.49446108E+00	2.46237108E-01	8.56265100E-01	1.08042336E+00	
186	92.5	9.25000000E-01					-2.14348990E-0
187	93.0	9.30000000E-01	-2.54281228E+00	2.18560594E-01	8.49256438E-01	1.08221067E+00	
188	93.5	9.35000000E-01					-4.59274879E-0
189	94.0	9.40000000E-01	-2.59227089E+00	1.90068925E-01	8.42080321E-01	1.08410444E+00	
190	94.5	9.45000000E-01					-7.16762332E-0
191	95.0	9.50000000E-01	-2.64289568E+00	1.60729195E-01	8.34732090E-01	1.08611187E+00	
192	95.5	9.55000000E-01					-9.87355877E-0
193	96.0	9.60000000E-01	-2.69474972E+00	1.30506319E-01	8.27206839E-01	1.08824071E+00	
194	96.5	9.65000000E-01					-1.27163419E-0
195	97.0	9.70000000E-01	-2.74790079E+00	9.93628446E-02	8.19499389E-01	1.09049933E+00	
196	97.5	9.75000000E-01					-1.57021307E-0
197	98.0	9.80000000E-01	-2.80242182E+00	6.72587365E-02	8.11604271E-01	1.09289677E+00	
198	98.5	9.85000000E-01					-1.88374881E-0
199	99.0	9.90000000E-01	-2.85839144E+00	3.41511424E-02	8.03515704E-01	1.09544279E+00	
200	99.5	9.95000000E-01					-2.21294185E-0
201	100.0	1.00000000E+00	-2.91589451E+00	-5.87079914E-06	7.95227567E-01	1.09814796E+00	
202	100.5	1.00500000E+00					-2.55854096E-0

```
DEXTER-MIKULAS      RDX124      FEBRUARY,1970.


INPUT DATA

UGUESS(1) =  5.00000000E-03
UGUESS(2) =  4.00000000E-03
       NN =  100
      ETA =  0.
        S =  0.
       MU =  3.00000000E-01
       E1 =  1.00000000E-09
       E2 =  1.00000000E-10
        M =    0

F(1) =  5.02644542E-01     F(2) = -9.64484385E-01     DEL =  6.57395793E-04     UGUESS(2) =  4.00000000E-03

LIMIT REACHED WITHOUT CONVERGENCE

F(1) = -9.64484385E-01     F(2) =  1.83550531E-01     DEL = -1.05105991E-04     UGUESS(2) =  4.65739579E-03

LIMIT REACHED WITHOUT CONVERGENCE

F(1) =  1.83550531E-01     F(2) =  6.42579832E-02     DEL = -5.66162688E-05     UGUESS(2) =  4.55228980E-03

LIMIT REACHED WITHOUT CONVERGENCE

F(1) =  6.42579832E-02     F(2) = -5.84799816E-03     DEL =  4.72273306E-06     UGUESS(2) =  4.49567353E-03

LIMIT REACHED WITHOUT CONVERGENCE

F(1) = -5.84799816E-03     F(2) =  1.76589496E-04     DEL = -1.38430230E-07     UGUESS(2) =  4.50039627E-03

LIMIT REACHED WITHOUT CONVERGENCE

CONVERGENCE MET

F(1) =  1.76589496E-04     F(2) =  4.76541336E-07     DEL =  8.00000000E-02     UGUESS(2) =  4.50025784E-03
```

I	N	RHO(I)	B(I)	NTHETA(I)	NR(I)	L(I)	U(I)
1	0.0	0.	0.	IIIII	IIIII	IIIII	
2	.5	5.00000000E-03					4.50025784E-0
3	1.0	1.00000000E-02	-2.19965996E-02	1.28572415E+00	1.28584744E+00	0.	
4	1.5	1.50000000E-02					1.34991405E-0
5	2.0	2.00000000E-02	-4.39949728E-02	1.28549085E+00	1.28579560E+00	0.	
6	2.5	2.50000000E-02					2.24909462E-0
7	3.0	3.00000000E-02	-6.59990228E-02	1.28506047E+00	1.28566773E+00	0.	
8	3.5	3.50000000E-02					3.14706627E-0
9	4.0	4.00000000E-02	-8.80120494E-02	1.28444176E+00	1.28547268E+00	0.	
10	4.5	4.50000000E-02					4.04333336E-0
11	5.0	5.00000000E-02	-1.10037258E-01	1.28363749E+00	1.28521338E+00	0.	
12	5.5	5.50000000E-02					4.93740139E-0
13	6.0	6.00000000E-02	-1.32077827E-01	1.28264875E+00	1.28489112E+00	0.	
14	6.5	6.50000000E-02					5.82877561E-0
15	7.0	7.00000000E-02	-1.54136930E-01	1.28147596E+00	1.28450657E+00	0.	
16	7.5	7.50000000E-02					6.71696029E-0
17	8.0	8.00000000E-02	-1.76217743E-01	1.28011919E+00	1.28406009E+00	0.	
18	8.5	8.50000000E-02					7.60145828E-0
19	9.0	9.00000000E-02	-1.98323455E-01	1.27857827E+00	1.28355187E+00	0.	
20	9.5	9.50000000E-02					8.48177056E-0
21	10.0	1.00000000E-01	-2.20457271E-01	1.27685293E+00	1.28298201E+00	0.	
22	10.5	1.05000000E-01					9.35739599E-0
23	11.0	1.10000000E-01	-2.42622414E-01	1.27494275E+00	1.28235054E+00	0.	
24	11.5	1.15000000E-01					1.02278309E-0
25	12.0	1.20000000E-01	-2.64822130E-01	1.27284722E+00	1.28165745E+00	0.	
26	12.5	1.25000000E-01					1.10925688E-0
27	13.0	1.30000000E-01	-2.87059694E-01	1.27056576E+00	1.28090266E+00	0.	
28	13.5	1.35000000E-01					1.19511001E-0
29	14.0	1.40000000E-01	-3.09338406E-01	1.26809769E+00	1.28008611E+00	0.	
30	14.5	1.45000000E-01					1.28029118E-0
31	15.0	1.50000000E-01	-3.31661601E-01	1.26544227E+00	1.27920768E+00	0.	
32	15.5	1.55000000E-01					1.36474871E-0
33	16.0	1.60000000E-01	-3.54032650E-01	1.26259868E+00	1.27826725E+00	0.	
34	16.5	1.65000000E-01					1.44843052E-0
35	17.0	1.70000000E-01	-3.76454959E-01	1.25956604E+00	1.27726465E+00	0.	
36	17.5	1.75000000E-01					1.53128408E-0
37	18.0	1.80000000E-01	-3.98931978E-01	1.25634339E+00	1.27619973E+00	0.	
38	18.5	1.85000000E-01					1.61325642E-0
39	19.0	1.90000000E-01	-4.21467203E-01	1.25292970E+00	1.27507230E+00	0.	
40	19.5	1.95000000E-01					1.69429403E-0
41	20.0	2.00000000E-01	-4.44064173E-01	1.24932387E+00	1.27388215E+00	0.	
42	20.5	2.05000000E-01					1.77434288E-0
43	21.0	2.10000000E-01	-4.66726484E-01	1.24552473E+00	1.27262908E+00	0.	
44	21.5	2.15000000E-01					1.85334836E-0
45	22.0	2.20000000E-01	-4.89457783E-01	1.24153104E+00	1.27131285E+00	0.	
46	22.5	2.25000000E-01					1.93125527E-0
47	23.0	2.30000000E-01	-5.12261775E-01	1.23734149E+00	1.26993321E+00	0.	

48	23.5	2.35000000E-01					2.00800774E-0
49	24.0	2.40000000E-01	-5.35142228E-01	1.23295467E+00	1.26848990E+00	0.	
50	24.5	2.45000000E-01					2.08354923E-0
51	25.0	2.50000000E-01	-5.58102976E-01	1.22836913E+00	1.26698264E+00	0.	
52	25.5	2.55000000E-01					2.15782247E-0
53	26.0	2.60000000E-01	-5.81147920E-01	1.22358333E+00	1.26541114E+00	0.	
54	26.5	2.65000000E-01					2.23076944E-0
55	27.0	2.70000000E-01	-6.04281036E-01	1.21859563E+00	1.26377510E+00	0.	
56	27.5	2.75000000E-01					2.30233130E-0
57	28.0	2.80000000E-01	-6.27506377E-01	1.21340434E+00	1.26207418E+00	0.	
58	28.5	2.85000000E-01					2.37244838E-0
59	29.0	2.90000000E-01	-6.50828077E-01	1.20800767E+00	1.26030805E+00	0.	
60	29.5	2.95000000E-01					2.44106009E-0
61	30.0	3.00000000E-01	-6.74250359E-01	1.20240375E+00	1.25847636E+00	0.	
62	30.5	3.05000000E-01					2.50810494E-0
63	31.0	3.10000000E-01	-6.97777533E-01	1.19659061E+00	1.25657873E+00	0.	
64	31.5	3.15000000E-01					2.57352042E-0
65	32.0	3.20000000E-01	-7.21414008E-01	1.19056622E+00	1.25461479E+00	0.	
66	32.5	3.25000000E-01					2.63724300E-0
67	33.0	3.30000000E-01	-7.45164291E-01	1.18432843E+00	1.25258411E+00	0.	
68	33.5	3.35000000E-01					2.69920807E-0
69	34.0	3.40000000E-01	-7.69032999E-01	1.17787500E+00	1.25048629E+00	0.	
70	34.5	3.45000000E-01					2.75934986E-0
71	35.0	3.50000000E-01	-7.93024856E-01	1.17120359E+00	1.24832089E+00	0.	
72	35.5	3.55000000E-01					2.81760142E-0
73	36.0	3.60000000E-01	-8.17144708E-01	1.16431179E+00	1.24608745E+00	0.	
74	36.5	3.65000000E-01					2.87389454E-0
75	37.0	3.70000000E-01	-8.41397522E-01	1.15719703E+00	1.24378550E+00	0.	
76	37.5	3.75000000E-01					2.92815969E-0
77	38.0	3.80000000E-01	-8.65788396E-01	1.14985669E+00	1.24141454E+00	0.	
78	38.5	3.85000000E-01					2.98032597E-0
79	39.0	3.90000000E-01	-8.90322564E-01	1.14228799E+00	1.23897408E+00	0.	
80	39.5	3.95000000E-01					3.03032102E-0
81	40.0	4.00000000E-01	-9.15005406E-01	1.13448807E+00	1.23646357E+00	0.	
82	40.5	4.05000000E-01					3.07807099E-0
83	41.0	4.10000000E-01	-9.39842448E-01	1.12645394E+00	1.23388247E+00	0.	
84	41.5	4.15000000E-01					3.12350043E-0
85	42.0	4.20000000E-01	-9.64839380E-01	1.11818247E+00	1.23123021E+00	0.	
86	42.5	4.25000000E-01					3.16653222E-0
87	43.0	4.30000000E-01	-9.90002058E-01	1.10967043E+00	1.22850620E+00	0.	
88	43.5	4.35000000E-01					3.20708753E-0
89	44.0	4.40000000E-01	-1.01533651E+00	1.10091445E+00	1.22570982E+00	0.	
90	44.5	4.45000000E-01					3.24508566E-0
91	45.0	4.50000000E-01	-1.04084896E+00	1.09191099E+00	1.22284045E+00	0.	
92	45.5	4.55000000E-01					3.28044405E-0
93	46.0	4.60000000E-01	-1.06654581E+00	1.08265642E+00	1.21989742E+00	0.	
94	46.5	4.65000000E-01					3.31307810E-0
95	47.0	4.70000000E-01	-1.09243367E+00	1.07314691E+00	1.21688006E+00	0.	
96	47.5	4.75000000E-01					3.34290113E-0
97	48.0	4.80000000E-01	-1.11851939E+00	1.06337852E+00	1.21378765E+00	0.	
98	48.5	4.85000000E-01					3.36982426E-0

99	49.0	4.90000000E-01	-1.14481000E+00	1.05334713E+00	1.21061948E+00	0.	
100	49.5	4.95000000E-01					3.39375630E-0
101	50.0	5.00000000E-01	-1.17131282E+00	1.04304843E+00	1.20737479E+00	0.	
102	50.5	5.05000000E-01					3.41460364E-0
103	51.0	5.10000000E-01	-1.19803537E+00	1.03247797E+00	1.20405279E+00	0.	
104	51.5	5.15000000E-01					3.43227014E-0
105	52.0	5.20000000E-01	-1.22498549E+00	1.02163111E+00	1.20065268E+00	0.	
106	52.5	5.25000000E-01					3.44665700E-0
107	53.0	5.30000000E-01	-1.25217125E+00	1.01050299E+00	1.19717361E+00	0.	
108	53.5	5.35000000E-01					3.45766263E-0
109	54.0	5.40000000E-01	-1.27960104E+00	9.99088599E-01	1.19361473E+00	0.	
110	54.5	5.45000000E-01					3.46518251E-0
111	55.0	5.50000000E-01	-1.30728355E+00	9.87382680E-01	1.18997513E+00	0.	
112	55.5	5.55000000E-01					3.46910903E-0
113	56.0	5.60000000E-01	-1.33522781E+00	9.75379775E-01	1.18625390E+00	0.	
114	56.5	5.65000000E-01					3.46933136E-0
115	57.0	5.70000000E-01	-1.36344318E+00	9.63074194E-01	1.18245065E+00	0.	
116	57.5	5.75000000E-01					3.46573527E-0
117	58.0	5.80000000E-01	-1.39193940E+00	9.50460012E-01	1.17856261E+00	0.	
118	58.5	5.85000000E-01					3.45820297E-0
119	59.0	5.90000000E-01	-1.42072657E+00	9.37531051E-01	1.17459055E+00	0.	
120	59.5	5.95000000E-01					3.44661289E-0
121	60.0	6.00000000E-01	-1.44981524E+00	9.24280871E-01	1.17053279E+00	0.	
122	60.5	6.05000000E-01					3.43083953E-0
123	61.0	6.10000000E-01	-1.47921636E+00	9.10702760E-01	1.16638823E+00	0.	
124	61.5	6.15000000E-01					3.41075322E-0
125	62.0	6.20000000E-01	-1.50894133E+00	8.96789714E-01	1.16215573E+00	0.	
126	62.5	6.25000000E-01					3.38621991E-0
127	63.0	6.30000000E-01	-1.53900207E+00	8.82534425E-01	1.15783411E+00	0.	
128	63.5	6.35000000E-01					3.35710092E-0
129	64.0	6.40000000E-01	-1.56941097E+00	8.67929268E-01	1.15342214E+00	0.	
130	64.5	6.45000000E-01					3.32325271E-0
131	65.0	6.50000000E-01	-1.60018100E+00	8.52966281E-01	1.14891854E+00	0.	
132	65.5	6.55000000E-01					3.28452662E-0
133	66.0	6.60000000E-01	-1.63132569E+00	8.37637145E-01	1.14432201E+00	0.	
134	66.5	6.65000000E-01					3.24076853E-0
135	67.0	6.70000000E-01	-1.66285918E+00	8.21933171E-01	1.13963118E+00	0.	
136	67.5	6.75000000E-01					3.19181862E-0
137	68.0	6.80000000E-01	-1.69479627E+00	8.05845273E-01	1.13484463E+00	0.	
138	68.5	6.85000000E-01					3.13751100E-0
139	69.0	6.90000000E-01	-1.72715244E+00	7.89363949E-01	1.12996089E+00	0.	
140	69.5	6.95000000E-01					3.07767339E-0
141	70.0	7.00000000E-01	-1.75994392E+00	7.72479258E-01	1.12497845E+00	0.	
142	70.5	7.05000000E-01					3.01212673E-0
143	71.0	7.10000000E-01	-1.79318773E+00	7.55180793E-01	1.11989572E+00	0.	
144	71.5	7.15000000E-01					2.94068477E-0
145	72.0	7.20000000E-01	-1.82690170E+00	7.37457653E-01	1.11471106E+00	0.	
146	72.5	7.25000000E-01					2.86315365E-0
147	73.0	7.30000000E-01	-1.86110458E+00	7.19298416E-01	1.10942277E+00	0.	
148	73.5	7.35000000E-01					2.77933147E-0
149	74.0	7.40000000E-01	-1.89581605E+00	7.00691104E-01	1.10402909E+00	0.	

150	74.5	7.45000000E-01					2.68900772E-0
151	75.0	7.50000000E-01	-1.93105684E+00	6.81623153E-01	1.09852817E+00	0.	
152	75.5	7.55000000E-01					2.59196281E-0
153	76.0	7.60000000E-01	-1.96684875E+00	6.62081373E-01	1.09291811E+00	0.	
154	76.5	7.65000000E-01					2.48796748E-0
155	77.0	7.70000000E-01	-2.00321474E+00	6.42051908E-01	1.08719691E+00	0.	
156	77.5	7.75000000E-01					2.37678215E-0
157	78.0	7.80000000E-01	-2.04017904E+00	6.21520195E-01	1.08136253E+00	0.	
158	78.5	7.85000000E-01					2.25815627E-0
159	79.0	7.90000000E-01	-2.07776720E+00	6.00470918E-01	1.07541279E+00	0.	
160	79.5	7.95000000E-01					2.13182760E-0
161	80.0	8.00000000E-01	-2.11600624E+00	5.78887954E-01	1.06934548E+00	0.	
162	80.5	8.05000000E-01					1.99752139E-0
163	81.0	8.10000000E-01	-2.15492471E+00	5.56754321E-01	1.06315824E+00	0.	
164	81.5	8.15000000E-01					1.85494955E-0
165	82.0	8.20000000E-01	-2.19455284E+00	5.34052118E-01	1.05684867E+00	0.	
166	82.5	8.25000000E-01					1.70380975E-0
167	83.0	8.30000000E-01	-2.23492266E+00	5.10762460E-01	1.05041421E+00	0.	
168	83.5	8.35000000E-01					1.54378433E-0
169	84.0	8.40000000E-01	-2.27606812E+00	4.86865408E-01	1.04385223E+00	0.	
170	84.5	8.45000000E-01					1.37453929E-0
171	85.0	8.50000000E-01	-2.31802531E+00	4.62339890E-01	1.03715997E+00	0.	
172	85.5	8.55000000E-01					1.19572302E-0
173	86.0	8.60000000E-01	-2.36083256E+00	4.37163621E-01	1.03033454E+00	0.	
174	86.5	8.65000000E-01					1.00696505E-0
175	87.0	8.70000000E-01	-2.40453068E+00	4.11313005E-01	1.02337293E+00	0.	
176	87.5	8.75000000E-01					8.07874559E-0
177	88.0	8.80000000E-01	-2.44916311E+00	3.84763042E-01	1.01627199E+00	0.	
178	88.5	8.85000000E-01					5.98038869E-0
179	89.0	8.90000000E-01	-2.49477625E+00	3.57487208E-01	1.00902842E+00	0.	
180	89.5	8.95000000E-01					3.77021668E-0
181	90.0	9.00000000E-01	-2.54141962E+00	3.29457342E-01	1.00163877E+00	0.	
182	90.5	9.05000000E-01					1.44361140E-0
183	91.0	9.10000000E-01	-2.58914618E+00	3.00643505E-01	9.94099409E-01	0.	
184	91.5	9.15000000E-01					-1.00432120E-0
185	92.0	9.20000000E-01	-2.63801265E+00	2.71013837E-01	9.86406547E-01	0.	
186	92.5	9.25000000E-01					-3.57877419E-0
187	93.0	9.30000000E-01	-2.68807989E+00	2.40534389E-01	9.78556195E-01	0.	
188	93.5	9.35000000E-01					-6.28526506E-0
189	94.0	9.40000000E-01	-2.73941321E+00	2.09168945E-01	9.70544162E-01	0.	
190	94.5	9.45000000E-01					-9.12966394E-0
191	95.0	9.50000000E-01	-2.79208289E+00	1.76878819E-01	9.62366045E-01	0.	
192	95.5	9.55000000E-01					-1.21182250E-0
193	96.0	9.60000000E-01	-2.84616465E+00	1.43622629E-01	9.54017205E-01	0.	
194	96.5	9.65000000E-01					-1.52576212E-0
195	97.0	9.70000000E-01	-2.90174017E+00	1.09356052E-01	9.45492757E-01	0.	
196	97.5	9.75000000E-01					-1.85549832E-0
197	98.0	9.80000000E-01	-2.95889776E+00	7.40315382E-02	9.36787549E-01	0.	
198	98.5	9.85000000E-01					-2.20179431E-0
199	99.0	9.90000000E-01	-3.01773306E+00	3.75980041E-02	9.27896140E-01	0.	
200	99.5	9.95000000E-01					-2.56546828E-0
201	100.0	1.00000000E+00	-3.07834978E+00	4.76541334E-07	9.18812782E-01	0.	
202	100.5	1.00500000E+00					-2.94739888E-0

```
04/08/70   LRC CM SCOPE 3.0  6600C-131K 02/24/70
10.18.14.SRD5799.          -  0408  0941
10.18.14.                      LRC COMPUTER COMPLEX
10.18.14.JOB,01,0500,050000.        A2358,      2,
10.18.14.CORNELIA CEXTER, RDK295, 1148,201I
10.18.14.RUN(S)
10.18.21.SETINDF.
10.18.22.LGO.
10.18.33.MEMORY  043000 CM
10.21.22.STOP
10.21.22.SPPRINT(OUTPUT,5)
10.21.24.CPU     98.000811 SEC.
10.21.24.PPU     21.331968 SEC.
10.21.24.DATE      04/08/70
10.51.55. SRD5799. PRINT-PP 00850 LINES,LP 25
```

Attention Patron:

The one-page vita has been removed

from the scanned document

BEHAVIOR OF DOUBLY CURVED PARTLY WRINKLED MEMBRANE STRUCTURES FORMED FROM AN INITIALLY FLAT MEMBRANE

by

Martin M. Mikulas, Jr.

ABSTRACT

A theory is presented for the elastic analysis of deep doubly curved, axisymmetric, partly wrinkled membranes which are formed from an initially flat sheet. The doubly curved membrane surface is analyzed separately in the wrinkled and unwrinkled regions and then properly matched together. The wrinkled region is considered as a zero hoop stress linear membrane, while in the unwrinkled region where stretching of the membrane surface is important, small strain nonlinear membrane theory is used. In addition, meridional and circumferential stiffening cords which are closely spaced so that their effects may be "smeared out" or averaged over the surface are included.

In order to demonstrate the application of the proposed theory, three illustrative wrinkled membrane problems are solved. The first problem is an initially flat circular membrane which has been pleated around its outer circumference to form a deep doubly curved axisymmetric surface which is then attached to a rigid boundary and pressurized. The second problem solved is the stretching of an initially flat circular membrane over a doubly curved, axisymmetric mandrel and the last problem solved is the very large deformation behavior of a pressurized membrane cylinder subjected to a radial line load.

In order to assess the validity of the theory presented, an experimental investigation of the first problem was conducted. In the experiments circular sheets of 1/2-mil Mylar were pleated around the circumference, attached to a rigid circular boundary, and then pressurized. Measurements were made for different levels of internal pressure of the depth and extent of the resulting unwrinkled region at the crown. The results were compared with theoretical predictions and the correlation between experiment and theory was very good until yielding of the Mylar occurred.